ANALYSIS OF PHOTOVOLTAIC PANELS PERFORMANCE AND POWER OUTPUT FORECASTING BASED ON OPTIMIZED DEEP LEARNING TECHNIQUE

MUHAMMAD NAVEED AKHTER

FACULTY OF ENGINEERING
UNIVERSITY OF MALAYA
KUALA LUMPUR

2021

ANALYSIS OF PHOTOVOLTAIC PANELS PERFORMANCE AND POWER OUTPUT FORECASTING BASED ON OPTIMIZED DEEP LEARNING TECHNIQUE

MUHAMMAD NAVEED AKHTER

THIS REPORT IS SUBMITTED IN FULFILMENT OF THE REQUIREMENTS FOR THE DEGREE OF DOCTOR OF PHILOSOPHY

FACULTY OF ENGINEERING
UNIVERSITY OF MALAYA
KUALA LUMPUR

2021

UNIVERSITY OF MALAYA

ORIGINAL LITERARY WORK DECLARATION

Name of Candidate: MUHAMMAD NAVEED AKHTER

Matric No: 17036114/1, KVA170031

Name of Degree: Doctor of Philosophy

Title of Thesis: Analysis of Photovoltaic Panels performance and power output forecasting based on optimized deep learning technique

Field of Study: Renewable Energy

I do solemnly and sincerely declare that:

(1) I am the sole author/writer of this Work;
(2) This Work is original;
(3) Any use of any work in which copyright exists was done by way of fair dealing and for permitted purposes, and any excerpt or extract from, or reference to or reproduction of any copyright work has been disclosed expressly and sufficiently, and the title of the Work and its authorship have been acknowledged in this Work;
(4) I do not have any actual knowledge, nor do I ought reasonably to know that the making of this work constitutes an infringement of any copyright work;
(5) I hereby assign all and every right in the copyright to this Work to the University of Malaya ("UM"), who henceforth shall be the owner of the copyright in this Work and that any reproduction or use in any form or by any means whatsoever is prohibited without the written consent of UM having been first had and obtained;
(6) I am fully aware that if, in the course of making this Work, I have infringed any copyright whether intentionally or otherwise, I may be subject to legal action or any other action as may be determined by UM.

Candidate's Signature Date: 21-08-2021

Subscribed and solemnly declared before,

Witness's Signature Date:

Name:

Designation:

ANALYSIS OF PHOTOVOLTAIC PANELS PERFORMANCE AND POWER OUTPUT FORECASTING BASED ON OPTIMIZED DEEP LEARNING TECHNIQUE

ABSTRACT

Alternative renewable energy sources have a significant contribution to meet the world's energy demand due to population climax and reduce global warming. Solar energy is a major alternative energy source to generate electricity through photovoltaic (PV) systems. However, the generated PV power is susceptible to unpredictable climate and seasonal factors, which cause an unfavorable effect on the stability, reliability, and operation of the grid. Therefore, proper monitoring of the PV system and accurate forecasting of PV power output is required to ensure the stability and reliability of the grid. The purpose of monitoring the PV systems is to keep the PV system in continuous functional status with improved performance. In the first part of this work, the performance of three grid-connected photovoltaic systems installed at the rooftop of the engineering tower building, University of Malaya, Kuala Lumpur, Malaysia, is evaluated. The grid-connected PV systems are based on poly-crystalline (p-s_i), mono-crystalline (m-s_i), and a-si (amorphous silicon (a-s_i)) technologies. The performance is evaluated on monthly and annual data monitored from January 2016 to December 2019. A comprehensive analysis is conducted on eleven performance parameters: performance ratio, capacity factor, array yield, final yield, PV array efficiency, PV system efficiency, inverter efficiency, AC energy, array losses, system, and the overall losses. Secondly, an hour ahead forecasting of solar power output is performed on an annual basis for the aforesaid three PV systems over the same period (2016-2019), based on forecasting accuracy measurement parameters such as RMSE, MSE, MAE, r and R^2. A deep learning method (RNN-LSTM) is proposed and compared with regression (GPR, GPR (PCA)),

machine learning (SVR, SVR (PCA), ANN), and hybrid methods (ANFIS (GP), ANFIS(SC), ANFIS(FCM)) for an hour ahead forecasting of PV power output on an annual basis for the whole period. Moreover, Salp Swarm Algorithm (SSA) is used to tune the hyperparameters of the developed deep learning method on an annual basis over four years to enhance its forecasting accuracy and is compared with RNN-LSTM, GA-RNN-LSTM, and PSO-RNN-LSTM. Performance analysis findings show that p-s_i PV system performs better with a higher annual average (array yield (1309.7 h), array efficiency (12.17 %), and system efficiency (11.33 %)) accompanied by less degradation in almost all performance parameters compared to a-s_i and m-s_i PV systems. Moreover, the composite PV system has the potential to avoid 28143.7 kg of CO_2 emissions in four years. The forecasting results show that the proposed deep learning technique (RNN-LSTM) has presented lower (RMSE, MSE) and higher (r and R^2) compared to other techniques. Moreover, the proposed hybrid method (SSA-RNN-LSTM) is found (19.14% and 21.57%), (15.4% and10.81%) and (22.9% and 25.2%) better in terms of (RMSE and MAE) than developed (RNN-LSTM) for p-si, m-si and a-si PV systems respectively. Furthermore, the proposed hybrid method (SSA-RNN-LSTM) has shown higher R^2 and maximum convergence speed compared to GA-RNN-LSTM and PSO-RNN-LSTM. In addition, the proposed deep learning and hybrid models (SSA-RNN-LSTM) are found to be robust and flexible in the prediction of power output for three different PV systems over four years duration.

Keywords: (performance analysis, forecasting, PV power output, machine learning, optimized deep learning, hybrid method)

ANALISA PRESTASI PANEL-PANEL FOTOVOLTA DAN PERAMALAN KUASA KELUARAN BERDASARKAN PENGOPTIMUMAM PELAJARAN DALAMAN

ABSTRAK

sumber tenaga alternatif boleh diperbaharui mempunyai sumbangan besar untuk memenuhi permintaan tenaga dunia kerana klimaks penduduk dan mengurangkan pemanasan global. Tenaga suria adalah sumber tenaga alternatif utama untuk menjana elektrik melalui sistem fotovoltaik (PV). Walau bagaimanapun, tenaga PV yang dihasilkan bergantung terhadap faktor iklim dan musim yang tidak dapat diramalkan, yang menyebabkan kesan yang tidak baik terhadap kestabilan, kebergantungan, dan operasi grid. Oleh itu, pemantauan sistem PV yang tepat dan peramalan tepat output kuasa PV diperlukan untuk memastikan kestabilan dan kebergantungan grid. Tujuan pemantauan sistem PV adalah untuk memastikan sistem PV sentiasa berfungsi dengan peningkatan prestasi. Pada bahagian pertama kajian ini, prestasi tiga sistem fotovoltaik bersambung grid yang dipasang di bumbung bangunan menara kejuruteraan, Universiti Malaya, Kuala Lumpur, Malaysia, dinilai. Sistem PV yang disambungkan ke grid didasarkan pada teknologi poli-kristal (p-si), mono-kristal (m-si), dan filem nipis (silikon amorf (a-si)). Prestasi dinilai berdasarkan data bulanan dan tahunan yang dipantau dari bulan Januari 2016 hingga Disember 2019. Analisis menyeluruh dilakukan terhadap sebelas parameter prestasi; nisbah prestasi, faktor kapasiti, hasil array, hasil akhir, kecekapan array PV, kecekapan sistem PV, kecekapan penyongsang, tenaga AC, kerugian array, sistem, dan kerugian keseluruhan. Kedua, ramalan satu jam lebih awal di jalankan terhadap output tenaga suria secara tahunan untuk tiga sistem PV di atas dalam tempoh yang sama (2016-2019), berdasarkan parameter pengukuran ketepatan ramalan seperti RMSE, MSE, MAE, r dan R2. Kaedah pembelajaran mendalam (RNN-LSTM) dicadangkan dan dibandingkan dengan regresi (GPR, GPR (PCA)), pembelajaran mesin

(SVR, SVR (PCA), ANN), dan kaedah hibrid (ANFIS (GP), ANFIS (SC) , ANFIS (FCM)) selama satu jam ke depan meramalkan output kuasa PV pada setiap tahun untuk keseluruhan tempoh. Tambahan pula, Salp Swarm Algorithm (SSA) digunakan untuk menyesuaikan hiperparameter kaedah pembelajaran mendalam yang dikembangkan secara tahunan melebihi empat tahun untuk meningkatkan ketepatan ramalannya dan dibandingkan dengan RNN-LSTM, GA-RNN-LSTM, dan PSO-RNN-LSTM. Analisis prestasi yang diperolehi menunjukkan bahawa sistem PV p-si bekerja lebih baik dengan purata tahunan yang lebih tinggi (hasil array (1309.7 jam), kecekapan array (12.17%), dan kecekapan sistem (11.33%)) disertai dengan penurunan yang kurang dalam hampir semua parameter prestasi berbanding ke sistem PV a-si dan m-si.Selain itu, sistem PV komposit berpotensi untuk mengelakkan 28143.7 kg pelepasan CO2 dalam empat tahun. Hasil ramalan menunjukkan bahawa teknik pembelajaran mendalam yang dicadangkan (RNN-LSTM) telah menunjukkan lebih rendah (RMSE, MSE) dan lebih tinggi (r dan R^2) berbanding dengan teknik lain. Di samping itu, kaedah hibrid yang dicadangkan (SSA-RNN-LSTM) didapati (19.14% dan 21.57%), (15.4% dan10.81%) dan (22.9% dan 25.2%) lebih baik dari segi (RMSE dan MAE) daripada yang dikembangkan (RNN-LSTM) masing-masing untuk sistem PV polikristalin, monokristalin dan filem nipis. Selain daripada itu, kaedah hibrid yang dicadangkan (SSA-RNN-LSTM) telah menunjukkan kelajuan penumpuan R^2 dan maksimum yang lebih tinggi berbanding dengan GA-RNN-LSTM dan PSO-RNN-LSTM. Seterunya, model pembelajaran mendalam dan hibrid yang dicadangkan (SSA-RNN-LSTM) didapati kukuh dan fleksibel dalam ramalan output kuasa untuk tiga sistem PV berbeza dalam tempoh empat tahun.

Kata kunci: (analisis prestasi, ramalan, output kuasa PV, pembelajaran mesin, pembelajaran mendalam yang dioptimumkan, kaedah hibrid)

ACKNOWLEDGEMENTS

Foremost, I praise and thank ALLAH Almighty for His faithfulness, grace, love, mercy, strength, and inspiration throughout the course of this work. I pay Darood and salam on the last Prophet of ALLAH (MUHAMMAD (PBUH), due to whom ALLAH has blessed me this honor. My profound appreciation goes to Prof. Dr. Saad Mekhilef and Prof Ir Dr. Hazli bin Mokhlis for their interest, contributions, and encouragement towards the successful completion of this research. My late mother and Grandmother who has prayed a lot for me. I have missed them a lot throughout my career. May ALLAH have mercy on them. My Parents, for their immeasurable sacrifices and encouragement towards my attainment in life. My lovely wife and children, for their love, encouragement, and understanding throughout the course of this work. My siblings for their continued prayers and encouragement. Dr. Munir Azam Muhammad has given valuable technical inputs towards the successful completion of this work. Finally, to everyone too numerous to mention that have contributed in one way or the other toward successful completion of this program.

TABLE OF CONTENTS

LIST OF FIGURES

LIST OF TABLES

LIST OF SYMBOLS AND ABBREVIATIONS

ANFIS	:	Adaptive neuro-fuzzy inference system
ANN	:	Artificial neural network
AC	:	Alternating current
AE	:	Autoencoder
ARMA	:	Autoregressive moving average
ARIMA	:	Autoregressive integrated moving average
ARMAX	:	Autoregressive moving average with exogenous input
ACO	:	Ant colony optimization
ADF	:	Augmented dickey-fuller
ARX-ST	:	Autoregressive with Exogenous Input based Statistical model
a-s_i	:	Amorphous Silicon
BIPV	:	Building-integrated photovoltaics
BNI	:	Beam normal irradiation
BPPT	:	Backpropagation through time
CO_2	:	Carbon dioxide
CIS	:	Copper–indium–selenide
CIGS	:	Copper indium gallium selenide
CMV	:	Cloud motion vector
CNN	:	Convolutional neural network
CARDS	:	Coupled autoregressive and dynamical system
CSRM	:	Clear sky solar radiation model
CdTe	:	Cadmium telluride
c-s_i	:	Crystalline silicon
CF	:	Capacity Factor (%)

DC	:	Direct current (A)
DCGSO	:	Divide and conquer Glow swarm optimization
DCNN	:	Deep convolutional neural network
DENFIS	:	Dynamic evolving neural-fuzzy inference model
DNI	:	Direct normal irradiance
DHR	:	Dynamic harmonic regression
DRNN	:	Deep recurrent neural network
DWT	:	Discrete wavelet transform
EEMD	:	Ensemble empirical mode decomposition
ELM	:	Extreme learning machine
ESDLS	:	Evolutionary seasonal decomposition least square
GHG	:	Greenhouse gases
FCM	:	Fuzzy cluster means
FFA	:	Firefly algorithm
FIS	:	Fuzzy inference system
FPA	:	Flower pollination algorithm
GA	:	Genetic algorithm
GARCH	:	The generalized autoregressive conditional heteroskedasticity
GAMMF	:	Genetic approach combined with the multi-model framework
GBRT	:	Gradient boosted regression trees
GP	:	Grid partitioning
GPR	:	Gaussian process regression
GRNN	:	General regression neural network
GW	:	Gigawatt
GHI	:	Global horizontal irradiance
HIT	:	Heterojunction including thin film

HRES	:	Hybrid renewable energy sources
IEA	:	International Energy Agency
KSI	:	Kolmogorov–Smirnov test integral
LASSO	:	Least absolute shrinkage and selection operator
LM	:	Levenberg Marquardt
LSTM	:	Long short-term memory
LS-GCPV	:	Large scale grid connected photovoltaics
LVQ	:	Learning vector quantization
MPPT	:	Maximum power point tracking
MARS	:	Multivariate adaptive regression spline
MAPE	:	Mean absolute percentage error
MAD	:	Mean absolute deviation
MAE	:	Mean absolute error
MBE	:	Mean bias error
MeAPE	:	Median absolute percentage error
MIL	:	Mean interval length
MLFFNN	:	Multi-layer feedforward neural network
MLP	:	Multi-layer percepteron
MLPNN	:	Multi-layer percpteron neural network
MLR	:	Multi-linear regression model
MSE	:	Mean square error
m-s_i	:	Monocrystalline
NWP	:	Numerical weather prediction
NSE	:	Nash Sutcliffe efficiency
NRMSE	:	Normalized root mean square value
NO_X	:	Nitrogen oxides

OOB	:	Out of bag
PV	:	Photovoltaic
PR	:	Performance Ratio (%)
PSO	:	Particle swarm optimization
PF	:	Power Factor
p-s_i	:	Polycrystalline
PCA	:	Principal component analysis
PEARL	:	Power Electronics and Renewable Energy Research Laboratory
PFLRM	:	Partial functional linear regression model
PCIP	:	Prediction interval coverage probability
RBNN	:	Radial basis neural network
RBFNN	:	Radial basis feedforward neural network
RMSE	:	Root mean square value
RE	:	Renewable energy
RF	:	Random forest
RNN	:	Recurrent neural network
RSM	:	Response surface method
SEDA	:	Sustainable Energy Development Authority
SFLA	:	Shuffled frog leaping algorithm
SC	:	Subtractive Clustering
SMAPE	:	Symmetric mean absolute percentage error
SO_2	:	Sulfur Dioxide
SSA	:	Salp Swarm Algorithm
SVM	:	Support Vector Machine
SVM-C	:	Support Vector Machine (classification)
SVM-R	:	Support Vector Machine (regression)

SVR	:	Support Vector Regression
SVR-KHA	:	Support Vector Regression-Krill Herd Algorithm
SOM	:	Self-organizing map
TDNN	:	Time Delay neural network
UM	:	University of Malaya
VMD	:	Variational mode decomposition
VAE	:	variational Auto Encoder
WD	:	Wavelet decomposition
WT	:	Wavelet transform
WOA	:	Whale optimization algorithm
d	:	Agreement index
E_{AC}	:	AC energy (kWh)
$E_{AC,h}$	:	Hourly AC energy (kWh)
$E_{AC,d}$	:	Daily AC energy (kWh)
$E_{AC,m}$	:	Monthly AC energy (kWh)
$E_{AC,y}$	:	Yearly AC energy (kWh)
E_{DC}	:	DC energy (kWh)
$E_{DC,h}$	:	Hourly DC energy (kWh)
$E_{DC,d}$	:	Daily DC energy (kWh)
$E_{DC,m}$	:	Monthly DC energy (kWh)
$E_{DC,y}$	:	Yearly DC energy (kWh)
f	:	Main's frequency (Hz)
I_{mp}	:	Current at maximum power (A)
I_{sc}	:	Current at short circuit (A)
I_{max}	:	Maximum input current per string (A)

I_{sc}	:	Short circuit current (A)
La	:	Array losses (h)
Ls	:	System losses (h)
P_{mp}	:	Peak power (W)
$P_{PV,\ rated}$	:	PV Rated power (KW_P)
P_{app}	:	Max. apparent AC power (VA)
P_{rated}	:	Rated power (at 230V, 50Hz) (W)
R^2	:	Coefficient of determination
r	:	Correlation coefficient
V_{mp}	:	Voltage at maximum power (V)
V_{oc}	:	Voltage at open circuit (V)
V_{max}	:	Maximum input voltage (V)
V_{rated}	:	Rated input voltage (V)
V_{min}	:	Min. input voltage (V)
$V_{initial}$	:	Initial input voltage (V)
V_{ac}	:	Nominal AC voltage (V)
$V_{nominal}$	:	Nominal AC voltage range (V)
Y_R	:	Reference yield (h)
H_t	:	In-plane solar irradiance (kW/m^2)
H_R	:	Solar radiation (kWh/m^2)
Y_F	:	Final yield (h)
$Y_{F,\ d}$	:	Daily Final yield (h)
$Y_{F,\ m}$	:	Monthly Final yield (h)
$Y_{F,\ y}$	:	Yearly Final yield (h)
Y_A	:	Array yield (h)

$Y_{A, d}$	:	Daily Array yield (h)
$Y_{A, m}$	:	Monthly Array yield (h)
$Y_{A, y}$	:	Yearly Array yield (h)
η_{PV}	:	PV module efficiency (%)
η_{sys}	:	System efficiency (%)
η_{inv}	:	Inverter efficiency (%)

LIST OF APPENDICES

CHAPTER 1: INTRODUCTION

1.1 Background

The drastic increase in world population has led to several developments and advancements in various technologies for improving the quality of human life. Among different types of energies, electrical energy is one of the key elements in ensuring the functioning of such technologies. With the increment demand for this energy due to globalization and modernization, researchers are now focusing to solve the problems of electricity shortage for 1.1 billion of the world population (Hossain, Mekhilef, & Olatomiwa, 2017). Currently, in the power system, electrical energy is commonly generated by three primary natural resources that are coal, natural gas, and oil. Although these resources are able to produce sufficient electrical energy for society, they also cause harmful impacts to the environment in terms of CO_2 emission, global warming, greenhouse gas (GHG) emission, and climate change. Furthermore, the excessive usage of these resources to keep up with the increasing demand for electrical energy also causes a significant reduction of these resources. This problem can lead to an energy crisis that will impact economic growth.

Keeping in view the above facts, the focus is now given to specific alternate resources of energy to meet the electrical demand. Among these resources, renewable energy (RE) has gained much attention due to its abandoned availability, sustainability, and cleanliness in nature. RE sources are fruitful and a blessing for society because they utilize zero fossil fuels (e.g., coal, oil, gas), have low maintenance cost, emit very low GHG emission, keep the environment clean, long-lasting, less costly than conventional energy sources in decentralized areas where transportation charges of fossil fuels are high (Das et al., 2018; Mellit, Kalogirou, Hontoria, & Shaari, 2009; Memon, Mekhilef, Mubin, & Aamir, 2018; Xin-gang & You, 2018).

Among different types of RE, the most dominant ones are solar and wind energies. They have a high penetration rate in the energy market (Das et al., 2018). However, wind energy is applicable only in specific areas, where air pressure is at a certain required level for the proper operation of wind turbines to generate electricity. In comparison with its application in generating electricity, solar energy is more dominant as compared to wind energy. Moreover, solar energy has a more coverage area with 1367 W/m^2/day generation over the atmosphere (Das et al., 2018; Gueymard, 2004). From a research, it was estimated that the total amount of power received by the earth from solar radiation is about 1.8×10^{11} MW at an instant (Shah, Yokoyama, & Kakimoto, 2015). Due to this, solar energy is under significant attention by policymakers, governments, investors, economists, and environmental experts. It is highly abundant and has a high potential for exploration in both rural and urban electrification. The solar energy application is categorized into various forms such as power generation, heating/cooling generation, passive systems, and combined power (Besharat, Dehghan, & Faghih, 2013; Bulut & Büyükalaca, 2007; GhaffarianHoseini et al., 2013; Halawa, GhaffarianHoseini, & Li, 2014; Hepbasli & Alsuhaibani, 2011).

The application of solar energy in generating electricity is through a Photovoltaic (PV) system. PV has attained global popularity in the past 10 years. In 2014, the total power generated from installed PV systems had surpassed 175 GW. Germany, China, Japan, and the USA are among the leading countries in which photovoltaic are expanding rapidly. The installed PV capacity in the last eleven years is improved from 17 GW in 2010 to about 140 GW in 2020 (Jäger-Waldau, 2020). The total installed PV electric power in 2015 is 59 GW. In a report by IHS company, it is stated that an additional 272.4 GW power is raised from the above potential to enhance the exponential rate of generative potential in the years 2016-2019. Figure 1.1 shows the current increase in installed PV

power from 2007 to 2020. The global PV power capacity installation can exceed 1700 GW by 2030, according to IEA's point of view (Das et al., 2018).

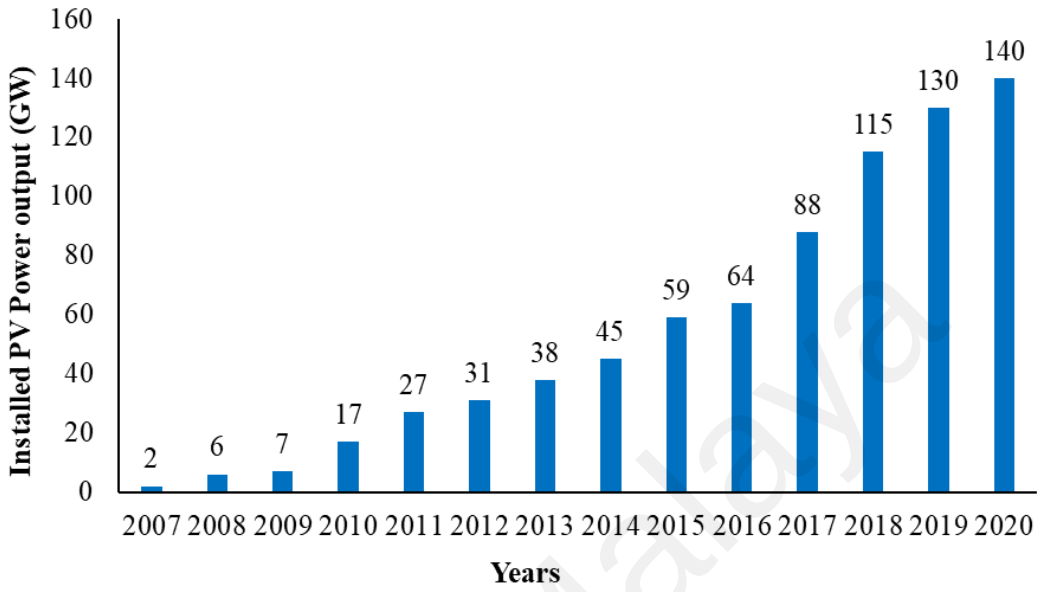

Figure 1.1: Increase in installed PV power output during the years from 2007-2020 (Bugała et al., 2018; Jäger-Waldau, 2020)

1.2 Problem statement

With the passage of time, the prime sources of energy (coal, oil, gas) are depleting due to their massive usage because of globalization and modernization of the world. Therefore, renewable energy sources have been focused on meeting the world energy demand and reduce global warming (Adaramola, Paul, & Oyewola, 2014). Among these energy sources, solar energy is the most abundant in the whole world (Das et al., 2018). Therefore, it is crucially important to study the performance of various PV technologies for maximum electricity generation.

The performance of PV systems depends upon solar cell technology, solar radiation, and other climate factors. Therefore, proper monitoring of PV systems is required to define the behavior of PV modules against different meteorological parameters for accurate performance evaluation. The purpose of monitoring the PV systems is to

facilitate a means to ascertain and extract valuable information pertaining to any operational problems. This will avoid similar issues in the future and keep the PV system functioning with improved performance (Brecl et al., 2016).

Different research studies have been performed to analyze the performance of different PV technologies in the tropical climate of Malaysia. The copper indium–selenide (CIS) modules have shown better performance ratio (PR) (84.1%) than PR (79.1%) of mono-crystalline (m-s_i) modules at Bangi Malaysia. However, the performance comparison of CIS with polycrystalline (p-s_i) and thin-film (a-s_i) was not provided (Humada et al., 2016). Furthermore, the inverter efficiency (η_{inv}) and the PV system efficiency (η_{sys}) were also not evaluated. The performance of Cadmium telluride (CdTe), Crystalline silicon (c-s_i), and CIS was evaluated in Malaysia (Kumar et al., 2019). The CdTe modules have shown a better PR of 76.20%-77.36% compared to the other two modules. However, the performance of p-s_i and a-s_i was not analyzed. A detailed analysis is also missing in this study based on several other performance parameters, which are the array yield, PV efficiency, system efficiency, and inverter efficiency.

The performance of thin-film PV system was found better compared to Heterojunction including thin film (HIT), m-s_i and p-s_i PV systems in a techno-economic study in Penang (Yatim et al., 2017). The annual energy produced was 4723 kWh, 4749.3 kWh, 4999.6 kWh, and 5179 kWh for HIT, m-s_i, p-s_i, and thin-film PV systems respectively. However, detailed performance analysis was not performed in this study. It was observed that the PR of p-s_i was found 3% better than the PR of the m-s_i system in a comparative study performed at Kuala Lumpur (Zain et al., 2013). However, a-s_i PV system was not considered in this study. The degradation effect in different performance parameters had not been appropriately included in all these studies due to the use of only one year data. Therefore, it is required to assess various PV technologies over a long duration within the

same environment to achieve better information about the performance deviations of a particular region for different environmental patterns. There is no detailed study in Kuala Lumpur which provides a comprehensive analysis based on several performance parameters for p-s_i, a-si, and m-s_i based PV systems over a long-monitored period. Moreover, the study of the composite PV system including these three PV technologies is also missing from the literature along with the environment-saving impact in terms of GHG (CO_2, SO_2, NO_x, Ash) reduction.

The performance of PV systems is directly related to their power output. The PV power production, however, is dependent upon various factors such as climatic conditions, wind pressure, humidity, solar radiation, ambient temperature, and module temperature. The natural variations in the climate may vary these parameters, altering the amount of power produced. The abrupt change in solar power output disturbs the reliability, stability, and planning of the power system for grid-connected PV systems. To avoid these circumstances, accurate and precise solar power output forecasting is required to ensure the reliability, stability, and quality of the power system.

In terms of PV output forecasting, various techniques have been explored, such as autoregressive moving average (ARMA), autoregressive integrated moving average (ARIMA), autoregressive moving average with exogenous input (ARMAX), coupled autoregressive and dynamic system (CARDS), regression and regression trees. These methods have a limitation to deal with nonlinear data. The sky images and satellite images were used to predict the solar irradiance for an ultra-short-term period based on cloud tracking and forecasting (Cheng, 2017; F. Wang et al., 2018; Zaher, Thil, Nou, Traoré, & Grieu, 2017). The forecasting accuracy of image-based methods is dependent directly on image processing algorithms. However, based on low-resolution satellite data and limited coverage of sky images from the ground, the forecasting accuracy of these methods needs further improvement. Numerical weather prediction (NWP) is used for 15 days ahead

solar irradiance forecasting, but its application is limited due to the data access restrictions imposed by the domestic meteorological departments (Lima, Martins, Pereira, Lorenz, & Heinemann, 2016; Mathiesen, Collier, & Kleissl, 2013; Perez et al., 2013; Verzijlbergh, Heijnen, de Roode, Los, & Jonker, 2015).

Among machine learning techniques, Artificial Neural Network (ANN) in (Alzahrani, Shamsi, Dagli, & Ferdowsi, 2017; Bou-Rabee, Sulaiman, Saleh, & Marafi, 2017; Hussain & AlAlili, 2017; Xue, 2017) and Adaptive Neuro-fuzzy inference system (ANFIS) in (Olatomiwa, Mekhilef, Shamshirband, & Petković, 2015) are deployed for solar power output forecasting. They have a better ability to deal with nonlinear systems and cope with the inconsistent behavior of solar power. However, the issues of random initial data, local minima, overfitting, and increased complexity due to multilayered structure affect the reliability of the power system (De Giorgi, Malvoni, & Congedo, 2016; Dolara, Grimaccia, Leva, Mussetta, & Ogliari, 2015; Mellit et al., 2009). The Support vector machine (SVM) has also shown better forecasting accuracy to predict solar power in (H. S. Jang, Bae, Park, & Sung, 2016; Junior et al., 2014; Wolff, Kühnert, Lorenz, Kramer, & Heinemann, 2016). However, it is highly sensitive to parameters such as kernel function, tube radius (ε) and penalty factor (C). Therefore, proper selection of these parameters is a challenging task (Das et al., 2018). In an extreme learning machine (ELM), the selection of input weights and biases of hidden nodes is random (Deo, Downs, Parisi, Adamowski, & Quilty, 2017; Hossain, Mekhilef, Danesh, Olatomiwa, & Shamshirband, 2017; Tang, Chen, & Hou, 2016).

To overcome the deficiencies of conventional neural networks and other machine learning techniques, deep learning models have been applied in certain areas (H. Wang, Lei, Zhang, Zhou, & Peng, 2019; Youssef, El-Telbany, & Zekry, 2017). Deep learning is also an advanced type of machine learning method. Convolutional neural network (CNN)

(Zang et al., 2018) and Recurrent neural network (RNN) (Shi, Xu, & Li, 2017; A. Yona, Senjyu, Funabashi, & Kim, 2013) are deep learning models used for forecasting of PV power. Deep learning has the ability to extract deep features from PV power output and provide better forecasting results than persistence, physical and statistical models.

An algorithm is proposed based on the Long short term memory (LSTM) network for day-ahead power output forecasting using the data provided by local meteorological authorities. It has shown 18.34% more forecasting accuracy than other benchmark methods (Qing & Niu, 2018). G Narvaez et al. have performed PV power prediction on a daily and weekly basis using the deep learning method (Narvaez, Giraldo, Bressan, & Pantoja, 2021). A grey theory-based deep belief network proposed for a day ahead forecasting of PV power output showed better forecasting accuracy and computational efficiency (Chang & Lu, 2018). F Wang et al. (F. Wang et al., 2020) have developed a time correlation modification method to enhance the accuracy of the deep learning model for a day ahead PV power forecasting. However, an hour ahead PV power forecasting based on a deep learning model for different PV systems over a large real dataset in Malaysia to ensure the robustness of the model, is missing in all these studies. According to the author's knowledge, the comparison of the deep learning method with regression (GPR, GPR(PCA)), artificial neural networks (ANN), machine learning (SVR, SVR(PCA)), and hybrid (ANFIS) methods altogether is also missing in literature for PV power output forecasting. Therefore, there is still room for improvement to develop a deep learning method for an hour ahead prediction of power output for different PV systems on annual basis over four years data period (2016-2019) in comparison with regression, machine learning and hybrid techniques.

The PSO was used to optimize the parameters of LSTM to enhance its 30 minutes ahead prediction accuracy for PV power output forecasting considering the time-series

approach (Zheng et al., 2020). However, only one-year data is considered. A genetic algorithm (GA) was also used with LSTM for 4 hours ahead forecasting of PV power output (Jaidee & Pora, 2019). However, GA is an old optimization algorithm and is preferred for discrete problems (Zheng et al., 2020). There is no study in literature, which has used some advanced optimization algorithm to tune the hyperparameters of LSTM for an hour ahead forecasting of PV power output for three different PV systems on an annual basis in Malaysia over a large data set. Furthermore, the comparison of advanced optimization algorithm with GA and PSO is also missing. Therefore, an advanced optimization algorithm with better convergence speed is also required to tune the hyperparameters of the developed deep learning method to enhance its forecasting accuracy in comparison with GA and PSO algorithms.

1.3 Motivation

This research is significant for short-term planning in Malaysia because it incorporates two aspects: (1) performance analysis; (2) PV power output forecasting. The justification is that by keeping in view the prior information obtained from this long-term performance of three different PV technologies, the Malaysian government and private renewable energy sector can plan to install large solar farms with higher PV efficiency and yield in the tropical climate of Kuala Lumpur.

In addition, an hour ahead (short-term) forecasting of solar power output in grid-connected PV systems will also enhance the grid reliability and improve the power system operation. This short-term forecasting can also be helpful for electricity price forecasting in Malaysia for hybrid systems connected with the grid. The two aspects of the research are interrelated with each other in such a way that the performance of any PV module can also be evaluated in advance if its power output is predicted at the first step. Therefore, this research is helpful to fulfill society's need for improving the life quality in Malaysia.

1.4 Research objectives

The main aim of this research is to develop a soft optimized deep learning technique for the prediction of solar power output for three different PV systems on an annual basis over the period (2016-2019). The research objectives are described as follows:

1. To evaluate and analyze the performance of three different PV systems: polycrystalline, monocrystalline, and thin-film, along with combined PV system based on various performance parameters accompanied by evaluation of environment saving impact in terms of CO_2 reduction.
2. To develop a deep learning algorithm for an hour ahead forecasting of the solar power output for three different PV systems.
3. To compare the deep learning algorithm with regression (GPR), machine learning (ANN, SVR), and hybrid (ANFIS) methods for an hour ahead forecasting of solar power output for three PV systems.
4. To optimize the developed deep learning algorithm using GA, PSO, and SSA optimization techniques for enhancing its forecasting accuracy.

1.5 Methodology of research

The methodology adapted to fulfill the research objectives is shown in Figure 1.2. It has two parts. In the first part, the actual PV data is used to evaluate the performance of three different PV systems: polycrystalline, monocrystalline, and thin-film, along with the calculation of greenhouse gases (GHG) emission reduced over four years recorded actual data period (2016-2019). In the second part of the methodology, preprocessing of data is performed, such as collection, division, and normalization before forecasting. After that, a deep learning method (RNN-LSTM) is proposed for an hour ahead forecasting of PV power output and compared with regression (GPR, GPR(PCA)), machine learning (SVR, SVR(PCA), ANN), and hybrid (ANFIS) methods. Moreover, the

developed deep learning method is further optimized using the SSA optimization algorithm in comparison with GA and PSO.

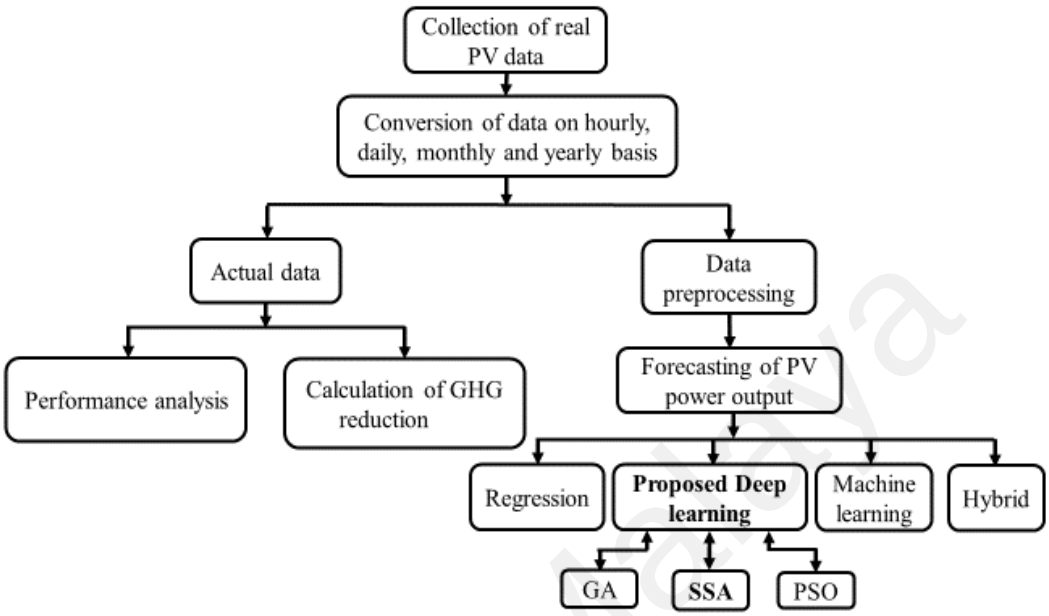

Figure 1.2: Flow chart of research methodology

1.6 Scope of the study

The scope of this study is divided into three parts. In the first part, the performance of grid-linked photovoltaic systems is evaluated and analyzed based on three PV technologies along with a composite PV system installed at the rooftop of the engineering tower building, UM, Kuala Lumpur Malaysia. It includes monthly and annual analysis based on eleven different performance indices such as the capacity factor, performance ratio, PV array efficiency, PV system efficiency, inverter efficiency, array yield, final yield, AC energy generated, array losses, system, and the overall losses. The data employed for estimating the PV systems performances were collected between January 2016 and December 2019. Furthermore, the comparison is performed with the results reported in some of the previous studies under similar and different climates. Moreover, the contribution of the composite PV system to the environment is also examined in terms

of Greenhouse gases (CO_2, SO_2, NO_x, and Ash) reduction. This performance analysis provides an insight into the need to observe the PV systems performance and extract valuable information regarding possible operational problems, to keep the PV system in continuous operational conditions with improved overall performance. This research is expected to deliver valuable statistics to individuals and organizations about the real performance of grid-integrated PV systems in Malaysia, including other tropical climate regions in the world.

Secondly, this research proposes a deep learning technique (RNN-LSTM) for an hour ahead forecasting of PV power output on an annual basis for the data period (2016-2019). Moreover, an hour ahead prediction of PV power output is also performed annually using GPR, SVR, GPR (PCA), SVR(PCA), ANN, and ANFIS (grid partitioning, subtractive clustering, and FCM) over the four years period to compare with the proposed deep learning method. These techniques are applicable to real recorded and meteorological data for enhancing the reliability and stability of the grid.

Finally, the hyperparameters of the developed deep learning method (RNN-LSTM) are optimized further to enhance its forecasting accuracy, using the SSA optimization in comparison with genetic algorithm (GA) and particle swarm optimization (PSO).

1.7 Thesis outline

The remaining part of the thesis is organized as follows: in chapter 2, the literature review about the performance analysis of PV systems and forecasting of solar power output is provided. Then, different types of forecasting horizons are discussed. Various mathematical forecasting techniques are discussed for the prediction of solar power output. In the next section, the machine learning techniques (ANN, SVM, ELM, deep learning) are described for forecasting solar power output along with the summary. Finally, the hybrid methods are elaborated, showing different combinations of statistical

and machine learning techniques. A comprehensive comparative analysis is performed at the end of this chapter.

In chapter 3, the description of a grid-connected PV system is provided, along with the collection of data. Then, different performance parameters are presented to evaluate and analyze the performance of the PV system. Secondly, different linear and machine learning techniques, such as GPR, SVR, PCA, ANN, ANFIS, and the proposed deep learning algorithm (RNN-LSTM), are described for an hour ahead prediction of solar power output. Finally, the methodology of GA, PSO, and SSA optimization algorithms is presented to optimize the forecasting accuracy of the developed deep learning (RNN-LSTM) technique.

In chapter 4, the performance of three different types of PV systems, along with combined PV system, is analyzed over four years recorded period (2016-2019) based on several performance parameters. The impact of the combined PV system on cleaning the environment is also presented. In the next section, the results for an hour ahead forecasting of the solar power output for three different PV systems based on Regression (GPR, GPR(PCA)), machine learning (SVR, SVR (PCA), ANN), hybrid (ANFIS (GP), ANFIS (SC), ANFIS (FCM)) and proposed deep learning method (RNN-LSTM), are discussed in detail. Finally, the results showing the optimization of the developed deep learning (RNN-LSTM) method using GA and PSO, and SSA algorithms are elaborated. In the end, the findings are concluded according to research objectives in chapter 5.

CHAPTER 2: LITERATURE REVIEW

2.1 Introduction

In this chapter, an assessment of different PV systems based on different performance parameters is reviewed. The forecasting of solar power output is briefly discussed, including previous solar power output prediction approaches used in literature. Then, different types of forecast methods based on time horizons are described. This chapter also reviews mathematical techniques for forecasting solar power output, such as the persistence model, statistical techniques. In addition, machine learning forecasting techniques such as ANN, SVM, ELM, and deep learning are critically analyzed. Furthermore, metaheuristic forecasting techniques are also briefly reviewed. Then, a comprehensive comparative analysis for all these forecasting techniques is provided, indicating the gap for this research. The importance of forecasting and grid management strategy with integration of renewable power generation is also discussed. Finally, the chapter is summarized at the end.

2.2 Performance assessment of PV systems

The proper monitoring of PV systems is necessary to analyze the performance of PV modules against different meteorological parameters (Khalid et al., 2016). Table 2.1 describes the recent literature analyzing the performance of different PV technologies in various world locations to determine the optimum PV technology under a specified condition. To attain the optimum performance of the PV system in Malaysia, there were some studies in the past. The performance of two grid-linked PV systems at Bangi Malaysia was analyzed (Humada et al., 2016); one was mono-crystalline (m-s_i), and the other was copper indium–selenide (CIS) based modules. It was observed that the maximum monthly performance ratio (PR) in a year for CIS and m-s_i was 84.1% and 79.1 %, respectively. It indicates that CIS modules performed better than m-s_i under tropical atmospheric conditions. However, the performance of CIS as compared to p-s_i and a-s_i

had not been evaluated. Furthermore, the efficiency of inverter (η_{inv}) and the PV system (η_{sys}) were also not assessed in this study.

Table 2.1: Assessments of PV performance reported in the literature

Ref	Location	PV types	AC energy (kWh)	PV Eff (%)	PR (%)	Final Yield (kWh/kWP/ day)
(Tripathi et al., 2014)	India	p-si a-si	2550 23996.5	11.07 6.56	75.3 70.8	2.79-5.14 2.62-4.84
(Al-Otaibi et al., 2015)	Kuwait	CIGS	9000 15000		76	4.5
(Ali and Khan, 2020)	Pakistan	p-si CIS	53751 54570	-	72.2 73.25	-
(Tahri et al., 2018)	Japan	p-si CIS	16.4-17.3 9.7-9.9	-	80.5-86.5 74.7-76.1	3.85-4.05 3.90-3.95
(Quansah et al., 2017)	Ghana	HIT m-si p-si a-si CIS	4490 4000 4572.1 4500 3133.2	-	74.8 67.9 76.3 75.8 52.3	3 2.8 3.10 3.08 2.12
(Ozden et al., 2017)	Anatolia	a-si m-si CdTe	-	11.86 6.40 5.30	-	-
(Ramanan and Karthick, 2019)	India	p-si CIS	1536.9 1698.4	12.19 14.19	78.5 86.7	4.31 4.68
(Elibol et al., 2017)	Turkey	m-si a-si p-si	___	13.26 4.79 11.36	91 73 81	12.3-14.5 3.8-5.2 9.8-11

Another study (Kumar et al., 2019) was conducted at Universiti Malaysia Pahang (UMP). The performance of three PV technologies is evaluated in this study, which are CdTe, c-si, and CIS. The CdTe modules performed better with a PR of 76.20%-77.36% as compared to the other two modules. Similar to the previous study, this study did not evaluate the performance of p-si and a-si under the tropical weather of Malaysia. Also, this study did not consider the analysis on several other performance parameters, i.e., array

yield (Y_A), PV system efficiency (η_{PV}), system efficiency (η_{sys}) and inverter efficiency (η_{inv}).

A techno-economic study (Yatim et al., 2017) was performed on a 3.3kW residential building-integrated PV (BIPV) system with HIT, m-s_i, p-s_i, and thin-film modules in Penang, Malaysia. It was found that thin-film modules performed better than the other three modules. The annual energy produced was 4723 kWh, 4749.3 kWh, 4999.6 kWh, and 5179 kWh for HIT, m-s_i, p-s_i, and thin-film modules, respectively. However, detailed performance analysis was not conducted in this study. In Kuala Lumpur, a comparative study (Zain et al., 2013) was performed between grid-connected p-s_i and m-s_i PV structures. It was observed that the PR of p-s_i was 3% higher than the PR of m-s_i. However, a-s_i PV system was not presented in this study. Another common shortcoming of these four studies is that the performance analysis was conducted on only one year of data; hence the impact of degradation in the performance parameter had not been incorporated in these studies.

It is evident from these similar climate studies that there is no single best technology for the tropical climate of Malaysia. Therefore, it is necessary to assess various technologies over a long period within the same environment to obtain better information with respect to performance deviations of a particular region for different environmental patterns. So far from the author's knowledge, no study in Kuala Lumpur provides a comprehensive analysis based on several performance parameters for p-s_i, a-si, and m-s_i based PV systems over a long-monitored period. Besides, the study of the composite PV system containing these three technologies is also missing from the literature, along with the environment-saving impact in terms of GHG reduction.

2.3 Forecasting of PV power output

In a grid system connected with solar PV plants, the variable and non-controllable nature of solar irradiation production poses critical problems to the performance of the power system. Voltage fluctuation, reactive power compensation, harmonics, frequency response, reliability, and stability are well-known problems. Therefore, an accurate power output forecasting of the PV system is an essential task to address these problems.

In the past, mathematical techniques have been applied to forecast the power generation output of PV systems. These methods can be categorized into the Persistence method and Statistical methods. Unfortunately, these techniques generally produce low forecasting accuracy and fail to work correctly with nonlinear data also. Due to these limitations, machine learning techniques such as Support Vector Machine (SVM), Artificial Neural Network (ANN), Extreme Learning Machine (ELM), deep learning, and metaheuristic techniques are used to deal with nonlinear data and enhance the forecasting accuracy (Antonanzas et al., 2016; Das et al., 2018; Raza & Khosravi, 2015; Sobri, Koohi-Kamali, & Rahim, 2018; Voyant et al., 2017).

Machine learning methods can deal with problems that explicit algorithms are not able to solve. The ability to develop a relationship between inputs and outputs, even when their representation is impossible, makes these models suitable for pattern recognition, classification, data mining, and forecasting (Voyant et al., 2017). There are three main groups of solar radiation forecasting methods, i.e., statistical/numerical methods, physical methods, and hybrid or ensemble methods. Machine learning models (ANN, SVM, ELM, deep learning) are an advanced form of statistical methods. Physical methods consist of three sub-models, (i) NWP model, (ii) sky imagery model, (iii) satellite imaging or remote sensing model. Statistical methods are based on historical data. They have the ability to extract information from the data to forecast time series. The physical methods are based

on the interaction between the physical state and dynamic motion of solar radiation in the atmosphere.

Statistical/numerical methods produce better solar forecasting results for time horizons between 1 hour and 6 hours, while for medium and longer time horizons, physical methods (NWP, remote sensing, etc.) become most attractive (Voyant et al., 2018). Numerical weather prediction (NWP) models are generally used for 15 days ahead forecasting. Three types of NWP models are global (entire earth), mesoscale (part of the earth), and regional (specific local region) (Diagne, David, Lauret, Boland, & Schmutz, 2013). Sky imagery models are used for short-term GHI forecast (6 hours) to deal with small-scale variability created by the cloud's variable motion. It has the advantage of having complete meteorological information for a very short-term forecast of future cloud patterns in solar generation facility areas (Sobri et al., 2018). Remote sensing or satellite imaging models are used to forecast solar irradiation without any need for ground sensors.

While metaheuristic methods with a combination of machine learning and physical methods provide more accurate solar forecasting for medium and long-term time horizons (Ghimire, Deo, Downs, & Raj, 2018). Metaheuristic techniques having various combinations of machine learning, deep learning, and physical methods are able to provide better solar forecasting by reducing the forecasting errors (RMSE, MAPE, MAE) compared to other methods (Diagne et al., 2013; Ghimire et al., 2018; Ogliari, Dolara, Manzolini, & Leva, 2017; Sobri et al., 2018; Verbois, Huva, Rusydi, & Walsh, 2018; Wolff et al., 2016)

In (Das et al., 2018), direct forecasting techniques for PV power generation have been reviewed. While machine learning methods for PV output prediction have been reviewed in (Voyant et al., 2017) and a brief review of ANN is performed for short-term load forecasting in (Raza & Khosravi, 2015). Statistical, physical, and ensemble methods have

been studied as solar PV generation forecasting methods in (Sobri et al., 2018). Antonanzas et al. highlighted some issues related to prediction planning (Antonanzas et al., 2016). In (H. Wang et al., 2019), a review of deep learning for renewable energy forecasting is discussed in detail. It becomes clear that there is no comprehensive analysis and comparative discussion on machine learning, deep learning together with metaheuristic techniques for PV power output forecasting. The detail of forecasting horizons, mathematical, machine learning, and hybrid methods are described as follows.

2.4 Forecasting horizon

The time duration for which the forecasting of PV power output is performed is known as the forecasting horizon. In the forecasting horizon, the time duration is the main factor that determines its classification. Proper selection of time horizon is compulsory before the design of the model to maintain the accuracy of PV forecasting at an acceptable level, as the forecasting accuracy is highly sensitive to the forecast horizon.

Prediction intervals (PIs) and confidence intervals (CIs) are valuable tools to minimize the effect of weather uncertainties, hence improve the efficiency of forecasting models. CIs represent statistical intervals calculated from existing data. While PIs develop upper and lower bounds of future realizations for a random variable with corresponding coverage probability. PIs point out prediction values and provide information to make decision-makers ready for best and worst cases in the future (Ni, Zhuang, Sheng, Kang, & Xiao, 2017; Voyant et al., 2018). In recent literature, several methods are used to generate PIs (Fliess, Join, & Voyant, 2018) and optimize (Quan, Srinivasan, & Khosravi, 2014) further in order to enhance their efficiency against uncertainties due to seasonal or geographical variations (van der Meer, Munkhammar, & Widén, 2018).

The accuracy of forecasting is affected by the change of forecasting horizon, even with similar parameters in the same model. Rohit et al. (Rawat, Vora, Manry, & Eapi, 2014)

analyzed the forecasting accuracy of the multivariable neural network for three types of forecasting horizons (1h, 26h, 51h ahead). The forecast error (MSE) for the proposed forecasting model is in the range of 1.068-7.8909 during the training session and 0.99253-8.1365 during the testing session for the above said forecasting horizons.

The forecasting accuracy decreases with the increase of the forecast horizon, even for the same forecasting technique. Thus, the selection of a proper time horizon is compulsory before designing a forecasting model to maintain the accuracy of PV forecasting at an acceptable level. In a multi-time-scale data-driven Spatio-temporal PV power forecast, the average RMSE found was 106.9, 154.8, 163.2, and 187.6 for a forecasting horizon of 5 min, 15 min, 1h, and 2h ahead forecasts, respectively (C. Yang, Thatte, & Xie, 2015).

Very short-term forecasting (1 sec - < 1 h) is helpful for real-time electricity dispatch, optimal reserves, and power smoothing. In contrast, short-term forecasting (1 h- 24 h) is useful to increase the security of the grid. Medium-term forecasting (1 week – 1 month) maintains the power system planning and maintenance schedule by predicting the available electric power in the near future. Long-term forecasting (1 month - 1 year) helps in electricity generation planning, transmission, and distribution authorities in addition to energy bidding and security operations. Figure 2.1 describes the relationship between forecasting horizon, forecasting model and related activities. Meanwhile, Figure 2.2 describes the recently mentioned four types of PV forecasting based on the time horizon.

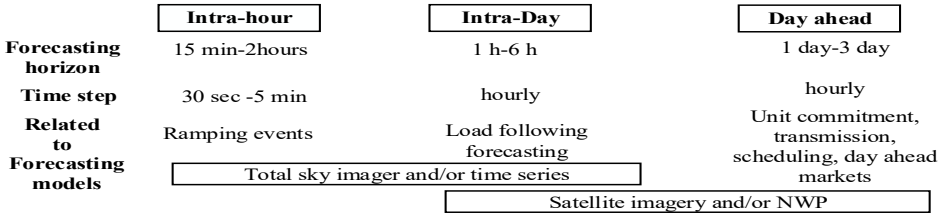

Figure 2.1: Relation between forecasting horizon, forecasting model and related activities

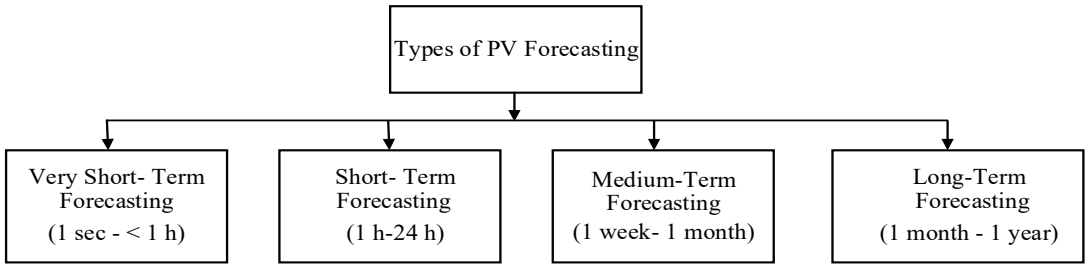

Figure 2.2: Classification of PV power forecasting based on time

2.5 Mathematical forecasting techniques

Mathematical forecasting techniques can be broadly divided into two techniques: (1) Persistence method and (2) Statistical techniques. Figure 2.3 describes both techniques of solar power forecasting in addition to machine learning and hybrid techniques based on historical data.

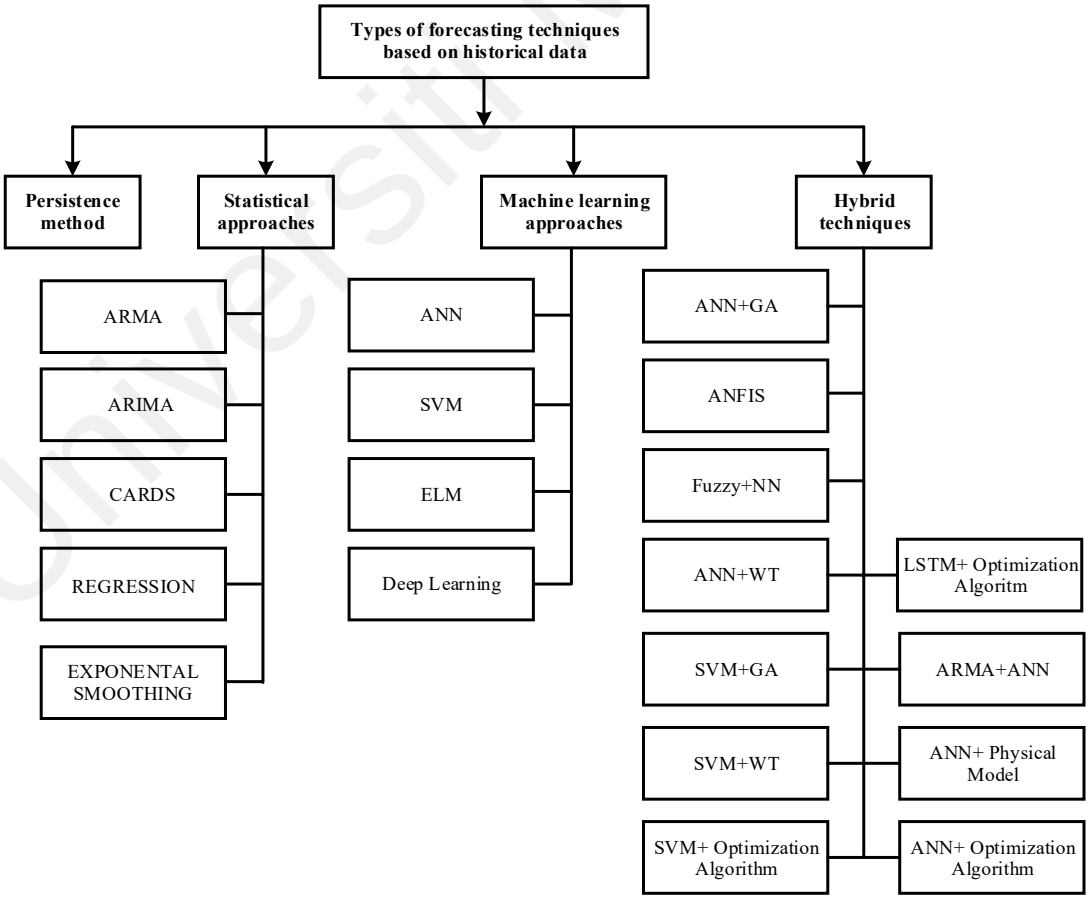

Figure 2.3: Types of PV power forecasting based on historical data

2.5.1 Persistence model

It is used as a standard model to test the forecasting accuracy of any proposed model. The historical data is required only in this model. From previous studies (Azimi, Ghayekhloo, & Ghofrani, 2016; Lipperheide, Bosch, & Kleissl, 2015; Nonnenmacher, Kaur, & Coimbra, 2016; Voyant, Muselli, Paoli, & Nivet, 2012) other proposed model showed better performance when compared with the persistence model. The solar power forecasting output is assumed to be similar to the power value measured on the last or coming day (Diagne et al., 2013). The persistence model is the most used model in the forecasting of solar power output for a time span of one hour. It is also known as a naive predictor. It is an improper method for forecasting more than 1 hour ahead forecasting and can only be used for comparative analysis with other advanced techniques (Lipperheide et al., 2015).

2.5.2 Statistical techniques

2.5.2.1 Time series models

*(a) **Autoregressive moving average (ARMA) model***

This model is a combination of two models known as the AR and MA models. It has an important role in the forecasting of PV power output from time series data and is represented by the following equation (R. Huang, Huang, Gadh, & Li, 2012)

$$X(t) = \sum_{i=1}^{p} \propto_i X(t-i) + \sum_{j=1}^{q} \beta_j e(t-j) \qquad (2.1)$$

Where

$X(t)$ = the forecasted solar output

p, q = order

$\propto_i, \beta_j$ = coefficients

e(t) = white noise that produces random uncorrelated variables with zero mean and constant variance (Rajagopalan & Santoso, 2009).

This model is usually applied to auto-correlated time series data. ARMA is a promising tool to understand and predict the future values of specific time series. The stationary time series requirement is a significant limitation of the ARMA model (Diagne et al., 2013). The key fact for its importance that it has the ability to extract the statistical properties and its adoption of the Box Jenkins method. ARMA was used in conjunction with TDNN for 10-minutes ahead prediction of hourly solar radiation, resulting in better forecasting accuracy. Augmented Dickey-Fuller (ADF) method was used to find the stationary behavior of the residual for the judgment of different de-trending models. ARMA is used to predict the linear component of trend time series only with a limitation that it can not deal with nonlinear components (Ji & Chee, 2011).

ARMA models are very flexible, where they can represent different types of time series using a different order. The deterministic component is removed to ensure the stationarity of the solar irradiance series in the case of solar energy forecasting. This is performed by dividing the measured value of solar irradiance at ground *G* by the corresponding quantity at the top of the atmosphere G_{ext} (Blaga et al., 2019)

$$K_t = \frac{G}{G_{ext}} \tag{2.2}$$

Where K_t is the clearness index, which separates out the stochastic component of the solar irradiance time series. ARMA models forecast the clearness index. A combination of ARMA and the generalized autoregressive conditional heteroskedasticity (GARCH) model was analyzed in short-term solar forecasting to assess the prediction intervals associated with the point forecasts. Furthermore, ARMA-GARCH needs a lower computational requirement than an ensemble method based on NWP (David,

Ramahatana, Trombe, & Lauret, 2016). Applications of the ARMA model in the solar forecasting energy field have also been discussed in (Boland, David, & Lauret, 2016). A general schematic diagram is shown for ARMA-based prediction in Figure 2.4.

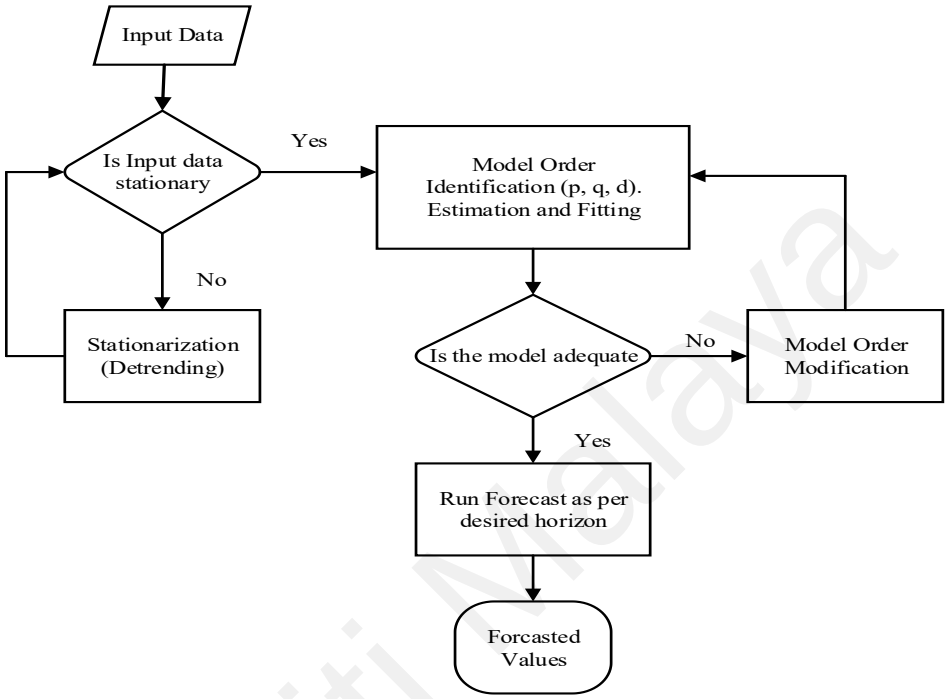

Figure 2.4: General schematic diagram for ARMA based prediction

ARIMA is an extended version of the ARMA model with an added integrated element. ARIMA models can process non-stationary time series data and were used as a reference estimator in the forecasting of the global irradiance field (Hamilton, 1994). The ARIMA model (a, b, c) of the time series (X_1, X_2, X_3) can be expressed as:

$$\emptyset_a(B)\Delta^b X_t = \theta_c(B)a_t \tag{2.3}$$

where

$$\emptyset_a\,(B) = 1 - \emptyset_1 B - \emptyset_2 B^2 \ldots\ldots\ldots \emptyset_a B^a \tag{2.4}$$

$$\theta_c\,(B) = 1 - \theta_1 B - \theta_2 B^2 \ldots\ldots\ldots \theta_c B^c \tag{2.5}$$

B is the backward shift operator, $BX_y = X_{y-1}$, Δ is the backward difference, $\emptyset_a$ and θ_c are polynomials of order a and c, respectively. ARIMA (a, b, c) model is the

combination of autoregressive part AR(a) (see (Eq. 2.4)) and integral part $I(b) = \Delta^b$ and MA(c) is moving average part (see (Eq. 2.5)). For a stable operation (bounded outputs for bounded inputs), both polynomials are designed in such a way that their zeros lie outside the unit circle. White noise process ($a_{t,}\ a_{t-1,}\ldots,$) is used for some random values (deviated from time-series average) drawn from a fixed distribution with zero mean and variance σ_a. a_t is the independent time step variation of the white noise process. After differentiating at appropriate time steps to remove any trends, the AR component is stochastically coupled with the MA component (Sobri et al., 2018).

Reikard (Reikard, 2009) developed an ARIMA model for forecasting solar irradiance by applying regression in logs to the inputs of this model. Best results were obtained by using the ARIMA in logs at low resolutions by producing RMSE (W/m^2) of 0.1321, 0.1897, and 0.1865 for 5, 15, and 30 minutes horizons, respectively where the data was dominated by the diurnal cycle. An ARIMA method is analyzed on high-resolution GHI (W/m^2) data to test its capabilities in Abu Dhabi by using the performance parameters such as coefficient of determination R^2 and RMSE. The best fit model showed R^2 of 88.63% and RMSE of 72.88 W/m^2 (Hussain & Al Alili, 2016).

Another version of the ARMA model is an autoregressive moving average with exogenous inputs (ARMAX). It does not rely on solar irradiance as ARIMA but considers the climatic information, unlike ARIMA. Yanting Li proposed a time series (ARMAX) model with exogenous inputs (temperature, air pressure, humidity, insolation duration, precipitation amount, wind speed, and direction) for 1-day ahead prediction of the power output for a grid-connected PV system, showing better prediction performance in terms of performance parameters (RMSE (125.84 W/m^2), MAPE (82.69%), MAD (98.61)) when compared with ARIMA, RBFNN and other techniques (Y. Li, Su, & Shu, 2014).

An Autoregressive with Exogenous Input based Statistical model (ARX-ST) was proposed to enhance the prediction accuracy of solar PV power production. The proposed models utilize both local and geographically correlated information of solar PV production from other sites. From simulation results, the suggested time scales for the ST forecast are at 1-h and 2-h ahead by using the actual solar data. For 1-h ahead, the MAE of the ST model is 50.79%, 41.8%, and 5.15% lower than the PSS, BPNN, and AR models, respectively. For 2-h ahead, the MAE of the ST model is 60.2%, 47.27%, and 8.09% lower than the PSS, BPNN, and AR model, respectively (C. Yang et al., 2015).

(b) ***CARDS model***

A coupled autoregressive and dynamical system model was developed by Jing for hourly and intra-hourly forecasting of solar irradiance. Lucheroni presented a model for the power market, which exploits the simultaneous presence of Hopf critical point and noise in a two-dimensional non-autonomous stochastic differential equation system for log-price and derivative of log-price (J. Huang, Korolkiewicz, Agrawal, & Boland, 2013). The equation for the dynamic system part, based on the Lucheroni model, is given as:

$$\dot{R} = z \tag{2.6}$$

$$\varepsilon \dot{Z} = k(z + R) - \lambda(3R^2 z + R^3) - \varepsilon z - \gamma R - b + \zeta \tag{2.7}$$

Where k, ε, γ, λ are the adjustable parameters and $\zeta$is the noise term. In the above equation, $\dot{R}$ is the first and, z is the second derivative of R. For de-seasoned solar radiation time series R_t, the following version of the model is used.

$$R_{t+1} = R_t + z_t \Delta_t + \omega_t \tag{2.8}$$

$$z_{t+1} = z_t + [k\big(z_t + R_{t)-} \lambda(3R_t^2 z_t + R_t^3) - \varepsilon z_t - \gamma R_t - b\big].\frac{\Delta_t}{\varepsilon} + a_t \tag{2.9}$$

Where ω_t and a_t are noise terms. The ordinary least square method is used to estimate the other parameters. Fourier series was used to perform de-seasoning. Autoregressive

process can not model the residual series individually, formed by subtracting the fourier series component from the original series. The reason is less efficiency of the AR process to reach the highest values in the series at mean reversion. Hence a resonating model was introduced by Luncheroni (Lucheroni, 2009) with a proxy for curvature, which provides much superior fitting to this residual series. After comparing the results of the CARDS model with Kostylev and Pavlovsk from their literature survey (Kostylev & Pavlovski, 2011), the best performing model for mostly clear days had 17% rRMSE and 32% for mostly cloudy, whereas it was 16.5% for all days for the CARDS model.

Huang et al. (J. Huang et al., 2013) developed a combination of AR and dynamical system model for 1-h ahead forecasting of global solar radiation in Mildura Town located in Australia. The forecasting ability of a mixture of AR and Luncheroni model were identified. The proposed model was analyzed using median absolute percentage error (MeAPE), MBE, Kolmogrov-Smirnov test integral (KSI), and NRMSE. The analysis showed that the combined model outperforms the other models, hence selected as the model that was upgraded by including added components, which led to the development of CARDS models. The error analysis shows that the CARDS model has successfully decreased forecasting error MeAPE in the combined model by 33.4%.

2.5.2.2 Regression method

This method is used to develop a connection between a dependent variable and an explanatory variable. Explanatory variables are required to determine the dependent variable. For example, solar irradiation forecast is the dependent variable, and climatic variable is the explanatory variable.

Behrooz et al. (Keshtegar, Mert, & Kisi, 2018) investigated the accuracy of different regression methods such as RSM, MARS, M5 model tree, and Kriging method for modeling of solar radiation in Adana and Antakya, Turkey. The best MARS model was

better than the best Kriging model for solar radiation in the Adana station. In Antakya, Kriging was best compared to all other three methods in terms of RMSE, d, NSE statistics. Model accuracies for estimating solar radiation were improved by including the periodic component in input variables. The conclusion was that the Kriging method was found superior for the modeling of solar radiation than other heuristic techniques such as RSM, MARS, and M5model tree.

Two models, simple and multiple linear regression models, were used for PV power generation forecasting. The regression model with two inputs proved to be better than with only one input. Therefore, the requirement for a large number of explanatory variables and a mathematical model is the limitation for this method (Oudjana, Hellal, & Mahamed, 2012).

Guochang Wang et al. (G. Wang, Su, & Shu, 2016) developed a regularized partial functional linear regression model (PFLRM) for one day ahead forecasting of PV power output. The results showed improved forecasting performance by generating the lowest RMSE (63.1742), MAD (35.0702), and MAPE (0.0886). MAPE of regularized PFLRM is 11.34% when compared with 20.92% in the multi-linear regression model (MLR) and 63.88% in RBFNN.

A multi-linear adaptive regression spline was developed to predict the day-ahead power output of a PV plant in Germany by using NWP and past historical data as inputs. The forecasted power output has a high correlation with the measured value of 0.706 and relatively low errors (RMSE of 177.8KW, MAE of 125.9KW) despite the low number of features and training samples. More accurate results can be obtained by increasing the temporal resolution in the near future (Massidda & Marrocu, 2017).

Juan R Trapero (Trapero, Kourentzes, & Martin, 2015) developed a dynamic harmonic regression model in the state space framework for short-term forecasting (1-24 h) of solar irradiation, illustrated by hourly aggregated time series of GHI and DNI. The DHR dynamic harmonic regression achieved the lowest RMSE of 30% and 47% for GHI and DNI, respectively, in comparison to naïve, ETS, and ARIMA models.

LASSO (least absolute shrinkage and selection operator) was developed for 5-min solar irradiation forecasting by collecting irradiance time series data at every one second from a monitoring network in Oahu, Hawaii. The proposed model showed better results compared to univariate models, especially with few training data and many predictors (D. Yang, Ye, Lim, & Dong, 2015).

An ensemble model was proposed having a combination of Multi-linear Regression (MLR), NN, boosting, and random forecast (RF) for the day ahead and week ahead prediction of PV output power. The results showed improvement in forecasting accuracy with the smallest RMSE of 1.00% and 4.42% for the day ahead and weak ahead forecast, respectively. The forecasting accuracy decreases with the increase of horizon. The problem of ramping up and down was managed by enhancing the sampling rate of historical measurement data (Guo et al., 2016).

2.5.2.3 Regression trees (RTs)

Regression trees are used mainly in machine learning, automatic learning, and data mining. In these trees, the target variables are represented by the leaves, and branch lines represent the input layer combinations. Regression tree (RT) learning methods are dependent on decision trees as a model for prediction. Decisions trees are not for decision purpose; they only represent data. The tree performance is validated by extrapolating its results to the test data set. There are certain types of classic RT methods, such as: boosted

regression trees and bagged regression trees. Boosted and bagged RTs are used for the improvement of classical RTs (Voyant et al., 2018).

(a) ***Boosting***

In boosted RT, there is a successive building of trees. It converts a combination of weak trees into powerful committees (Voyant et al., 2017). An additional coefficient is used to represent the weight of trees used for prediction improvement. The prediction is performed by the weighted linear combination of the trees (Voyant et al., 2018). A quantile gradient boosting method, combined with NWP utilizing principal component analysis (PCA), was used for day-ahead hourly forecasting of solar irradiance. The proposed model developed 41% and 39% reduction in MAE and RMSE as compared to the NWP model (Verbois, Rusydi, & Thiery, 2018). The gradient boosted regression trees (GBRT) proved to be an attractive method and showed comparable results in terms of RMSE with other conventional forecasting techniques on all forecasting horizons (1 to 6 h) for multi-site prediction of solar power generation (Persson, Bacher, Shiga, & Madsen, 2017). Jing Huang proved that the combination of gradient boosting and k-nearest neighbors regression were accurate for probabilistic forecasting of solar power for Global Energy Forecasting Competition 2014 (J. Huang & Perry, 2016).

(b) ***Bagging***

In bagged RT, there is no dependency on earlier trees, and the bootstrap sampling method is utilized to construct each node. Decisions from the majority of nodes is used as the prediction. Cyril voyant et al. used RT methods (normal, pruned, boosted, and bagged) for GHI prediction (1 h to 6 h) and estimated good prediction bands for Ajaccio (France) with a mean interval length (MIL) of 113Wh/m^2, 70% prediction interval coverage probability (PCIP) and lower (0.9) gamma index value (Voyant et al., 2018).

(c) ***Random forests***

Random forests put an extra layer of randomness to bagging. The growth of each regression tree is different, although there are equally divided samples from the given data. Random forests enhance the robustness of the model and diminish the over-training risks (Fouilloy et al., 2018). The main points of random forests are; 1) random feature selection, 2) bootstrap sampling, 3) out-of-bag (OOB) error estimation, and 4) full depth decision tree growing (Ahmad, Mourshed, & Rezgui, 2018). Random forest approach and bagged regression tree were proved best among eleven models for high weather variability in solar irradiation forecasting for a time horizon of (1 to 6 h) (Fouilloy et al., 2018). L Benali et al. (Benali, Notton, Fouilloy, Voyant, & Dizene, 2019) found that the RF method is the most efficient in comparison with smart persistence and ANN method, with an nRMSE from 19.65% for h + 1 to 27.78% for h + 6 for GHI; an nRMSE from 34.11% for h +1 to 49.08% for h + 6 for BNI; an nRMSE from 35.08% for h + 1 to 49.14% for h + 6 for the hourly prediction of solar irradiation. Random forests were used along with the firefly algorithm for the prediction of hourly global solar radiation and showed minimum RMSE, MAPE, MBE of 18.98%, 6.38%, 2.86%, respectively (Ibrahim & Khatib, 2017).

2.5.3 Summary of mathematical techniques

Mathematical techniques have been used for solar irradiation forecasting of linear systems and data patterns. The persistence model is used as a benchmark to assess the performance of other models. ARMA requires stationary time series (Diagne et al., 2013) and is able to handle nonlinear systems to a certain extent (Hamilton, 1994). ARMAX is also an extended version of ARMA using meteorological variables as an exogenous input (Y. Li et al., 2014). Regression trees have been used widely for boosting and bagging purpose in some articles. Boosting and bagging phenomena are used to enhance the performance of classical regression trees (Persson et al., 2017; Voyant et al., 2018).

The forecasting accuracy of these techniques, however, decreases with the increase in forecasting horizon. Therefore, these techniques are suitable for short-term forecasting horizons (Guo et al., 2016; Reikard, 2009).

2.6 Machine learning techniques

These techniques have four main types, Artificial neural networks (ANN), Support vector machine (SVM), Extreme learning machine (ELM), and deep learning techniques. A comprehensive discussion is given below for all these three techniques.

2.6.1 Artificial neural networks (ANNs)

The limitation of statistical techniques in dealing with non-linearity data due to weather variation had led to the application of Artificial Neural Networks (ANNs) in forecasting PV power output. ANNs have three main parts, the input layer, hidden layer, and output layers. The input layer takes the input information. The hidden layer analyzes the input information and consists of several layers. The output layer gives the output after acquiring analyzed information from the hidden layer (Das et al., 2018). Radial basis function, sigmoid and hyperbolic tangent sigmoid functions are commonly used for forecasting PV power output. The ANN model can be expressed as

$$U_N = b + \sum_{j=1}^{N} (W_j \times I_j) \tag{2.10}$$

Where U_N, W_j, I_j, b, N are the final network output, connection weight, input number, bias weight, and a number of inputs, respectively.

Several different architectures of ANNs has been reviewed in literature to solve complex systems, such as multilayer feedforward neural network (MLFFNN), multilayer perceptron neural network (MLPNN), Radial basis function neural network (RBFNN), recurrent neural network (RNN), general regression NN (GRNN) and adaptive neuro-

fuzzy inference systems (ANFIS) (Chen, Duan, Cai, & Liu, 2011; Das et al., 2018; Ghofrani, Ghayekhloo, & Azimi, 2016; Mellit & Pavan, 2010; A. Yona et al., 2013). Figure 2.5 shows the schematic of ANN architecture, and Figure 2.6 describes its equivalent model.

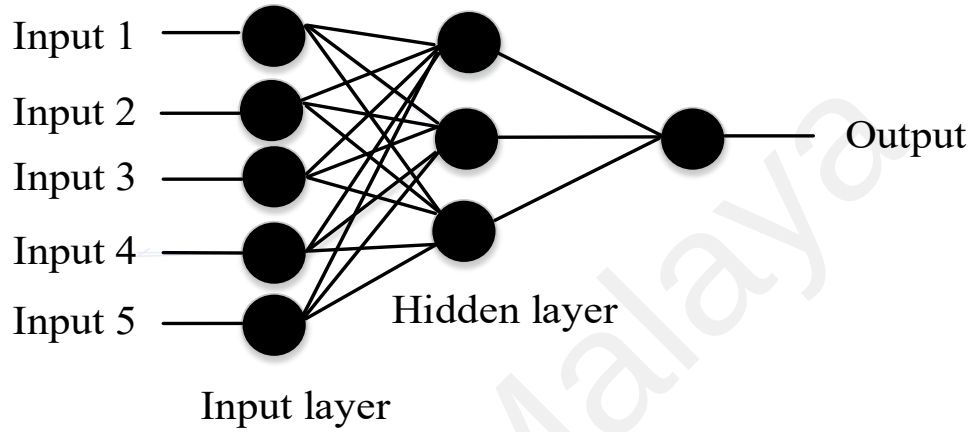

Figure 2.5: Schematic of ANN structure

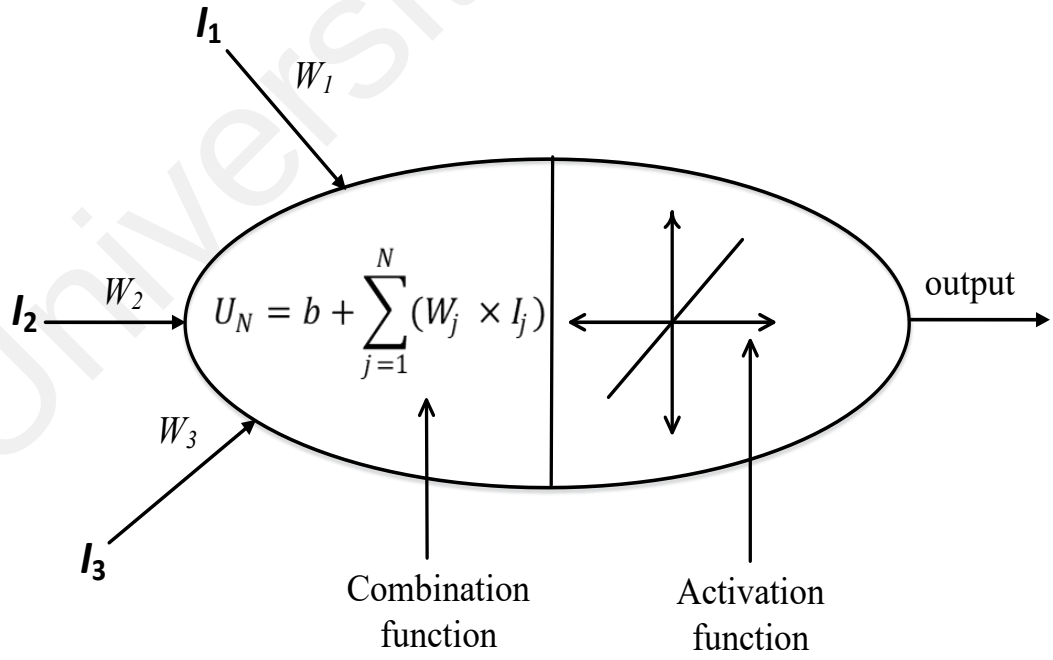

Figure 2.6: An ANN model

2.6.1.1 Multilayer feedforward neural network (MLFFNN)

MLFFNN is a supervised feedforward ANN which consists of more than one hidden layer. Its architecture is less complex because the information does not travel via a feedback path. The information takes the straight path only from input to output layer. The selection of hidden layers is dependent on the complexity of the problem (Das et al., 2018). Three multilayer FFNN techniques with BP were developed for designing a model forecaster to forecast the daily average solar radiation in five different cities in Kuwait. ANN1 (gradient descent method) and ANN2 (LM algorithm) with MAPE of 86.3 and 85.6 were proven to be more feasible for prediction purposes as compared to ANN3 having MAPE of 94.75 (Bou-Rabee et al., 2017).

Mellit et al. developed a comprehensive comparison of three ANN techniques (AFFNN, RBNN, DRNN) for the short-term hourly prediction of power production in a large-scale grid-connected photovoltaic plant (LS-GCPV). They concluded that the performance of the AFFNN (sunny, overcast) model is best, with the lowest MAPE (1.92%) and highest R (0.9986) compared to RBFNN and DRNN (Mellit, Pavan, & Lughi, 2014). A MLFFNN based on a backpropagation algorithm produced less MAPE (5.9%) for a day before forecasting compared to MAPE (7.6%) for a day after forecasting of global horizontal solar irradiation (Chiteka & Enweremadu, 2016).

ANFIS is used to forecast nonlinear values, in which previous sample information is used to forecast the sample in advance (Yun et al., 2008). It has a wide area of application among fuzzy systems because of robust results, less expensive, and transparency. Its performance can be enhanced by proper tuning of the membership function (Diagne et al., 2013).

2.6.1.2 Multilayer perceptron (MLP) neural network

MLP is a branch of FFNN. Among the three layers of nodes (input, output, hidden), each node except the input node is a neuron that uses a nonlinear activation function. It differentiates from linear perceptron due to its multilayer structure and nonlinear activation function. Adel Mellit et al. (Mellit & Pavan, 2010) used the MLPNN technique for 24 hours ahead forecasting of solar irradiance and showed a good correlation coefficient of 98-99% for sunny days and 94-96% for cloudy days.

A methodology was developed for the daily prediction of global solar radiation on a horizontal surface by using a Multi-layer Perceptron (MLP) neural network and an ad-hoc time series preprocessing. The proposed approach has reduced forecasting error to 6% compared to Markov chains or Bayesian inference. Validation of the proposed prediction methodology was done using six other prediction methods. The cumulated DC PV energy for a 6-month period showed remarkable similarity between simulated and measured data ($R^2 > 0.99$ and nRMSE < 2% on 1.175 kW mono-Si PV power grid (Paoli, Voyant, Muselli, & Nivet, 2010).

A MLPNN along with a clustering (T.S.C.K) algorithm was analyzed for hourly forecasting of global horizontal solar irradiation (GHI) and direct normal irradiance for different time horizons (1h, 24h, 48h). In a case study, the proposed method developed more accurate solar forecasting for a 1h horizon, with lower RMSE and MAE compared to 24h and 48h time horizons (Ghofrani et al., 2016).

2.6.1.3 Radial basis function neural network (RBFNN)

RBFNN uses radial basis function as an activation function. RBFNN is a bilayer NN. There are two stages of the learning process based on synaptic weight (Gupta, Jin, & Homma, 2004). RBFNN has achieved a good performance accuracy, with more computational speed for learning, less computing power, and time (Mandal, Madhira,

Meng, & Pineda, 2012). Structural simplicity and universal approximation property are the main reasons for this technique (Atsushi Yona et al., 2007). It is strictly limited to exactly one hidden layer called feature selection. RBFNN was used for a 24-h ahead forecasting of power generation in an experimental system using input parameters such as daily air temperature, mean daily wind speed, pressure, mean daily relative humidity, mean daily solar irradiance, and mean daily power output of the system. RBFNN was found suitable for sunny and cloudy days with a very high correlation coefficient (sunny (99.39%), cloudy (99.48%)) and very low MAPE (sunny (8.29%), cloudy (8.89%) (Chen et al., 2011). In (Atsushi Yona et al., 2007), RBFNN outperformed the result of FFNN in some months for 24 hours - ahead forecasting for PV system power output based on insolation prediction.

2.6.1.4 Recurrent neural network (RNN)

It is a type of neural network in which a directed graph is constructed based on the connection between nodes. It is utilized in specific tasks such as un-segmented data and speech recognition due to its ability to use internal memory. Different complex structures and computational relationships are learned well by RNN. It is mainly deliberated for time series forecasting (Das et al., 2018). In (Atsushi Yona et al., 2007), RNN outperformed the result of FFNN in some months for 24 hours-ahead forecasting of PV power output and is validated by simulation. The RNN method proposed by Yona (A. Yona et al., 2013) showed minimum MAE (0.1567KW) compared to FFNN for 24 hours ahead forecasting using weather data, fuzzy theory, and neural network.

Mashud Rana (Rana, Chandra, & Agelidis, 2016) presented a Cooperative Neuro-evolutionary RNN technique for half an hour ahead forecasting of PV power output. The advantage of using this approach is to create an ability to predict the PV power output directly compared to other techniques where solar irradiance is first predicted and then

converted to power output. The proposed technique has (0.40-35.18)% accuracy enhancement over the other three baseline models. Multivariate models also showed better forecasting results (MRE: 7.33%) than univariate models (MRE: 7.45%). R-DNN was proved best in electricity load forecasting in comparison with FF-DNN. Both techniques showed less MAPE, RMSE for the day ahead compared to a week ahead forecasting horizon (Din & Marnerides, 2017). Table 2.2 describes the summary of different ANN techniques used in recent literature based on different forecasting horizons together with their advantages and disadvantages.

2.6.2 Support vector machine (SVM)

SVM is a supervised learning technique in the field of machine learning theory and structural risk minimization. It is used to enhance its generalization capability by reducing the empirical risk and confidence interval of the learning machine (Quej, Almorox, Arnaldo, & Saito, 2017). Support vector machine (SVM) has a fundamental principle of applying nonlinear data mapping in some spaces and linear mapping in future space.

Another method, which is developed to deal with different regression problems, is known as support vector regression (SVR). It is based on statistical learning theory and the structural risk minimization (SRM) method (Gorunescu, 2011). The kernel functions are key features of SVM, which maps data into higher dimensional space. The nonlinear kernel function is defined as:

$$k = \exp\left(-{}^{1}/_{\sigma^2}\ \left\|X - X_i^2\right\|\right) \tag{2.11}$$

Where X and X_i are the vectors in input space and the vector of features computed from training or test samples, respectively. The targets in higher dimensional space show resemblance with the targets of similar or lower dimensional input space (Hossain, Mekhilef, & Olatomiwa, 2017).

Table 2.2: Summary of ANN methods

Ref	Forecast horizon	Methods	Advantages	Disadvantages	Input variables
(Theocharides et al., 2020)	Hourly Day ahead	ANN (K-means clustering)	MAPE value of 4.7% and 6.7% for hot and cold semi-arid climate condition	Increased complexity	Global irradiance, ambient temperature, relative humidity, wind direction and speed, azimuth and elevation angles
(Ozoegwu, 2019)	Month up to 2 years	ANN	Improves the forecasting accuracy to 0.96 and 0.98	-	Sunshine, temperature, cloudiness, precipitation, relative humidity, dewpoint and soil temperatures, evaporation, and pressure
(Bugała et al., 2018)	Hourly, a day ahead	ANN	Quality test (93%) and RMSE of 0.02%	-	A number of sunny hours, length of the day, air pressure, maximum air temperature, daily insolation, and cloudiness.
(Din & Marnerides, 2017)	Days and weeks ahead	FF-DNN	Reduced MAPE (0.067) as compared with RNN in the frequency domain	Complexity increased due to the use of the TF procedure	Date, hour, Elec Price, Dry Bulb, DEW point, SYS load
(Leva, Dolara, Grimaccia, Mussetta, & Ogliari, 2017)	24-ahead	ANN, MLPNN, training procedure is EBPNN	Less WMAE, RMSE, and NMAE for a sunny day	Forecasting reliability and accuracy are affected by critical samples values of a training data set	The weather forecast, power & irradiance measurements, historical data sets
(Ghofrani et al., 2016)	Multiple cases(1h,26 h, 51 h) ahead	MLPNN+ feature selection method	1. Reduce the number of neural net inputs by 70%. 2. Training MSE(1.509) and testing MSE(1.1531) for multivariable forecaster	A little increase in MSE for a multivariable forecaster as compared single variable forecaster	Solar radiation, wind speed, wind direction, relative humidity, air temperature

Table 2.2 (continued)

Ref	Forecast horizon	Methods	Advantages	Disadvantages	Input variables
(Renno, Petito, & Gatto, 2016)	Daily GR and hourly DNI	Two MLPNN methods	GR has MAPE(4.57%), RMSE(160.3Wh/m^2), and R^2(0.9918), hourly DNI has the MAPE, RMSE, and R2 values of 5.57%, 17.7 W/m^2 and 0.994	Comparative to some other methods in other studies	Meteorological, astronomical parameters as inputs for prediction by GR, while DNI used astronomical for target site
(Chiteka & Enweremadu, 2016)	Day-ahead and day before	MLFFNN based on BP algorithm	R^2(99.894%), RMSE (0.223KW/m^2/day), MAE (0.17KW/m^2/day), MAPE(2.56%)	Increased complexity	Latitudes, longitudes and altitudes, humidity, pressure, clearness index, average temperature
(Rawat et al., 2014)	Multiple cases(1h,26h, 51 h) ahead	MLPNN+ feature selection method	1. reduce the number of neural net inputs by 70%. 2. Training MSE(1.509) and testing MSE(1.1531) for multivariable forecaster.	A little increase in MSE for a multivariable forecaster compared to a single variable forecaster.	Solar radiation, wind speed, wind direction, relative humidity, air temperature.
(J. Wu & Chan, 2013)	hourly	TDNN +clustering algorithm	Lowest RMSE (122W/m^2) in comparison with TDNN and ARMA.	Increased complexity	Solar radiation data

A model based on SVM was developed for an intra-day (15-300 minutes) power forecasting. The findings showed that the proposed SVM model produced better forecasting accuracy, with the lowest [RMSE (10.8661), MRE (9.9677%)] and highest R^2 (0.9104) than NAR and ANN. But the prediction during the presence of medium clouds was found to be difficult. RMSE and MAE ranges are 5.7367-24.7855 and 5.2825%-26.6654% for time horizons of 15min and 300 min, respectively. This means that forecasting accuracy decreases with the increase of time horizon (H. S. Jang et al., 2016).

Three strategies were evaluated for one day ahead forecast of PV power generation. Strategy 3 (principal component analysis) was found best with 10.24 KWH RMSE, which is 2.7% lower than the one achieved with strategy 1. Strategy 2 had the worst performance with RMSE of 11.16 kWh. It was deduced that the use of the principal component analysis technique along with feasible forecasting strategies increases the forecasting accuracy by having a low RMSE (Junior et al., 2014). Support vector regression SVR with PV power measurements, NWPs, and cloud motion vectors irradiation forecasts (CMV) were analyzed for PV power forecasting based on RMSE for 15 min to 5 h ahead forecast horizons. SVR based on PV measurements has shown better accuracy for a 1h ahead forecast. NWP based predictions were better for a horizon greater than 3h. The combined model was better than all models for all forecast horizons (Wolff et al., 2016). A summary on SVM methods for various forecasting horizons is given in Table 2.3.

2.6.3 Extreme learning machine (ELM)

Extreme learning machine has a property of simple training and anti-jamming (Tang et al., 2016). The training algorithms of the neural network slows down the learning speed of FFNN. To increase the computation speed, an extreme learning machine was developed by Huang (G.-B. Huang, Zhu, & Siew, 2004). The selection procedure of ELM

Table 2.3: Summary of SVM methods

Ref	Methods	Forecast horizon	Advantages	Disadvantages	Input parameters
(Ağbulut, Gürel, & Biçen, 2021)	SVM, KNN	daily	R^2 varies between 85.5% and 93.6%	-	daily minimum and maximum ambient temperature, cloud cover, daily extraterrestrial solar radiation, day length, and solar radiation
(Belaid, Mellit, Boualit, & Zaiani, 2020)	SVM	an hour ahead	Lowest RMSE(60.42Wh/m^2)	Monthly developed models are inferior to annual models	temperature, relative humidity, wind speed, pressure, and global solar radiation
(Guermoui, Rabehi, Gairaa, & Benkaciali, 2018)	SVM	daily	RMSE, rRMSE, and (R^2), of 1.59 (MJ/m2), 8.46 and 97,4% respectively	Only one input parameter is considered	Sunshine ratio
(Quej et al., 2017)	ANFIS, ANN, SVM	Daily	SVM better than ANN having lowest RMSE(2.523MJ/m^2/d), MAE(1.76MJ/m^2/d), R^2(0.719)	Low value of R^2 with abundance rainfall or cloudiness	Daily air temperature, extraterrestrial solar radiation, rainfall, precipitation
(Lauret, Voyant, Soubdhan, David, & Poggi, 2015)	Neural networks, SVM	Hour ahead	Have rMAE (26.15%) as compared with persistence model	2% rRMSE for unstable sky conditions	Pat measured GHI values

for hidden nodes is random and determines the output weights of SLFNs. A brief discussion of ELM structure is given as follows. For N arbitrary distinct samples ($\boldsymbol{x}_i$, $\boldsymbol{t}_i$), $\boldsymbol{x}_i = [x_{i1}, x_{i2} \dots \dots . x_{in}]^{\mathrm{T}} \in \boldsymbol{R}^n$ and $\boldsymbol{t}_i = [t_{i1}, t_{i2} \dots \dots . t_{in}]^T \in \mathbf{R}^{\mathrm{m}}$, a standard SLFN with L hidden neurons and activation functions, $g(x)$ can be modeled mathematically as shown in Eq (2.12). Figure 2.7 shows the structure of ELM.

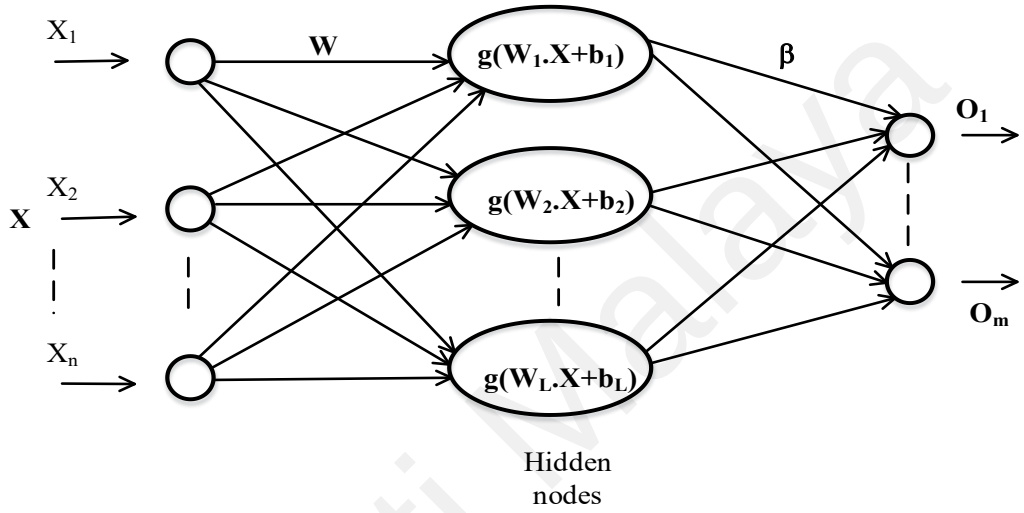

Figure 2.7: Structure of an ELM network

$$o_i = \sum_{j=1}^{L} \beta_j \, g\left(w_j . X_i + b_j\right) \qquad \text{For } i = [1 \dots \dots \dots . N] \tag{2.12}$$

Where $\boldsymbol{w}_i = [w_{i1}, w_{i2} \dots \dots . w]^T$ is a weight vector connecting the j^{th} hidden node and input nodes, and $\boldsymbol{\beta}_i = \left[\beta_{i1}, \beta_{i2} \dots \dots . \beta_{in}\right]^{\mathrm{T}}$ is a weight vector connecting the j^{th} hidden node and output nodes, $w_j . X_i$ is the inner product of w_j and X_i, while b_j is the threshold of the j^{th} hidden node. For the standard SLFN, we can approximate those N samples with zero error. Thus, there exist β_j, w_j, b_j that satisfies (Z. Li, Zang, Zeng, Yu, & Li, 2015)

$$\sum_{i=1}^{N} \left\| \sum_{j=1}^{L} \beta_j \, g\left(w_j . X_i + b_j\right) - t_i \right\| = \sum_{i=1}^{N} \| \, o_i - t_i \| \; = 0 \tag{2.13}$$

The compact form of the equation (2.13) can be written as (2.14)

$$\boldsymbol{H\beta} = 1 \tag{2.14}$$

Where $\boldsymbol{\beta} = [\beta_1^T + \beta_2^T \ldots\ldots\ldots \beta_L^T]_{L\times M}$ and $\boldsymbol{T} = [t_1^T + t_2^T \ldots\ldots\ldots t_L^T]_{N\times M}$ and the hidden layer output matrix H (G.-B. Huang, Zhu, & Siew, 2006) is defined as

$$H = \begin{bmatrix} g(w_1.X_1 + b_1) & \cdots & g(w_L.X_1 + b_L) \\ \vdots & \ldots & \vdots \\ g(w_1.X_N + b_1) & \cdots & g(w_L.X_N + b_L) \end{bmatrix}_{N\times L} \tag{2.15}$$

After the input weights β_j and biases are assigned randomly; the output vector $\boldsymbol{\beta}$ can be calculated by the following equation:

$$\boldsymbol{\beta = H^{-1}T} \tag{2.16}$$

$\boldsymbol{H^{-1}}$ is called Moore-Penrose inverse of matrix $\boldsymbol{H}$. The entropy and ELM methods were combined for 1-hour and 2-hours ahead forecasting of PV power generation. The data results showed that the proposed method has less MAPE (2.5538%), less CPU time (14.1337 ms), and a higher value of R^2 (0.99929), which indicated that the proposed method has high convergence speed, fewer setting parameters, and high forecast accuracy, when compared with GRNN and RBFNN, but have a slight difference in R^2 value with RBFNN (Tang et al., 2016).

The ELM model was proposed for the prediction of global solar radiation for several sites in Australia. Training of the proposed algorithm was performed for 26 sites, and validation is done for 15 sites. The proposed ELM model had shown lower RMSE (3.715–7.19%) than random forest (RF), M5Tree, and MARS methods. The proposed model had practical significance for energy modeling at the national level using satellite data (Deo, Şahin, Adamowski, & Mi, 2019).

2.6.4 Deep learning

Deep learning has the ability to extract deep features from PV power output and provide better forecasting results in comparison with persistence, physical and statistical

models. With the development of artificial intelligence (AI) methods, deep learning models have been applied in certain areas to overcome the deficiencies of conventional neural networks and other machine learning techniques (H. Wang et al., 2019; Youssef et al., 2017). Deep learning is also an advanced type of machine learning method. Convolutional neural networks (CNN) (Zang et al., 2018) and Recurrent neural networks (RNN) (Shi et al., 2017; A. Yona et al., 2013) are deep learning models used for forecasting PV power.

A grey theory-based deep belief network proposed for a day ahead forecasting of PV power output in (Chang & Lu, 2018) showed better forecasting accuracy and computational efficiency compared to RBFNN, BPNN, and ARIMA methods. F Wang et al. (F. Wang et al., 2020) have developed a time correlation modification method to enhance the accuracy of the deep learning model for a day ahead PV power forecasting in comparison with the conventional deep learning method.

An algorithm is proposed based on the LSTM network for day-ahead power output forecasting using provided data from local meteorological authorities (Qing & Niu, 2018). It has shown 18.34% more forecasting accuracy than BPNN, LR, and persistence methods for the half-year testing data set. The proposed method has also presented 42.9% higher RMSE skill than other methods for a testing data set of 1 year. G Narvaez et al. have performed PV power prediction on a daily and weekly basis using the deep learning method. The results showed that the proposed method had performed 38% better than other methods based on site adaptation (Narvaez et al., 2021).

A deep learning method (LSTM) was proposed for the day ahead solar energy forecasting and showed an average forecast skill of 52.2% compared to the persistence method (Srivastava & Lessmann, 2018). The LSTM model revealed 21% RMSE skill

score compared to 12% and 7% RMSE skill score of CNN and MLP network, respectively, for a 1- min ahead prediction of PV power (Zhang et al., 2018).

Lulu Wen et al. proposed a deep learning approach for 1-h ahead prediction of solar power output. It has given better prediction results than MLP and SVM methods. In the end, the PSO algorithm was also used for load dispatch optimization (Wen, Zhou, Yang, & Lu, 2019). The LSTM method proposed in Canada has shown the lowest RMSE (0.086) and MBE (0.004) compared to SVR and FFNN methods for solar power prediction (Alzahrani et al., 2017).

2.6.5 Summary of machine learning techniques

Machine learning techniques (ANN, SVM, ELM) are being widely used nowadays in solar power generation forecasting to achieve the best forecasting accuracy based on performance parameters such as RMSE, MAPE, MABE, R, and R^2. These techniques can deal with non-stationary data patterns. Through effective training, ANN is popular in dealing with nonlinear systems because they are more robust and have strong inference capabilities. However, the reliability of the system is affected by the random initial data, local minima, and over-fitting. Large data is required during the training stage, and due to its multi-layered structure, the system complexity also increased (De Giorgi et al., 2016; Dolara et al., 2015; Mellit et al., 2009).

SVM is a modern and reliable tool used in nonlinear systems for both solar and wind forecasting. SVM has no local minima problem and is able to learn without much dependence on prior knowledge, unlike ANN (Voyant et al., 2017). It can also simplify complex mathematical issues (Mojumder, Ong, Chong, & Shamshirband, 2016). But SVM is highly dependent on parameters such as tube radius (ε), kernel function parameter, and penalty factor (C).

Therefore, proper selection of these parameters is mandatory, which is a difficult task (Das et al., 2018). In ELM, input weights and hidden node biases are selected randomly using the linear regression method (Tang et al., 2016).

To overcome the deficiencies of conventional ANN and machine learning techniques (SVM, ELM), the trend is shifting towards the use of deep learning techniques for solar power output forecasting. Deep learning has the ability to get in-depth features from PV power output and provide better forecasting results in comparison with persistence, physical and statistical models. Based on the analysis of machine learning techniques for different forecasting horizons, it becomes clear that forecasting accuracy decreases with an increase in forecasting horizon. These techniques provide better forecasting accuracy for short and medium-term forecasting horizon instead of long-term forecasting horizon (Chiteka & Enweremadu, 2016; Ghofrani et al., 2016; H. S. Jang et al., 2016; Wolff et al., 2016).

2.7 Hybrid methods

Hybrid methods are a combination of two or more methods together with some optimization theorem. This combination increases the overall forecasting accuracy of the hybrid method by incorporating the benefits of individual techniques. From a detailed review, it can be observed that in most cases, a single technique or method is not enough to fulfill the demand for better PV forecasting accuracy and system reliability. Several methods were combined to improve the forecasting accuracy of the PV system and showed better results in comparison with the use of a single method (Dolara et al., 2015).

The advantages of the hybrid system include the positive points of both methods, excluding their limitations. As a result, the PV forecasting accuracy is enhanced compared to a single method. However, the combination of two or more methods increases the computational complexity of the hybrid systems. Particular issues that need

to be observed include cost, space, structural maintenance, robustness, reliability for the proper running of systems, and improvement to the PV forecasting accuracy. Another reason is that the performance of the hybrid model is totally dependent on the performance of the individual models. In a mix of two or more methods, if one method has inferior performance, then it will also lower the overall efficiency of the complete hybrid systems (Das et al., 2018). Therefore, a trade-off exists between the limitations and benefits of a hybrid in improving its forecasting accuracy.

Hybrid methods also have the capability to improve the performance of complex systems by addressing individual issues and using a combination of best-suited techniques. A number of combinations have been used as hybrid methods by different researchers. These combinations are 1). GAs and ANNs, 2). Fuzzy and ANNs, 3). ANFIS, 4). ANNs and physical model, 5). ANNs and ARMA 6). Wavelets and ANNs, 7). ANN and Optimization algorithms, 8). LSTM and Optimization algorithms, 9). WT and SVM, 9). SVM and Optimization algorithms, 10). SARIMA and SVM (Das et al., 2018; dos Santos, Escobedo, Teramoto, & da Silva, 2016; Mellit et al., 2009; Raza & Khosravi, 2015). These hybrid combinations are reviewed in detail as follows.

2.7.1 Genetic algorithms and artificial neural networks

A genetic algorithm (GA) is developed as a computer-based technique for search and optimization purposes based on natural genetics and natural selection. By using stochastic and non-deterministic operators, GA will generate optimal solution at each iteration of the population. This is the reason for its higher efficiency than other optimization algorithms in searching discontinuous and nonlinear spaces. The genetic operations are crossover, reproduction, and mutation. Among ANN, most of its applications are in FFNN along with the back propagation (BP) algorithm. The main advantage of FFNN is that it does not require a user-specified problem-solving algorithm (Mellit, Kalogirou, &

Drif, 2010). GA-ANN showed better results than other forecasting models in comparison with five techniques for 1-hour and 2-hour ahead forecasting of the average power output for a 1MWp PV power plant in California without using any exogenous input such as solar irradiance telemetry; thus, the solar panels were the only sensor used to generate the input data. GA/ANN showed an improvement in forecasting with the lowest RMSE of 32.2% and 35.1% for 1 h and 2 h forecasting horizon, respectively, compared to ARIMA, KNN, and ANN methods. However, the gains are more expensive (H. T. Pedro & Coimbra, 2012). Forecasting accuracy has decreased with the increase of horizon.

A hybrid approach using GA for 1-hour ahead PV power output forecasting was reported in (Y.-K. Wu, Chen, & Abdul Rahman, 2014). The hybrid model showed higher forecasting accuracy by producing the lowest forecasting error of 5.64%, 3.43%, and 6.57% in comparison to other methods. However, there is still a need for additional and accurate data to monitor the prediction process for larger data variations of PV power output.

A GA-based neural network approach was proposed for a distributed photovoltaic forecasting method. The weights and thresholds for the BP neural network were optimized using GA, which enhances the forecasting accuracy by reducing error (Tao & Chen, 2014).

A genetic approach combined with the multi-model framework (GAMMF) for the prediction of solar radiation time series was proposed in (J. Wu, Chan, Zhang, Xiong, & Zhang, 2014). From the findings, the GAMMF model has shown better forecasting accuracy with a low SMAPE of 19.60 compared to ARMA, TDNN, and hybrid models. However, the SMAPE value was higher than ARMA only for the range of 35000-40000 Whm^2.

2.7.2 Fuzzy and artificial neural networks

Neuro-fuzzy computing is a combination of neural network recognizing patterns and fuzzy inference systems. A fuzzy system contains human knowledge and implements decision-making and differentiation. It is very beneficial to mix several methods to give a synergistic way instead of focusing on one method exclusively (Olatomiwa, Mekhilef, Shamshirband, & Petković, 2015). FIS does not need the information of the main physical process as a pre-condition for its operation.

H. T. Yang et al. proposed one day ahead hourly forecasting using a hybrid method (SOM+LVQ+SVM+FIS) for the prediction of PV power output based on one-year weather information collected from the Taiwan Weather Central Bureau (TWCB). The results showed better prediction accuracy (3.295% MRE and 350.2 RMSE (W)) for the proposed hybrid scheme as compared to ANN (5.412% MRE and 529.2 RMSE (W)) and SVR(4.017% MRE and 402.5 RMSE (W)) for weather types other than sunny days (similar performance), with worst results on typhoon days (August 3 and 4) (H.-T. Yang, Huang, Huang, & Pai, 2014).

2.7.3 Adaptive neuro-fuzzy inference system

ANFIS is a combination of FIS and BP neural network learning algorithms. It splits the previous knowledge into certain subsets to reduce the search space, and BP neural network is used to adjust the fuzzy parameters. It is similar to the fuzzy network with distributed parameters. Its structure consists of five layers named: fuzzy layer, product layer, normalized layer, de-fuzzy layer, and total output layer (Quej et al., 2017). The variables in the first layer are called premise variables. The output of the second layer is generated by combining with the output of the first layer. In the third layer, known as the ruler layer, every node finds the individual firing strength to the total firing strength. The

fourth layer normalizes the firing strengths. Finally, the fifth layer combines all the inputs from the de-fuzzy layer and converts fuzzy data into the final output.

Olatomiwa proposed an ANFIS model for the estimation or prediction of solar radiation in Iseyin, Nigeria. The parameters considered are maximum mean temperature, minimum mean temperature, and sunshine duration. Findings showed that the proposed model (ANFIS) had a coefficient of determination R^2 =0.8544 and RMSE=1.0854 in the training phase, while R^2=0.6567 and RMSE = 1.7585 in the testing phase. As a result, the ANFIS model proved to be the best technique compared to other empirical models based on R^2. The hybrid model developed the ability to learn for fuzzy systems (Olatomiwa, Mekhilef, Shamshirband, & Petković, 2015).

The proposed method, which combines the optimized multivariate regression model for sunny weather; bi-level model consisting of an optimized regression model and ANFIS for cloudy weather; outperformed the ANN, ANFIS, LSE-regression models, and LS-SVM, with an average MAPE of 8.56% and MAE of 10.22 in 24 hours ahead forecasting of solar irradiation. FPA outperformed other algorithms in tuning the model parameters and convergence time (Bigdeli, Borujeni, & Afshar, 2017).

2.7.4 Artificial neural networks and physical model

The physical hybridized neural network is a combination of ANN and a physical model, known as the clear sky solar radiation model (CSRM). CSRM is a theoretical model used to find the solar radiation with respect to the geographical coordinates of the specific site. The purpose of CSRM is to limit the maximum available daily solar radiation by computing the time duration between sunrise and sunset of each day. A hybrid model (PHANN) was proposed and compared with the conventional ANN for a day ahead forecasting of PV plant power output. Hybrid model PHANN was found to be more accurate by producing NRMSE of 13.4% compared to 17.4% for ANN. The ANN is a

statistical method that requires an appropriate size of the historical data set and a suitable choice of network parameters (Dolara et al., 2015).

Emanuele Ogliari et al. developed a model for a day-ahead hourly power prediction, known as Physical Hybrid Neural Network (PHANN), which is a combination of clear sky solar radiation algorithm (CSRM) and statistical ANN. The improvement in the results was noticeable, but there was a chance that even a properly trained network can produce wrong results due to the variation in the weather forecast. This issue was addressed in that research by; 1) the use of larger NN (having a larger number of neurons), 2) the inclusion of tolerance threshold in error assessment, and 3) the addition of correction factor to reduce the final error (Ogliari, Gandelli, Grimaccia, Leva, & Mussetta, 2016).

Ogliari, E compared physical and hybrid methods for one day ahead forecasting of PV output power, using actual data from the existing power plant in Milan, Italy. ANN hybridized with clear sky solar radiation provides the best forecasting results (NMAE 5.6%), compared to two deterministic models (NMAE 8.5% (three parameters)) vs NMAE 9.0% (five parameters)) (Ogliari et al., 2017).

2.7.5 Autoregressive moving average and ANNs

ARMA is a linear model and deals only with stationary data. In contrast, ANN is able to handle nonlinear models. Therefore, a mix of these two techniques combines the specialties of the two techniques. This combination is used to deal with the non-stationary time series with some preprocessing. Without pre-processing, it can be less beneficial for many non-stationary problems. The solution to this problem is to convert a non-stationary to stationary one (weak or strong if possible) and then model the remainder as a stationary process. Employing the meteorological forecasts of the ALADIN NWP model, a hybrid technique ARMA/ANN was used in the hourly forecasting of global radiation in five sites

in the Mediterranean. The proposed model: 1). improved the forecasting accuracy by reducing the nRMSE by 11.3% in comparison to other persistence model, 2). used confidence intervals to increase the reliability of forecasting, 3). make corrections for forecasting the future values of insolation (average nRMSE gain up to 1.7%), due to its ability to determine stationarity. However, the drawback of the proposed method is the increase in cost and complexity (Voyant et al., 2012).

Both ARMA and TDNN were used in a 10 minutes-ahead prediction phase for a specific day because ARMA is more sensitive and is used to forecast linear parts of series, while TDNN is less stable and is used to predict nonlinear component of series. The hybrid technique generated better prediction results by overcoming the drawbacks of individual schemes, especially the stationary time series requirement for ARMA (Ji & Chee, 2011).

R. Azimi et al. (Azimi et al., 2016) proposed a new hybrid technique having a combination of K-means algorithm (for clustering purpose) with a time series analysis and multilayer perceptron neural network (MLPNN) for forecasting of solar radiation, where the RMSE is varied from (58.5-93) W/m^2 for forecasting horizon of 1-3 days ahead.

2.7.6 Wavelets and ANNs

Wavelets are used to decompose the sample data sequence of solar radiations into various time-frequency domain components. RNN is used to forecast all domains, and a relatively better forecast is achieved by incorporating an algebraic sum. A wavelet recurrent neural network (WRNN) was proposed for 2 days ahead forecasting of solar radiation. The obtained simulation showed a very low mean square error compared to hybrid neural networks in previous studies (Capizzi, Napoli, & Bonanno, 2012).

A hybrid model (DA-GRBFN-EPSO-WD) was developed for forecasting PV generation output in Japan. The proposed method significantly had reduced errors in comparison with the conventional ANN (MLP, RBFN, GRBFN) and had a minor improvement over the hybrid model (DA-RBFN-PSO-WD) (Mori & Takahashi, 2012).

WT-DCNN hybrid model with quantile regression was used for forecasting PV power output. The average values of interval sharpness (IS) for the proposed approach were -5.04, -6.73, -11.65, and -21.84 for 30, 60, 90, and 120 minutes forecasting horizons, respectively. It was concluded that the sharpness of predicted quantiles goes worse with the increase of time horizon (H. Wang et al., 2017).

2.7.7 ANNs and optimization algorithms

An hour ahead forecasting of solar power output was executed for three simulated PV sites in the state of Florida, using a novel technique (BP-SFLA-ANN). The results showed that WMAPE for the first site was 8.8% in comparison to previous models (WMAPE = 9.57%) and classical ANN (WMAPE = 10.78%). To resolve the issue of a high computational burden by SFLA, BP was initially used to find the ANN parameters. The solutions were used as the initial values of optimization processes. It was concluded that the proposed model was able to produce more accurate prediction and faster convergence when BP was employed in the initial step to decide on the starting population of SFLA (Asrari, Wu, & Ramos, 2017).

WT-GRNN-PSO hybrid model was proposed for the solar forecast with bootstrap confidence intervals to quantify the uncertainties. Analysis was performed over four seasons for three different horizons. NMAE was found 6.72% (1h forecast), and NRMSE was found to be 16.89% (3h forecast) and 3.33% (6h forecast). It was clear that both errors (NRMSE, NMAE) increased with the increase of horizon, hence decreasing the forecasting accuracy as a result (AlHakeem et al., 2015). A radial basis function neural

network with a decoupling method was proposed for the day ahead prediction of the PV power. It presented better forecasting results than RBFNN, BPNN, and ARIMA methods (Lu & Chang, 2018).

2.7.8 LSTM and optimization Algorithms

The PSO-LSTM was proposed for 30 minutes ahead forecasting of PV power output for multi-region solar systems. The sensitivity analysis was performed for different data sets. The results showed that the proposed hybrid method had the lowest RMSE (15.49) compared to basic LSTM, ANN methods (Zheng et al., 2020). A hybrid algorithm containing GA and a deep neural network was used to forecast solar irradiation and showed better forecasting results for different seasons (H. Wang et al., 2019).

A variational Auto Encoder (VAE) based LSTM model has shown less testing RMSE value of 5.471 for short-term prediction of solar power output for different data sets compared to other machine learning models (Dairi, Harrou, Sun, & Khadraoui, 2020). A hybrid method with a combination of deep convolutional neural network (DCNN) and variational mode decomposition (VMD) method was proposed for short-term forecasting of PV power. The VMD method was used to decompose the frequency components from historical time series. The proposed hybrid method has shown better forecasting results than SVR, GPR, VMD-GPR, VMD-SVR, and CNN (Zang et al., 2018).

A (CNN+LSTM) method has presented the lowest RMSE (0.0987), MAE (0.0506), and MAPE (13.42) for one hour ahead prediction of PV power compared to (AE+LSTM) and other methods. The proposed method has also shown better forecasting accuracy for 2h and 6h ahead time period (Lee, Kim, Park, Kim, & Kim, 2018). A hybrid method (WT-DCNN) was proposed for monthly and seasonal PV power forecasting and showed better forecasting results compared to BPNN, SVM, and WT+SVM methods. The wavelet

transform (WT) was used to convert the original signal into several frequency components (H. Wang et al., 2017).

2.7.9 Wavelet transform and Support vector machine

Wavelet transform is used to divide time-series signals into separate components. The continuous wavelet transform (CWT) is the integral (sum) of all the signals over the entire time. CWT is defined mathematically as the following equation.

$$W_x(a,b,\psi) = \frac{1}{\sqrt{a}} \int_{-\infty}^{+\infty} f(t)\, \psi^* \left(\frac{t-b}{a}\right) dt \tag{2.17}$$

Where a is the scale index parameter, b is the time-shifting parameter known as translation, $\psi(t)$ is a mother wavelet function, $\psi^*(t)$ is the complex conjugate of ψ and t is time. While discrete wavelet transform (DWT) is described as follows (Shamshirband et al., 2016):

$$a = {a_0}^m, b = n{a_0}^m b_0,\ a_0 > 1, b_0 \in R \tag{2.18}$$

Where n and m are integer numbers, the separated components act as an input for the SVM model. A SVM-WT method was modeled for forecasting diffused solar radiation using the cloudiness index as an input variable, which was correlated with the clearness index. SVM-WT showed better prediction accuracy (MABE of 0.5757MJ/m^2, RMSE of 0.9640 MJ/m^2, R of 0.9631) compared to SVM-RBF (MABE of 1.0877 MJ/m^2, RMSE of 1.2583 MJ/m^2, R of 0.8599), ANN (MABE of 1.1267, RMSE of 1.3184, R of 0.8392) and 3rd-degree empirical model (MABE of 1.2171, RMSE of 1.4548, R of 0.8156). The limitation is that the minimum predicted diffused radiation deviation was high (Shamshirband et al., 2016).

Kasra Mohammadi et al. developed a hybrid (SVM-WT) technique for daily and monthly prediction of horizontal GSR in an Iranian city. The findings showed that the

hybrid model gave promising forecasting results for daily [MAPE (6.9996%), MABE (0.8405MJ/m^2), RMSE (1.4245%), rRMSE (7.9467%), R^2 (0.9086)] and monthly mean estimation [MAPE (3.2601%), MABE (0.5104MJ/m^2), RMSE (0.6618MJ/m^2), rRMSE (3.6935%), R^2 (0.9742)] compared to GA, ANN and ARMA (K. Mohammadi et al., 2015).

2.7.10 Support vector machine and optimization algorithms

SVM uses non-linear mapping to correlate data. In the direct computation method, the kernel function denoted as K enables it to operate in a high dimensional space without computing the data coordinates in that space. There are four types of kernel functions for SVM, namely, linear, sigmoid, polynomial, and radial basis functions. RBF is the best among all these due to its simplicity, reliability, computational efficiency, and ease of adaptation to optimization. Different optimization theorems are used to enhance the efficiency of SVM, such as Firefly algorithm (FFA), Ant colony optimization (ACO), ensemble empirical mode decomposition (EEMD), Feedforward neural network (FFNN), Evolutionary seasonal decomposition least square (ESDLS) and Radial basis function (RBF) (Jiménez-Pérez & Mora-López, 2016; Lin & Pai, 2016; Mao, Gong, & Chang, 2013; Niu, Wang, & Wu, 2010; Olatomiwa, Mekhilef, Shamshirband, Mohammadi, et al., 2015; Wolff et al., 2016).

The firefly algorithm is based on the dashing social behavior of fireflies in nature. In FFA, there are two main parameters, one is a variation of light intensity and the second parameter is the formulation of attractiveness. For optimal design, the objective function is proportional to the emitted light intensity of the firefly. Olatomiwa et al. developed a support vector machine with the firefly algorithm for forecasting monthly mean daily global solar radiation on a horizontal surface. Findings showed that the proposed model (SVM-FFA) had the best forecasting results such as [R^2 (0.8024), r (0.8956), RMSE

(0.6988), MAPE (6.1768) in training phase] and [R^2 (0.53), r(0.7280), RMSE (1.8661), MAPE (11.592) in testing phase] compared to both ANN and GP. This model is only feasible for sites with similar climatic conditions (Olatomiwa, Mekhilef, Shamshirband, Mohammadi, et al., 2015).

An SVM model based on ant colony optimization for forecasting short-term power load is established in this research. The proposed method (ACO-SVM) achieved greater forecasting accuracy (1.50% error) in comparison with SVM (2.01% error) and BP Neural network (2.18% error). This hybrid approach has the ability to overcome the disadvantage of huge data and low processing speed (Niu et al., 2010).

A new approach having a combination of clustering and classification algorithms was developed to enhance the next-day prediction of hourly GSR. The combination of SVM-C and SVM-R was best, having rMAE of 16.7% and RMSE of 25.3% for one type of input data set, with independent variables for previous day values of meteorological parameters. The model had also shown rMAE of 15.2% and RMSE of 22.9% for another type of data set. It also had independent meteorological variables for the same-day forecast except for the daily clearness index that relates to the previous day. The estimated value of the forecasting skill was 49.3% greater than previous values, but the computing time was large (Jiménez-Pérez & Mora-López, 2016).

Meiqin Mao et al. proposed a new hybrid technique (EEMD-SVM) for a day ahead hourly power output forecasting for large PV plants. The results showed that the proposed method reduced the MAPE (0.0813, 0.118) and RMSE (3.95, 5.5) for both normal and abnormal days respectively when compared with the traditional SVM [MAPE (0.112, 0.162), RMSE (5.1, 7.2)] and BPNN method [MAPE (0.102, 0.151), RMSE (5.23, 7.9)] respectively. However, randomness has a negative impact on its forecasting accuracy (Mao et al., 2013).

A group of two techniques named LS-SVR and FFNN, trained with LM, was used for an intra-hour (15 minutes) ahead prediction of solar power output for the PV field located in EMSI School Morocco. The results showed that both methods had better prediction accuracy, but LS-SVR was better, with MSE, MAE, RMSE, R^2, and RRMSE of 0.0043, 0.047, 0.0653, 0.96, and 15.23%, respectively (Fentis, Bahatti, Mestari, & Chouri, 2017).

K-Ping Lin et al. (Lin & Pai, 2016) analyzed an evolutionary seasonal decomposition least square support vector regression (ESDLS-SVR) for the monthly forecast of power output. ESDLS-SVR (DS) model with linear kernel function proved to be superior in its forecasting performance (0.1618 RMSE, 7.8434% MAPE) in comparison with ESDLS-SVR (DT), ARIMA, SARIMA, GRNN, and LS-SVR models.

Two models named "SVM-RBF" and "SVM-POLY" were considered for the prediction of global solar radiation (GSR). SVR-RBF outperformed ANN and SVR-POLY with low RMSE (3.2), high coefficient of determination (0.900), low computation time, and has approximately similar performance to ANFIS (Wolff et al., 2016).

A genetic algorithm combined with a support vector machine (GA-SVM) has performed better than the conventional SVM model for short-term forecasting of solar power for a residential PV system. The proposed method has beaten the conventional SVM model by RMSE difference of 669.624W and MAPE error of 98.7648% (VanDeventer et al., 2019).

2.7.11 Seasonal auto-regressive integrated moving (SARIMA) average and Support vector machine

ARIMA represents an important example of Box and Jenkins approach to time series modeling. SARIMA model adds a seasonal component and is used for time series analysis and forecasting. A hybrid method consisting of SARIMA-SVM was developed for

hourly forecasting of a grid-connected PV plant. SARIMA estimated the linear part, and SVR estimated the nonlinear part of the produced power. The proposed model produced low NRMSE (9.5678%), NMBE(-0.3552%), MPE(5.1951%), and higher R(0.9905) than SARIMA and SVM, with slightly less NRMSE than individual SARIMA and SVR (Bouzerdoum, Mellit, & Pavan, 2013).

2.7.12 Summary of hybrid methods

Hybrid models are a combination of two or more techniques used in conjunction with each other to minimize the forecasting error. These methods have produced the best forecasting results as compared to individual statistical and machine learning techniques for all types of time horizons.

The prediction accuracy is affected by the increase of forecasting horizons (Azimi et al., 2016; Cherkassky & Ma, 2004; Cristaldi, Leone, & Ottoboni, 2017; C. Yang et al., 2015). It is found that the combination of machine learning techniques with some physical techniques (NWP, clear sky, satellite imaging) produced better forecasting results for long-term time horizon also (Cristaldi et al., 2017; Ghimire et al., 2018; Wolff et al., 2016). An utmost care is required in the selection of the individual techniques to form the composite hybrid model. Poor performance of any single technique affects the total performance of the composite hybrid model, thus limiting the overall forecasting accuracy as a result. As the number of techniques incorporated in the hybrid system increases, it becomes more complex and costly (De Giorgi et al., 2016). But the enhancement of forecasting accuracy is the ultimate task, in which a balance between accuracy, computational complexity, and the cost is required. A summary of several hybrid models is listed with forecasting horizons, advantages, and disadvantages in Table 2.4.

Table 2.4: Summary of Hybrid methods

Ref	Forecasting horizon	Methods	Advantages	Disadvantage	Input parameters used
(Fan, Wu, Ma, Zhou, & Zhang, 2020)	daily	SVM-PSO, SVM-BAT, SVM-WOA	SVM-BAT, SVM-WOA, and SVM-PSO have RMSD values of (2.9%–5.6%), (1.9%–4.9%), and (1.1%–3.3%), respectively	-	Temperatures, sunshine duration, suspended particulate matter, ozone, global and diffused solar radiation, standard deviation, kurtosis, coefficient of skewness
(B. Mohammadi & Aghashariatmadari, 2020)	-	SVR-KHA	the RMSE, MAPE, and R^2 values for this model were 1.98 MJ/m2 /day, 7.4%, and 0.93, respectively.	Performance is low in some stations due to different climatic conditions	Radiation data of neighboring stations
(Kisi, Heddam, & Yaseen, 2019)	daily	DENFIS	Enhanced solar radiation prediction over the MARS, M5 model tree, and least square SVR models by 20–42%, 29–47%, and 19–43% based on the RMSE	Considerable overestimation of compared models in summer months	Historical data of solar radiation and air temperature
(Hou et al., 2018)	daily	FOS-ELM	an enhancement in the RMSE and MAE by (68.8-79.8%).	-	Temperature, humidity, evaporation, and vapor pressure deficiency
(Jiang, Dong, & Xiao, 2017)	5-days-ahead on daily basis.	DCGSO-LASSO	Lowest MAPE(13.247%), RMSE(28.058W/m^2),RMSE/ avg (6.345%)	Week agreement with the actual data	temperature, pressure, relative humidity, solar zenith angle, precipitation, wind speed and direction, and global horizontal radiation.
(Asrari et al., 2017)	An hour ahead	BP-SFLA-ANN	1. fast convergence. 2. reduced WMAPE of 8.8% as compared to 9.57% in previous work.	Not given	previous solar data.

Table 2.4 (continued)

Ref	Forecasting horizon	Methods	Advantages	Disadvantage	Input parameters used
(Akarslan & Hocaoglu, 2016)	hourly	Linear + empirical model	Lowest RMSE (34.86%) as compared to previous empirical model studies	Accuracy still needs improvement	Solar radiation data from different regions
(Shamshirband et al., 2016)	Daily	SVM-WT	RMSE(0.6940MJ/m^2), MABE(0.5757MJ/m^2), R(0.9631).	Minimum predicted diffused radiation deviation is higher.	Clearness index
(Azimi et al., 2016)	1h,2h……48h ahead	k-means algorithm+ MLPNN.	1. less processing time. 2. less value of RMSE(58.5w/m^2), nRMSE (28.91%) and better forecasting skill (0.5714) was noticed for 1h horizon	Forecasting accuracy decreases with the increase of horizon.	Historical solar data
(Ghayekhloo, Ghofrani, Menhaj, & Azimi, 2015)	Each individual hour	GTSOP+ NG+ CHL.	2.Superior performance in terms of RMSE (53.929), rRMSE(0.845) than other algorithms.	Accuracy decreases with the horizon increase.	Temperature, wind speed, wind direction as inputs. Historical solar radiation data
(AlHakeem et al., 2015)	1-h, 3-h, and 6-h ahead horizons.	WT+GRNN+PSO	Increased forecast accuracy for 1-h, 3-h, and 6-h ahead horizons.	Slight variations in forecasting accuracy.	PV output power, global solar radiation, and temperature.
(C. Yang et al., 2015)	5 min, 15 min, 1h, and 2h ahead forecast.	(ST-ARX) forecast model	Reduced RMSE(154.5)and MAE(111.4) than PSS method.	Spatial-temporal method (ST) not better than PSS for 5 and 15 minutes forecast.	Historical data of both local and nearby solar sites.
(Salcedo-Sanz, Casanova-Mateo, Pastor-Sánchez, & Sánchez-Girón, 2014)	daily	CRO-ELM	1. Better than simple ELM and SVR algorithms. 2. CRO-ELM(5-gen) has RMSE (0.00125) in comparison with RMSE(0.00136) classical ELM.	RMSE increases with the increase of generation number	Aerosol optical depth, water vapor, theoretical extraterrestrial solar irradiation. Clearness index.

The selection of input parameters is also critical. An accurate historical data with a higher number of input parameters such as temperature, pressure, the humidity result in better forecasting results, but complexity increased with the increase of input parameters, so an optimum number of input parameters must be selected based on a strong correlation with PV power output for accurate forecasting results (Das et al., 2018). From a comprehensive review, it can be observed that keeping all these constraints within limits; the hybrid models are prime and efficient models compared to any other individual techniques.

2.8 A comparative analysis of forecasting Methods

Several statistical techniques have been used for forecasting the PV power output, such as ARMA, ARIMA, ARMAX, CARDS, regression, and regression trees. These methods have a limitation to deal with non-linear data. The sky images and satellite images were used to predict the solar irradiance for an ultra-short-term period based on cloud tracking and forecasting (Cheng, 2017; F. Wang et al., 2018; Zaher et al., 2017). The forecasting accuracy of image-based methods is dependent directly on image processing algorithms. However, the forecasting accuracy of these methods needs further improvement based on low-resolution satellite data and limited coverage of sky images from the ground. Numerical weather prediction (NWP) is used for 15 days ahead solar irradiance forecasting, but its application is limited due to the data access restrictions imposed by the domestic meteorological departments (Lima et al., 2016; Mathiesen et al., 2013; Perez et al., 2013; Verzijlbergh et al., 2015).

Among machine learning techniques, ANN in (Alzahrani et al., 2017; Bou-Rabee et al., 2017; Hussain & AlAlili, 2017; Xue, 2017) and ANFIS in (Olatomiwa, Mekhilef, Shamshirband, & Petković, 2015) are deployed for solar power output forecasting. They have a better ability to deal with nonlinear systems and cope with the erratic behavior of

solar power. However, the issues of random initial data, local minima, overfitting, and increased complexity due to multilayered structure affect the reliability of the power system (De Giorgi et al., 2016; Dolara et al., 2015; Mellit et al., 2009). The SVM has also shown better forecasting accuracy to predict the solar power in (H. S. Jang et al., 2016; Junior et al., 2014; Wolff et al., 2016). However, it is highly sensitive to parameters such as kernel function, tube radius (ε) and penalty factor (C). Therefore, proper selection of these parameters is a challenging task (Das et al., 2018). In an extreme learning machine (ELM), the selection of input weights and biases of hidden nodes is random using linear regression (Deo et al., 2017; Hossain, Mekhilef, Danesh, et al., 2017; Tang et al., 2016).

To overcome the deficiencies of conventional neural networks and other machine learning techniques, deep learning models have been applied in certain areas (H. Wang et al., 2019; Youssef et al., 2017). Deep learning is also an advanced type of machine learning method. Convolutional neural networks (CNN) (Zang et al., 2018) and Recurrent neural networks (RNN) (Shi et al., 2017; A. Yona et al., 2013) are deep learning models used for forecasting PV power. Deep learning has the ability to extract deep features from PV power output and provide better forecasting results in comparison with persistence, physical and statistical models.

An algorithm is proposed based on the Long short term memory (LSTM) network for day-ahead power output forecasting using the data provided by local meteorological authorities. It has shown 18.34% more forecasting accuracy than other benchmark methods (Qing & Niu, 2018). G Narvaez et al. have performed PV power prediction on a daily and weekly basis using the deep learning method (Narvaez et al., 2021). A grey theory-based deep belief network proposed for a day ahead forecasting of PV power output showed better forecasting accuracy and computational efficiency (Chang & Lu, 2018). F Wang et al. (F. Wang et al., 2020) have developed a time correlation

modification method to enhance the accuracy of the deep learning model for a day ahead PV power forecasting.

Based on the deep learning review, an hour ahead PV power forecasting based on a deep learning model for different PV systems over a large real dataset in Malaysia to ensure the robustness of the model is missing in the literature. According to the author's knowledge, the comparison of the deep learning method with regression (GPR, GPR(PCA)), artificial neural networks (ANN), machine learning (SVR, SVR(PCA)), and hybrid (ANFIS) methods altogether is also missing in literature for an hour ahead PV power output forecasting. Therefore, there is still room to develop a deep learning method for an hour ahead prediction of power output for different PV systems on an annual basis over four years recorded period (2016-2019) in comparison with regression, machine learning, and hybrid techniques.

From the literature review, it can be observed that hybrid methods have shown better forecasting accuracy compared with conventional methods. The PSO was used to optimize the parameters of LSTM to enhance its 30 minutes ahead prediction accuracy for PV power output forecasting considering time series (Zheng et al., 2020). However, only one-year data is considered. A genetic algorithm (GA) was also used with LSTM for 4 hours ahead forecasting of PV power output (Jaidee & Pora, 2019). However, GA is an old optimization algorithm and is preferred for discrete problems. There is no study in literature, which has used some advanced optimization algorithm to tune the hyperparameters of LSTM for an hour ahead forecasting of PV power output for three different PV systems on an annual basis in Malaysia over a large data set. Furthermore, the comparison of advanced optimization algorithm with GA and PSO is also missing. Therefore, an advanced optimization algorithm with better convergence speed is also

required to tune the hyperparameters of the developed deep learning method (RNN-LSTM) to enhance its forecasting accuracy in comparison with GA and PSO algorithms.

2.9 Importance of forecasting and grid management strategy with integration of renewable power generation

Due to the integration of PV power at latrge scale, the negative effects on the smart grid energy management, are getting more attention. These problems are power flow, grid losses, short circuit current of distribution networks, voltage fluctuations. The accurate forecatsing provides better information to grid operators, electricity participants and decision makers for planning of electric power. The PV outputs are found more smoother in very short time prediction model (30 sec to several minutes) compared to short-time PV prediction model (Wan et al., 2015).

To control the fluctuation rate of PV generations, certain techniques have been used such as electric vehicles, battery storage systems, an electic double-layer capacitor, fast ramping generators (Shivashankar, Mekhilef, Mokhlis, & Karimi, 2016). To schedule interaday electric power of smart grids integrated with PV generation, differents methods are used.

To integrate RES with energy storage systems (ESSs) in power system, energy management is an obligatory tool. The electricity bills are reduced for consumers and peak generations are reduced for utility companies with proper energy management system. An optimal way is to shift all the load and ESS charging to solar energy in day time instead of taking from utility. On the other hand, energy management is also needed to enhance the life of batteries by controlling their charging and discharging within specified limits. Therefore, precise forecasting of energy is required to obtain effective energy managemenr system due to variable behavior of PV power output (Aslam et al., 2021).

2.10 Summary

This chapter has reviewed the performance assessment of PV systems and forecasting of PV power output. Different forecasting horizons are discussed, followed by the review of mathematical techniques such as the persistence model, statistical techniques for forecasting solar power output. In addition, machine learning forecasting techniques such as ANN, SVM, ELM, and deep learning are reviewed and critically analyzed. Machine learning techniques can deal with nonlinear systems. The hybrid methods are elaborated in detail, showing different combinations of machine learning, deep learning, physical and optimization methods, along with the summary at the end of the section. A comprehensive comparative analysis of all these forecasting methods is presented to elaborate the research gap. Finally, the importance of forecasting and grid management strategy with integration of renewable power generation is elaborated.

CHAPTER 3: METHODOLOGY

3.1 Introduction

In this chapter, the methodology employed to achieve the research objectives is presented. The site of the three different grid-connected PV systems installed at the rooftop of the engineering tower UM is described, along with data collection. Moreover, different performance parameters are briefly discussed, which are used for evaluating the performance of three different grid-connected PV systems. The steps for data preprocessing are elaborated for use in forecasting methodology. Furthermore, the proposed methodology (deep learning (RNN-LSTM)) for an hour ahead forecasting of PV power output on an annual basis for three PV systems over the duration (2016-2019) is elaborated. In addition, the methodology of other forecasting methods such as regression [GPR, SVR, GPR(PCA) and SVR(PCA)], artificial neural network, and ANFIS (grid partitioning, subtractive clustering, and FCM) is also discussed for comparison with the proposed deep learning technique. The measurement indices are discussed to assess the accuracy of forecasting techniques by evaluating the difference between predicted and actual value. Furthermore, the methodology of three optimization algorithms, namely: GA, PSO, and SSA, is presented to tune the hyperparameters of the developed deep learning method (RNN-LSTM) to enhance its forecasting accuracy.

3.2 Site description and data set

The PV system is installed at latitude and longitude of 3.07^{o}N and 101.39^{o}E, respectively, about 66 meters above sea level. It has three types of modules. Mono-crystalline PV array (SHELL/SQ75 model) has an installed capacity of 1.875 kW_P for 25 modules, with 75W_P capacity for each module. Poly-crystalline PV array (MITSUBISHI/PV-AE125MF5N model) has an installed capacity of 2.0 kW_P for 16 modules, with 125 W_P capacity for each module. PV array based on amorphous silicon technology (SHARP/NS-F135G5 model) has an installed capacity of 2.7 kW_P for 20

modules, with 135 W_P for each module. Therefore, the overall capacity of the composite PV system is 6.575 kW_P. The individual PV structures were installed at a proper distance according to IEC 61730 standards which are being followed by the Sustainable Energy Development Authority (SEDA) (Authority and Malaysia, 2013). SEDA is responsible for monitoring renewable energy projects in Malaysia. In Kuala Lumpur, there is no winter season. Therefore, the shading effect is minimum. However, there are two main seasons; sunny and rainy seasons. An optimum tilt angle of 10^0 for this PV system is also a key factor in reducing the shading effect (Saadatian et al., 2013).

All modules are fixed and oriented towards true south at azimuth and tilt (inclination) angles of 0^o and $10^{o,}$ respectively. For a fixed configuration, the angle of inclination is determined as an angle of PV modules from the horizontal level, while the azimuth angle is specified as an angle of PV modules relative to the south direction. Both angles are considered optimal. The Liu and Jordan model (1962) is used for the optimization of these angles (Khatib et al., 2015). Research in (Saadatian et al., 2013) reported that the solar radiation received at a tilt angle of 10^0 was maximum for PV panels in Kuala Lumpur. The PV panels have experienced minimum shading effects and dust accumulation at this angle.

In Malaysia, true south-facing (Azimuth 0^o) is an optimum orientation at which PV systems have maximum annual average PV yield due to their location in the northern hemisphere (Ahmed et al., 2019). The phenomenon of natural cooling is adopted in the installation of this PV system by mounting the modules with an open back. Figure 3.1 indicates the main parts of the rooftop fixed system. A schematic diagram of PEARL's grid-connected PV system at the Faculty of Engineering, UM, Malaysia, is presented in Figure 3.2.

(a)

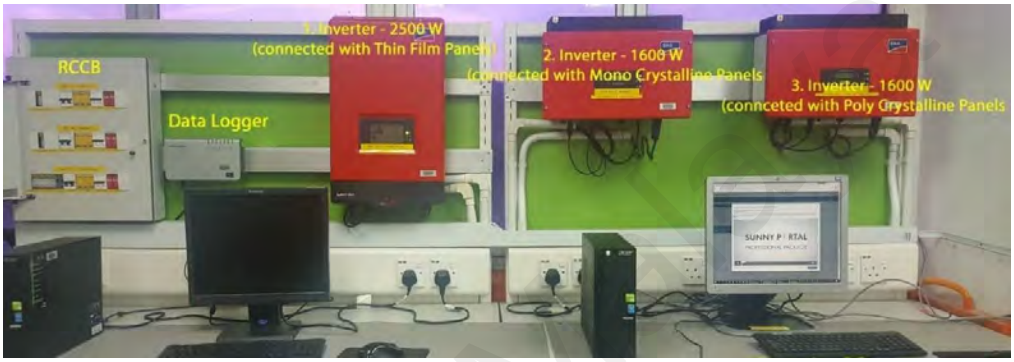

(b)

Figure 3.1: Main parts of the rooftop fixed system (a) Photo of the installed three technologies PV systems (b) Grid-connected inverters

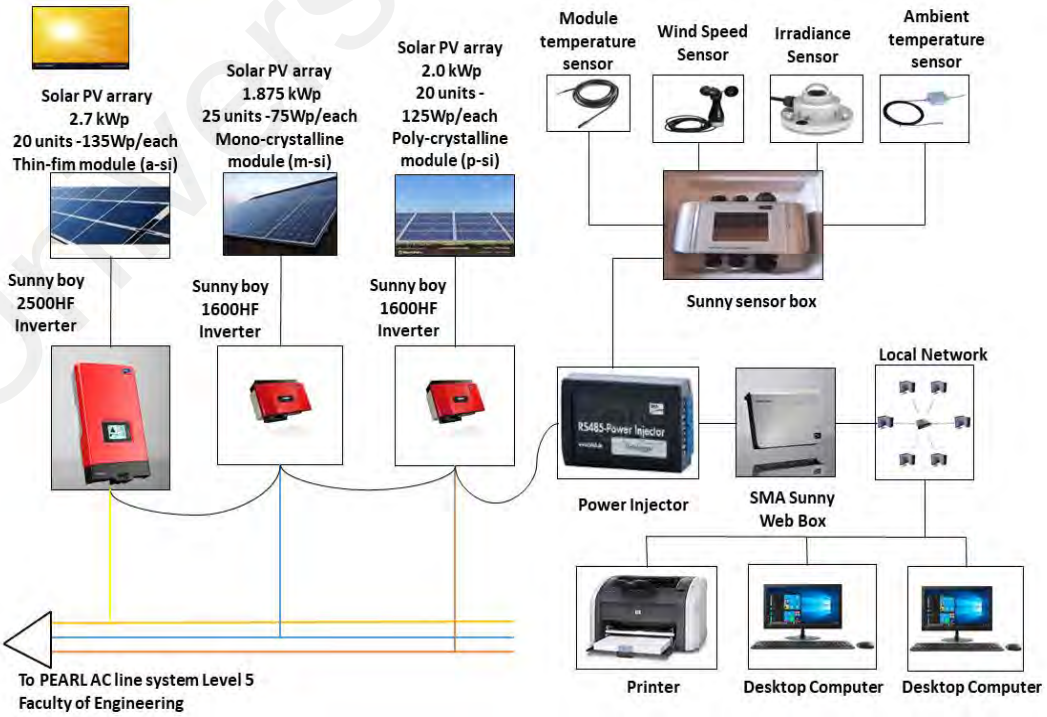

Figure 3.2: Schematic diagram of PEARL's grid-connected PV system at faculty of engineering, UM, Malaysia

PEARL's grid-linked PV system was commissioned for use in October 2015. However, the results calculated in this study are based on data measured between January 2016 and December 2019. The data was recorded by a web server integrated with the inverter for 5-minutes intervals, from which related performance parameters are calculated at hourly, daily, monthly, and yearly intervals by using relative mathematical formulas.

The SMA SUNNY SENSOR BOX is used to measure wind speed, solar irradiance, ambient, and PV module temperatures. The SMA power injector is used to power the sensor box and is connected with the SMA SUNNY Web box through a communication bus. The Sunny Web box is used to record all the data from sensors and grid-connected inverters. Table 3.1 shows the technical specifications of the PV modules.

Table 3.1: Technical specifications of PV module

Model	**NS-F135G5**	**PV-AE125MF5N**	**SQ75**
Maker	**SHARP**	**MITSUBISHI**	**SHELL**
Cell type	**Thin film**	**Poly-crystalline**	**Mono-crystalline**
Peak power, $P_{mp}\ (W)$	135	125	75
$V_{mp}\ (V)$	47	17.30	17
$I_{mp}(A)$	2.88	7.90	4.40
$V_{oc}\ (V)$	61.30	21.80	21.70
$I_{sc}\ (A)$	3.41	7.23	4.80
Temperature coefficients			
power, P_{mp} (%/ °C)	-0.30	-0.478	-0.52
V_{oc} (%/°C)	-0.24	-0.346	-0.37
I_{sc} (%/°C)	+ 0.07	+0.057	0.0290
Mechanical specifications			
Dimensions: Length X Width X Thickness (mm)	1402 X 1001 X 24	1495 X 674 X 46	1200 X 527 X 34
Weight (Kg)	26	13.50	7.257
Number of modules	20	16	25

The Sunny Web box is connected with the local network and desktop computers to save and monitor the data measurements. The data can be downloaded with a resolution of 5, 15, and 30 minutes, depending upon the requirement. The data for the previous 12 months remains available and can be downloaded at any time. The two inverters for p-s_i and m-s_i PV arrays have rated power of 1600W each. The third inverter for a-s_i PV array has a rated power of 2500W. Table 3.2 describes the technical specifications of inverters, respectively.

Table 3.2: Technical specifications of inverters used in the PV system

Model	**Sunny Boy 1600TL**	**Sunny Boy 2500 HF**
Model. No	**10**	**30**
Maker	**SMA**	**SMA**
No of units	2	1
DC		
$V_{max}\,(V)$	600	700
V($V_{rated}\,(V)$)	400	530
$V_{min}\ /\ V_{initial}\,(V)$	125/150	175/220
$I_{max}\ (A)$	12	15
$I_{sc}\ (A)$	18	-
MPP inputs/ strings per MPP input	1/ 1	1/ 2
AC		
$P_{rated}(W)$	1600	2500
$P_{app}\ (VA)$	1600	2500
$V_{ac}\,(V)$	220/230/240	220/230/240
$V_{nominal}\,(V)$	180-260	180-280
$f(Hz)$	50Hz/ 60Hz	50Hz/ 60Hz
PF	1	1
Maximum efficiency (%)	96	96.3
European efficiency (%)	96	95.3
Dimensions: Length X Width X Thickness (mm)	440 X 339 X 214	348 X 580 X 145
Weight (kg)	16	17

3.3 Methodology for performance analysis of PV Systems

To evaluate the performance of the PEARL's grid-linked system, the followingparameters are used: total AC (E_{AC}) and DC energy (E_{DC}) outputs (kWh),

performance yields (reference yield (Y_R), array yield (Y_A), and final yield (Y_F)) (kWh/kWp), system efficiencies (inverter efficiency, array efficiency, and system efficiency) (%), CF (%), system losses (array losses, system losses, and overall losses) (L_s)) (kWh/kWp) and PR (%). The analysis of the PV system is performed based on these parameters and can be compared with similar rooftop grid-tied systems regardless of capacity and location.

3.3.1 AC energy output

The alternating current (AC) energy produced over a certain time by the system is called the energy output of the system. The total hourly ($E_{AC,h}$), daily ($E_{AC,d}$), monthly ($E_{AC,m}$) and yearly ($E_{AC,d}$) energy of the PV system are defined as follows (de Lima et al., 2017):

$$E_{AC,h} = \sum_{t=1}^{t=60} (E_{AC,t}) \tag{3.1}$$

$$E_{AC,d} = \sum_{h=1}^{h=24} (E_{AC,h}) \tag{3.2}$$

$$E_{AC,m} = \sum_{d=1}^{N} (E_{AC,d}) \tag{3.3}$$

$$E_{AC,y} = \sum_{m=1}^{P} (E_{AC,m}) \tag{3.4}$$

The $E_{AC,t}$ is the generated AC energy (in minutes). While $E_{AC,h}$, $E_{AC,d}$, $E_{AC,m}$ and $E_{AC,y}$ are the hourly, daily, monthly, and yearly generated AC energies. N and P are the number of days and months in equations (3.3) and (3.4), respectively. The energy created by the PV system is known as DC energy output. This DC energy becomes the input of an inverter. The daily ($E_{DC,d}$), monthly ($E_{DC,m}$) and yearly ($E_{DC,d}$) energy produced by the PV system is shown as:

$$E_{DC,h} = \sum_{t=1}^{t=60} (E_{DC,t}) \quad (3.5)$$

$$E_{DC,d} = \sum_{h=1}^{h=24} (E_{DC,h}) \quad (3.6)$$

$$E_{DC,m} = \sum_{d=1}^{N} (E_{DC,d}) \quad (3.7)$$

$$E_{DC,y} = \sum_{m=1}^{P} (E_{DC,m}) \quad (3.8)$$

3.3.2 System yields

The yields represent the pragmatic action of the PV array comparative to its rated capacity. There are three types of system yields, which are reference, array, and final yields. The ratio of DC energy output to the rated power of the PV system for a specific time is known as the array yield. It points out the number of PV array operating hours at its rated capacity to generate the equal DC energy, as measured. It is defined as (Attari et al., 2016):

$$Y_A = \frac{E_{DC}}{P_{pv,rated}} \text{ (h)} \quad (3.9)$$

The daily, monthly, and yearly array yield is given as:

$$Y_{A,d} = \frac{E_{DC,d}}{P_{pv,rated}} \text{ (h)} \quad (3.10)$$

$$Y_{A,m} = \frac{E_{DC,m}}{P_{pv,rated}} \text{ (h)} \quad (3.11)$$

$$Y_{A,y} = \frac{E_{DC,y}}{P_{pv,rated}} \text{ (h)} \quad (3.12)$$

The ratio of AC output energy to the PV-rated power at standard test conditions (STC) for a specific time is called the final yield. It implies the number of PV array operating

hours at its rated capacity to generate the equivalent AC energy, as measured. It is given as (Adaramola and Management, 2015):

$$Y_F = \frac{E_{AC}}{P_{pv,rated}} \text{ (h)} \quad (3.13)$$

Where Y_F is the final yield and E_{AC} is the AC energy output (kWh). The daily, monthly, and yearly final yields are defined as:

$$Y_{F,d} = \frac{E_{AC,d}}{P_{pv,rated}} \text{ (h)} \quad (3.14)$$

$$Y_{F,m} = \frac{E_{AC,m}}{P_{pv,rated}} \text{ (h)} \quad (3.15)$$

$$Y_{F,y} = \frac{E_{AC,y}}{P_{pv,rated}} \text{ (h)} \quad (3.16)$$

The ratio of overall in-plane solar radiation (kWh/m^2) to PV reference irradiance (1 kW/m^2) over a given period is called reference yield. Peak sun hours are calculated from this yield. The reference yield is shown as:

$$Y_R = \frac{H_t}{H_R} \text{ (h)} \quad (3.17)$$

Where H_R is the reference irradiance and H_t is the in-plane solar radiation.

3.3.3 Capacity factor

For a defined time, the ratio of the generated output energy of the PV system to the energy output when the system is operated at its maximum capacity is known as a capacity factor (Sharma and Goel, 2017).

The annual CF is shown as:

$$C_F = \frac{\text{Total annual energy output } (E_{AC}) * 100}{P_{PV,Rated} * 8760} \text{ (h)} \quad (3.18)$$

3.3.4 System efficiencies

There are three types of efficiencies to evaluate PV system performance: PV module efficiency, system efficiency, and inverter efficiency. PV module efficiency is determined from DC energy output, while system efficiency is deduced from AC energy output. The PV module efficiency is given as:

$$\eta_{PV} = \frac{100 * E_{DC}}{H_t * A_m} \ (\%) \tag{3.19}$$

Where A_m is the area of the module (m^2), and H_t is the in-plane solar radiation. The system efficiency is determined as:

$$\eta_{sys} = \frac{100 * E_{AC}}{H_t * A_m} \ (\%) \tag{3.20}$$

The inverter efficiency is given as:

$$\eta_{inv} = \frac{100 * E_{AC}}{E_{DC}} \ (\%) \tag{3.21}$$

3.3.5 PV array and system losses

The losses produced in the PV array during the conversion of solar radiation into DC power are known as array losses. They are defined as:

$$L_a = Y_r - Y_a \ (h) \tag{3.22}$$

Where L_a, Y_r and Y_a represent array losses, reference yield, and array yield, respectively. The losses produced when the inverter converts DC power to AC power are known as the system losses. It is given as follows (Emmanuel et al., 2017):

$$L_s = Y_a - Y_f \ (h) \tag{3.23}$$

Where L_s, Y_a and Y_f represent system losses, array, and final yields, respectively.

3.3.6 Performance ratio

The performance ratio is the ratio of final yield to reference yield. PR shows the familiarity of the system to its actual performance during real operation and provides the comparison of different PV systems irrespective of nominal rated power capacity, tilt angle, and location (de Lima et al., 2017). PR explains the effect of losses on the PV output power due to module temperature and the imperfect use of solar radiation. It is represented as (Kumar and Sudhakar, 2015):

$$\mathrm{PR} = \frac{\mathrm{Y_F} * 100}{\mathrm{Y_R}} = 1 - (\mathrm{L_A} + \mathrm{L_{s)}}\ (\%) \tag{3.24}$$

Where Y_F, Y_R, $\mathrm{L_A}$, $\mathrm{L_S}$ and PR are the final yield, reference yield, array losses, system losses, and performance ratio, respectively.

3.4 Methodology for PV power output forecasting

In this section, the methodology of certain methods such as regression [GPR, SVR, GPR(PCA) and SVR(PCA)], artificial neural network (ANN), ANFIS (grid partitioning, subtractive clustering, and FCM), and proposed deep learning (RNN-LSTM) method for an hour ahead forecasting of PV power output is described in detail. The prediction is executed on an annual basis for four years recorded data period (2016-2019). The annual data is divided into two segments, 70% for training and 30% for testing purpose, to compare the proposed deep learning technique with all other techniques on an equal basis. The methodology flow chart of the proposed deep learning (RNN-LSTM) and other forecasting models is shown in Figure 3.3.

3.4.1 Data preprocessing

Data preprocessing involves certain steps such as data collection, data division, and data normalization. The 5 minutes duration database recorded over the four years period

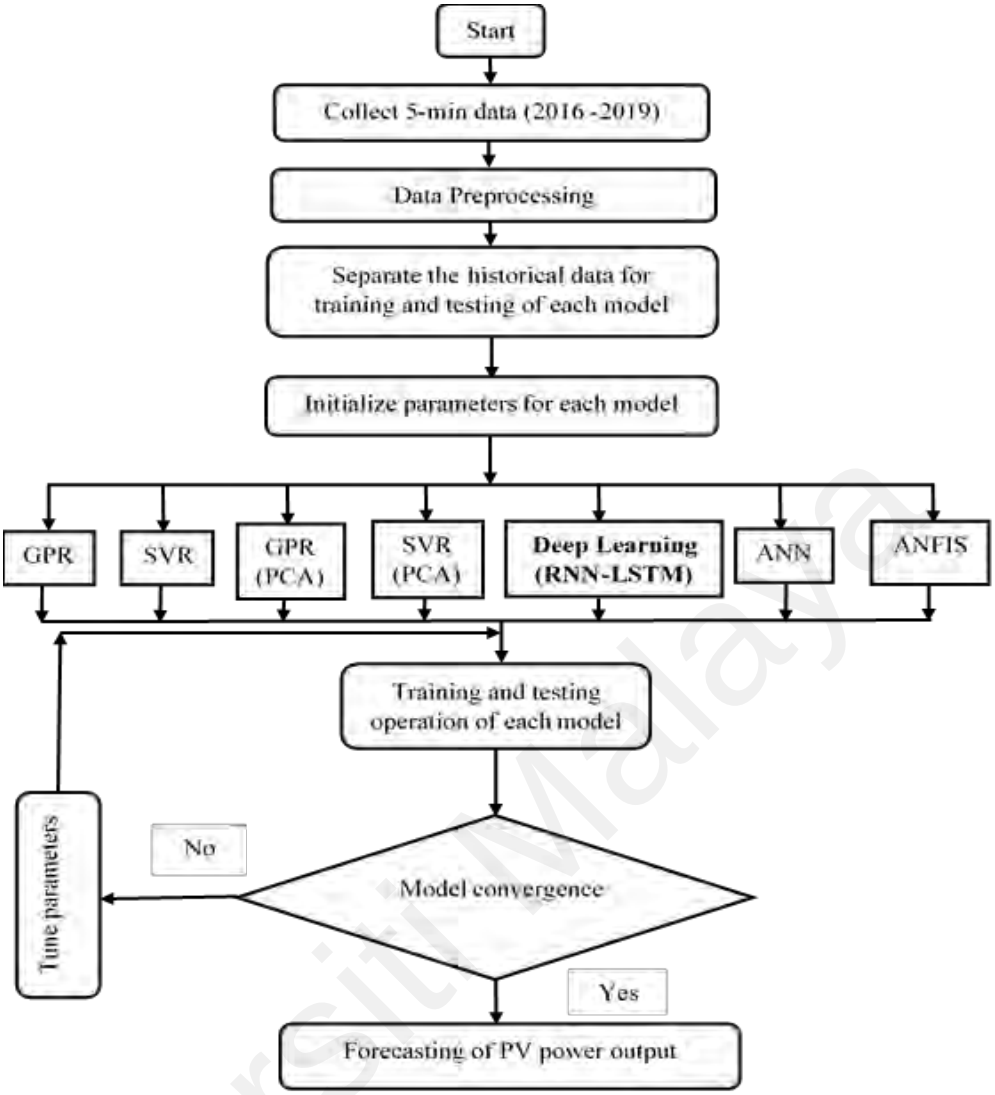

Figure 3.3: The methodology for forecasting models

(2016-2019) is used in this research. Four inputs, which are solar irradiance, wind speed, ambient, and PV module temperature, are considered. Among these four inputs, the solar irradiance, ambient temperature and wind speed are the weather parameters, considered for forecasting to improve the regional PV production. The three PV power outputs (one for each PV system) are collected using SMA SUNNY SENSOR BOX. The prediction is executed on an annual basis. Each year data is divided into two segments, 70% for training and 30% for testing, to provide a proper comparison of the proposed deep learning technique (RNN-LSTM) with other regression, machine learning, and hybrid techniques. The data is normalized before prediction and denormalized after prediction to retrieve the

actual values of forecasting accuracy measurement parameters. The formulas for normalization and denormalization are given as follows.

$$D_{norm} = (D_{actual} - D_{min})/(D_{max} - D_{min}) \quad (3.25)$$

$$D_{actual} = ((D_{max} - D_{min}).D_{norm}) + D_{min} \quad (3.26)$$

Where D_{norm}, D_{actual}, D_{min} D_{max} are the normalized, actual, minimum, and maximum values of data, respectively.

3.4.2 Regression for PV power output forecasting

Two regression methods are presented below for an hour ahead forecasting of PV power output. The principal component analysis is also discussed.

3.4.2.1 Gaussian process regression

This is the nonparametric probabilistic model based on some kernel functions. It represents that the joint Gaussian distribution is followed by a finite set of values. GP model provides a way of indicating prior distributions over functions. For a training data set D, $D = \{x_n, y_n\}$ for $n = 1, 2, \ldots, N$; where the input is $x_n \in \mathbb{R}^{dx}$ and output $y_n \in \mathbb{R}$, the output in $y_n \in R$. Suppose the observation model is

$$y = f(x) + \varepsilon \quad (3.27)$$

where f is the latent function and ε is Gaussian noise with zero mean and variance σ_n^2, i.e. $\varepsilon \sim N(0, \sigma_n^2)$. While y is the actual target value $y - [y_1 \ldots\ldots\ldots y_n]^T$ and x is the input features as $x - [x_1 \ldots\ldots\ldots x_n]^T$. A GP can be defined as $f(x) \sim GP(m(x), k(x, x'))$, where f(x) is the latent function, m(x) is mean variance and $k(x, x')$ is covariance function. For a real process, both of them are defined as:

$$m(x) = E[f(x)] \quad (3.28)$$

$$k(x, x') = E[(f(x) - m(x))(f(x') - m(x'))] \quad (3.29)$$

$\mathrm{x}, \mathrm{x}' \in \mathbb{R}^{dX}$ are two input vectors. Considering zero mean for simplicity, the kernel function used is given as

$$\mathrm{k}(\mathrm{x}, \mathrm{x}') = \exp\left(-\frac{\|\mathrm{x} - \mathrm{x}'\|}{2c^2}\right) \tag{3.30}$$

Where c is the hyperparameter. The Gramian matrix is described as:

$$\mathrm{k}(\mathrm{X}, \mathrm{X}) = \begin{bmatrix} k(\mathrm{x}_1, \mathrm{x}_1) & k(\mathrm{x}_1, \mathrm{x}_2) \dots & k(\mathrm{x}_1, \mathrm{x}_n) \\ k(\mathrm{x}_2, \mathrm{x}_1) & k(\mathrm{x}_2, \mathrm{x}_2) \dots & k(\mathrm{x}_2, \mathrm{x}_n) \\ \cdots & \cdots \quad \ddots & \cdots \\ k(\mathrm{x}_n, \mathrm{x}_1) & k(\mathrm{x}_n, \mathrm{x}_2) \dots & k(\mathrm{x}_n, \mathrm{x}_n) \end{bmatrix} \tag{3.31}$$

The marginal distribution over any specific set of input points must have a multivariate joint gaussian distribution shown as:

$$\begin{bmatrix} \boldsymbol{f} \\ \boldsymbol{f}_* \end{bmatrix} |\mathrm{x}, \mathrm{x}_* \sim \mathrm{N}\left(0, \begin{bmatrix} \boldsymbol{K}(\mathrm{x}, \mathrm{x}) & \boldsymbol{K}(\mathrm{x}, \mathrm{x}_*) \\ \boldsymbol{K}(\mathrm{x}_*, \mathrm{x}) & \boldsymbol{K}(\mathrm{x}_*, \mathrm{x}_*) \end{bmatrix}\right) \tag{3.32}$$

Where $\boldsymbol{k}(\mathrm{x}_*, \mathrm{x})$ and $\boldsymbol{k}(\mathrm{x}_*, \mathrm{x}_*)$ are found by putting x and x_* in eq (3.32) and $\boldsymbol{k}(\mathrm{x}_*, \mathrm{x}) = \boldsymbol{k}(\mathrm{x}, \mathrm{x}_*)^T$. From the independent identically distributed Gaussian noise assumption,

$$\begin{bmatrix} \varepsilon \\ \varepsilon_* \end{bmatrix} \sim \mathrm{N}\left(0, \begin{bmatrix} \sigma_n^2 \boldsymbol{C} & \boldsymbol{0} \\ \boldsymbol{0} & \sigma_n^2 \boldsymbol{C} \end{bmatrix}\right) \tag{3.33}$$

$$\begin{bmatrix} \boldsymbol{y} \\ y_* \end{bmatrix} |\mathrm{x}, \mathrm{x}_* \sim \mathrm{N}\left(0, \begin{bmatrix} \boldsymbol{K}(\mathrm{x}, \mathrm{x}) + \sigma_n^2 \boldsymbol{C} & \boldsymbol{K}(\mathrm{x}, \mathrm{x}_*) \\ \boldsymbol{K}(\mathrm{x}_*, \mathrm{x}) & \boldsymbol{K}(\mathrm{x}_*, \mathrm{x}_*) + \sigma_n^2 \boldsymbol{C} \end{bmatrix}\right) \tag{3.34}$$

The distribution $P(y_*, |\boldsymbol{y})$ indicates the closeness of the predicted value y_* with the actual data, $\boldsymbol{y}$ is described as

$$y_*, |\boldsymbol{y}\, \mathrm{x}, \mathrm{x}_* \sim \mathrm{N}(\boldsymbol{\mu}_*, \boldsymbol{\Sigma}_*) \tag{3.35}$$

Where the mean vector $\boldsymbol{\mu}_*$and covariance vector $\boldsymbol{\Sigma}_*$ can be calculated as

$$\boldsymbol{\mu}_* = \boldsymbol{K}(\mathrm{x}_*, \mathrm{x})\, (\boldsymbol{K}(\mathrm{x}, \mathrm{x}) + \sigma_n^2 \boldsymbol{C})^{-1} \mathbf{y} \tag{3.36}$$

$$\boldsymbol{\Sigma}_* = \boldsymbol{K}(\mathrm{x}_*, \mathrm{x}_*) - \boldsymbol{K}(\mathrm{x}_*, \mathrm{x})\, (\boldsymbol{K}(\mathrm{x}, \mathrm{x}) + \sigma_n^2 \boldsymbol{C})^{-1} + \boldsymbol{K}(\mathrm{x}, \mathrm{x}_*) + \sigma_n^2 \boldsymbol{C} \tag{3.37}$$

P is the total number of new complete data set. For the new sample $\boldsymbol{X}_{test}$, prediction is the average of prediction results for all models

$$\boldsymbol{y}_{predicted} = \frac{1}{P}\sum_{P=1}^{P} M_p\,(\boldsymbol{X}_{test}) \tag{3.38}$$

where $M_p(\boldsymbol{X}_{test})$ is the prediction result for the new test data set.

3.4.2.2 Support Vector Regression

A support vector machine (SVM) is a supervised learning technique in the field of machine learning theory, applicable to both classification and regression problems (Quej et al., 2017). It is used to enhance the generalization ability by minimizing the empirical risk and confidence interval using the hypothesis of structural risk minimization.

In addition to classification, SVM can also be applied successfully for regression problems known as support vector regression (SVR). For a data set of $\{(x_n, y_n)\}\frac{N}{n}$, where x_n and y_n are the input and output vectors, respectively. While N is the complete data set. A nonlinear function $\varphi(x)$ maps the input x into a feature space, and the resultant regression function is as follows:

$$f(x) = \omega.\varphi(x) + b \tag{3.39}$$

This function approximates the actual output y_n with an error tolerance value ε, where ω, $\varphi(x)$, and b are the weight vector, nonlinear mapping function, and bias value respectively. The general mathematical function for SVM is given as:

$$y = f(x) = \sum_{n=1}^{M} \propto_n.\varphi(x) = w\varphi(x) \tag{3.40}$$

Where $\varphi(x)$ perform the nonlinear transformation and output is the linearly weighted sum of M. The decision function of SVM is described as:

$$y = f(x) = \sum_{n=1}^{N} \propto_n . k(x_n, x) + b \tag{3.41}$$

Where k is the kernel function. Proper choice of kernel function is necessary to make the data separable in feature space. While N, $\propto_n$ and b are the number of training data, objective function parameter, and the bias values, respectively. x and x_n are independent vector and the vector used in training, respectively.

3.4.2.3 Principal Component Analysis (PCA)

It is a method to pick principal components from the data and use these components to perform the change of basis on data. It transforms the set of correlated variables into small sets of variables which are not correlated and preserves most of the information of original data.

Let W be the input dataset where each column represents the sequence of n-dimensional input. The average of each function in a dataset is considered zero $E(W) = 0$. The original data matrix is represented with m samples and n variables as follows:

$$W = [w_1, w_2, \dots \dots . w_m]^T = \begin{pmatrix} w_{11} & \dots & w_{1n} \\ \vdots & \ddots & \vdots \\ w_{m1} & \cdots & w_{mn} \end{pmatrix} \tag{3.42}$$

Therefore, the orthonormal transformation z can be used to transform w to new space y as follows:

$$Y = ZW \tag{3.43}$$

The Y matrix elements are derived from the linear combination of W matrix elements, which translates the pattern of linkage between the samples. The Y covariance matrix is defined as:

$$C_Y = ZC_W Z^Y \tag{3.44}$$

Where C_W is the covariance of matrix W. The loading matrix Z can be found from the eigenvalue equation shown as:

$$(C_Y - \boldsymbol{\lambda} I)e_i = 0 \tag{3.45}$$

Pairwise covariance is stored between the various input variables. This equation performs the decomposition of covariance matrix eigenvectors and eigenvalues. The related eigenvectors describe the new orthogonal components known as principal components. In contrast, the corresponding eigenvalues determine the magnitude of these principal components. Putting all the eigenvectors and eigenvalues in descending order, the covariance of the first principal component is maximum.

3.4.3 Artificial neural network (ANN) for PV power output prediction

The ANN performs the computational simulation of neuron behavior in the human brain to generate results based on training data set learning to follow the pattern of human behavior. The ANN model can be expressed as

$$U_N = b + \sum_{j=1}^{N} (W_j \times I_j) \tag{3.46}$$

Where U_N, W_j , I_j, b, N are the final network output, connection weight, input number, bias weight, and a number of inputs, respectively.

In this study, a typical multi-layer feedforward neural network with Levenberg-Marquardt backpropagation (BP) algorithm is used. The back-propagation method is used to update the weights of hidden neurons. It refers to the error propagated from the output back to the input through the hidden layer. The LM method takes less time as compared to other algorithms. The algorithm is executed for many training cycles known as epochs to minimize the error and specifies the accuracy. The input layer of MLFNN consists of four inputs, while the hidden layer has ten neurons. The output layer represents one

output. The structure of the used ANN network is shown in Figure 3.4, while Table 3.3 shows certain defined parameters of the ANN model.

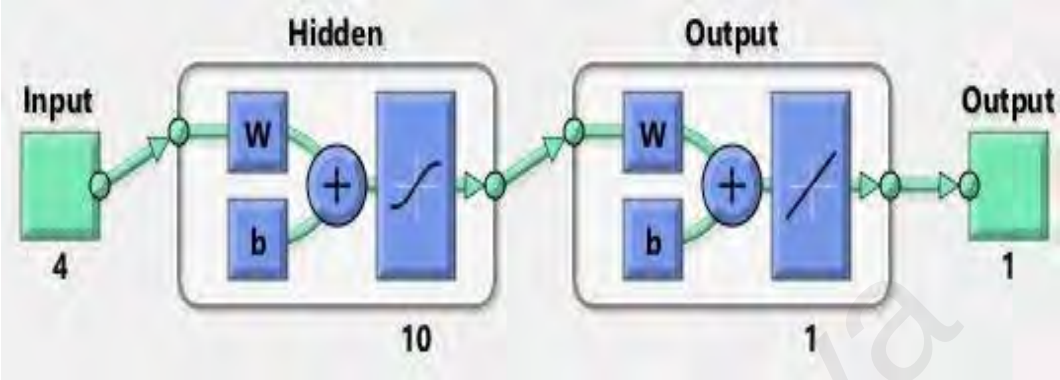

Figure 3.4:The structure of the ANN model

Table 3.3:Defined parameters for ANN

Learning rate	Momentum	Hidden Nodes	Number of iterations	Activation function
0.2	0.1	10	40-150	Continuous tangent-Sigmoid function

3.4.4 Adaptive neuro-fuzzy inference system (ANFIS) for PV power output prediction

ANFIS is a combination of ANN and fuzzy logic. It merges the FIS with a backpropagation neural network. This technique uses less search space by dividing the prior information into a certain number of subsets. The backpropagation algorithm is used to adjust the FIS parameters (Quej et al., 2017). In a first-order Takagi-Sugeno inference system with two fuzzy (IF/THEN) rules are used as follows (J.-S. R. Jang, Sun, Mizutani, & Computing, 1997):

Rule 1: If W is A, X is C, Y is E and Z is G, then

$$K_1 = p_1 W + q_1 X + r_1 Y + s_1 Z + t_1 \quad (3.47)$$

Rule 2: If W is B, X is D, Y is F and Z is H, then

$$K_2 = p_2W + q_2X + r_2Y + s_2Z + t_2 \quad (3.48)$$

Where W, X, Y and Z represents solar irradiance, ambient temperature, module temperature, and wind speed respectively, while K_i is PV power output in the fuzzy region. There are eight fuzzy sets from A-H. While p_i, q_i and r_i are the design coefficients which are decided during the process of training. In this study, the structure of the ANFIS model with four inputs (W, X, Y and Z), two rules, and one output K is presented in Figure 3.5.

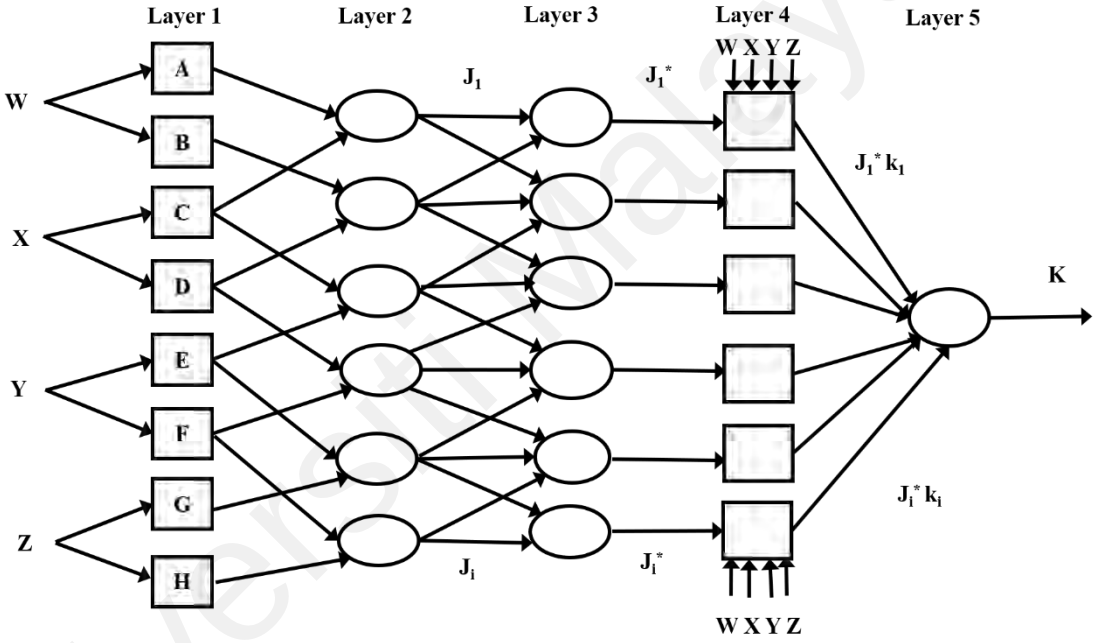

Figure 3.5: The structure of ANFIS with four inputs, two rules, and one output

The ANFIS structure has five layers named: fuzzy layer, product layer, normalized layer, de-fuzzy layer, and total output layer (Quej et al., 2017). Layer 1 has the output of the i^{th} node designated as $O_{1,i}$. The variables in the first layer are called premise variables. There are input variable membership functions (MFs) in the first layer. This layer transfers the input values to the next layer. Following node functions are used for every node i.

$$\begin{aligned} O_{1,i} &= \mu_{Ai}(W) \quad for\ i = 1,2 \\ O_{1,i} &= \mu_{Ci-2}(X) \quad for\ i = 3,4 \\ O_{1,i} &= \mu_{Ei-2}(Y) \quad for\ i = 5,6 \\ O_{1,i} &= \mu_{Gi-2}(Z) \quad for\ i = 7,8 \end{aligned} \tag{3.49}$$

Where W, X, Y and Z are the inputs to node i. While A_i, C_{i-2}, E_{i-2} and G_{i-2} are the linguistic label (e.g. 'small' or 'large') represented by suitable membership functions (MFs) $\mu_{Ai}(W)$, $\mu_{ci-2}(X)$, $\mu_{Ei-2}(Y)$ and $\mu_{Gi-2}(Z)$. The Gaussian membership function is used for each input variable. It is selected based on an arbitrary process of testing all member functions. The Gaussian MF is given as follows.

$$\mu_{Ai}(W) = e^{\frac{-(W-c)^2}{2\sigma^2}} \tag{3.50}$$

The Gaussian function adjusts itself according to variation of the variables presenting various membership functions for fuzzy set A. The second layer is the product layer which uses the rule operators (AND/OR) to generate the product of incoming inputs.

$$O_{2,i} = J_i = \mu_{Ai}(W) * \mu_{Ci-2}(X) * \mu_{Ei-2}(Y) * \mu_{Gi-2}(Z) \qquad for\ i = 1,2 \tag{3.51}$$

Where $O_{2,i}$ is the output of the second layer, while J_i represents the firing strength of the rule. The third layer is a normalized layer which provides the ratio of individual firing strength of rule i to sum of firing strengths for all rules. Therefore, this layer has normalized outputs, which are described as:

$$O_{3,i} = J_i^* = \frac{J_i}{J_1 + J_2} \tag{3.52}$$

Where $O_{3,i}$ and J_i^* are the third layer output and normalized firing strength, respectively. The fourth layer is a de-fuzzy layer. It provides weighted output because of the inference rules applied based on consequent parameters. Every node in this layer is an adaptive node.

$$O_{4,i} = J_i^*.K_i = J_i^*.(p_i W + q_i X + r_i Y + s_i Z + t_i) \tag{3.53}$$

Where $O_{4,i}$, J_i^* and K_i are fourth layer output, normalized firing strength from layer 3, and weighted sum, respectively. While p_i, q_i, r_i, s_i and t_i are the consequent parameters. Finally, the fifth layer combines all the inputs from the de-fuzzy layer and converts fuzzy data into the estimated overall output denoted as $O_{5,i}$.

$$O_{5,i} = \sum_i J_i^*.K_i = \frac{\sum_i (J_i.K_i)}{\sum_i J_i} \tag{3.54}$$

The information travels up to layer 4, where the least square regression method is used to optimize the consequent parameters. The error value propagates through the feedback or backward path. The gradient descent (GD) method is used to update the premise variables (J.-S. R. Jang et al., 1997). The overall output in Figure 3.5 can be rewritten as:

$$\begin{aligned} K_{output} = {} & (J_1^*.W)p_{1+}(J_1^*.X)q_1 + (J_1^*.Y)r_1 + (J_1^*.Z)s_1 + (J_i^*)t_1 \\ & + (J_2^*.W)p_{2+}(J_2^*.X)q_2 + (J_2^*.Y)r_2 + (J_2^*.Z)s_2 + (J_2^*)t_2 \end{aligned} \tag{3.55}$$

Three ANFIS methods used to generate the Takagi-Sugeno fuzzy inference structure; are described as follows:

3.4.4.1 Grid partitioning

The grid partitioning method divides the input into various spaces by using the axis paralleled method in which each input represents a fuzzy MF. The MF is evenly distributed for each input. The fuzzy rule base contains one rule for each input member function combination. Table 3.4 represents the parameters for grid portioning ANFIS.

Table 3.4:Parameters for Grid partitioning ANFIS

No. of MFs	Input MF	Output MF	Number of epochs	Initial Step size	Step size decrease rate	Step size increase rate
2	Gaussian	Linear	100	0.01	0.9	1.1

3.4.4.2 Subtractive clustering

In this method, data clusters are used to derive the rules and membership function to generates a Sugeno fuzzy system. There is one gaussian input MF for each input variable and one linear output MF for each output variable. Each fuzzy cluster has one rule. Table 3.5 describes the parameters of subtractive clustering ANFIS.

Table 3.5: Parameters for Subtractive clustering ANFIS

Influence radius	Number of epochs	Initial Step size	Step size decrease rate	Step size increase rate
0.55	100	0.01	0.9	1.1

3.4.4.3 Fuzzy cluster means (FCM)

In this method, data clusters are used to derive the rules and membership function to generate a Sugeno fuzzy system. Each input variable has one gaussian input MF. In contrast, each output variable has one linear output MF for Sugeno fuzzy system and gaussian MF for the Mamdani systems. Each fuzzy cluster has one rule. Table 3.6 elaborates the parameters for the FCM ANFIS model.

Table 3.6: Parameters for FCM ANFIS

No. of clusters	Partition matrix exponent	Iterations	Number of epochs	Initial Step size	Step size decrease rate	Step size increase rate
10	2	100	100	0.01	0.9	1.1

3.4.5 Proposed deep learning (RNN-LSTM) method for PV power output prediction

ANN lacks the time correlation approach and performs direct mapping between input and output data. Therefore, the application of ANN in time series forecasting is limited. To overcome this drawback, RNN built up sequence to sequence mapping by adding up

cyclic connections to neurons. The input of the previous time step affects the output of each time step (LeCun, Bengio, & Hinton, 2015; Shalev-Shwartz & Zhang, 2016). The basic structure of the RNN and its unfolded version is shown in Figure 3.6.

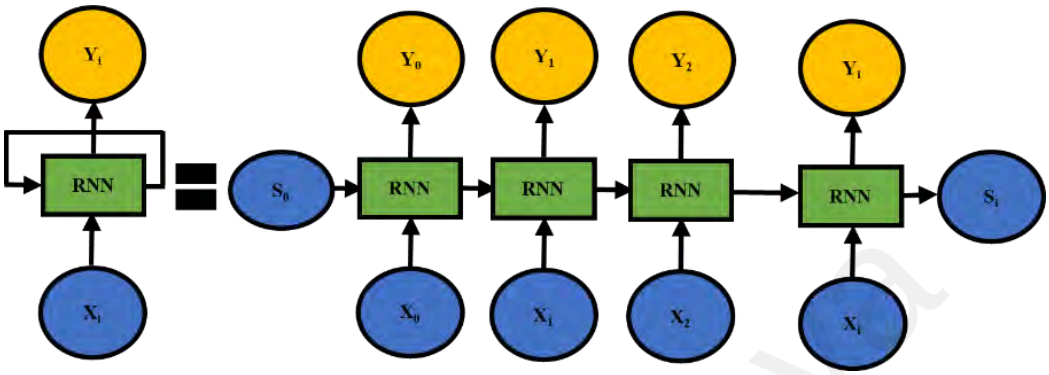

Figure 3.6: A basic RNN and unfolded version

In the training of RNN, both forward and backward passes are involved. The forward pass of RNN is the same as MLP ANN with a single hidden layer, except the activation of the hidden layer from the current inputs and previous time steps. The weights of RNN are adjusted by backward pass, known as backpropagation through time (BPPT). BPPT comprises repetitive usage of the chain rule like standard backpropagation.

The RNN has an important feature of using contextual information for mapping between input and output. However, the range of context is limited for standard RNN architectures. The RNN loses the most deleted input information. However, the problem of gradient vanishing is there in RNN like ANN. When the back-propagation phenomena update the parameters, they are also optimized in a negative way. As a result, the gradient vanishes, and the network is not updated. As a remedy, the long-short term memory (LSTM) is proposed to enhance the performance of the traditional RNN model (Zheng et al., 2020).

The RNN-LSTM is proposed to overcome the issues faced by regression, ANN, ANFIS, and machine learning techniques. Figure 3.7 describes the layered structure of

RNN-LSTM. The proposed model is based on four layers named as sequence input layer, LSTM layer, fully connected layer, and regression output layer. The four inputs (solar radiation, wind speed, ambient, and module temperatures) with the one-hour resolution are induced in the sequence input layer, with each input shown by a sole circle for 12 hours a day. Layer 2 is the LSTM layer in cascade with a fully connected layer to enhance the performance of the model. The LSTM layer considers several hidden units, while a number of responses are shown by the fully connected layer. Finally, the output is recorded in the regression layer. The power output of each PV system is the output response.

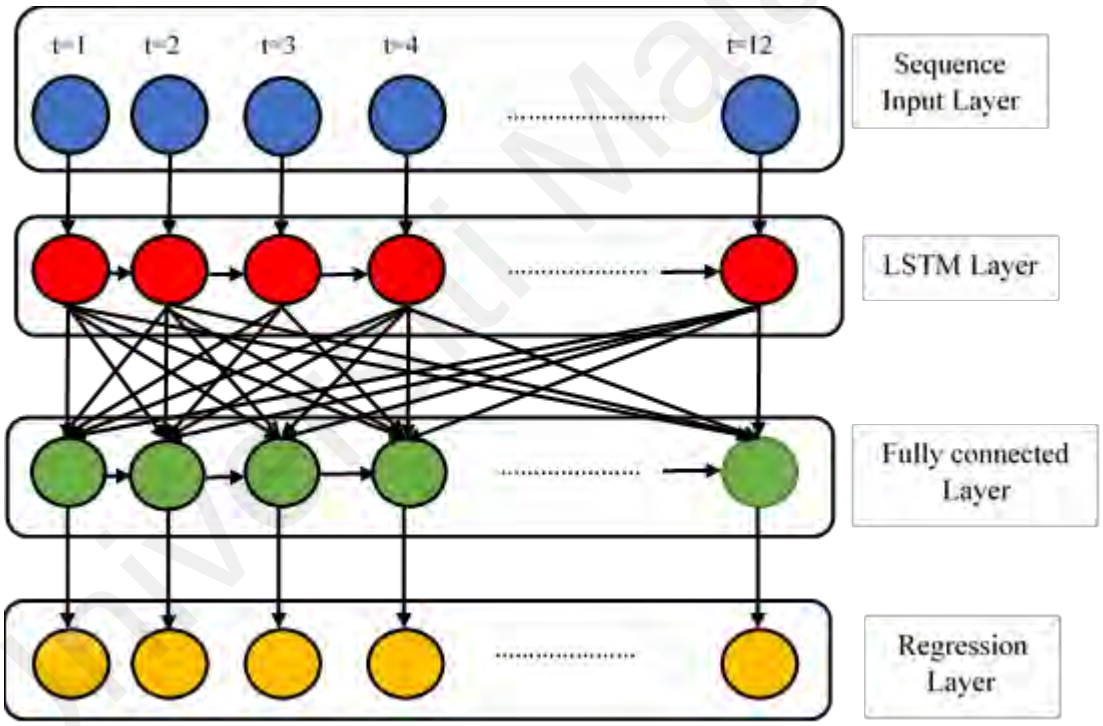

Figure 3.7: The Layered structure of the proposed RNN-LSTM model

The hyperparameters selection is based on the hit and trial method to achieve better forecasting accuracy of the proposed model. The hyperparameters considered are (1) the number of hidden units; (2) the maximum number of epochs; (3) initial learn rate; (4) learn rate drop period; (5) learn rate drop factor. Different LSTM structures are also

investigated for each PV plant based on 2019 data to choose the best structure. The structure of the basic LSTM cell is also described as follows:

3.4.5.1 A Basic LSTM Structure

Figure 3.8 describes the basic LSTM cell structure. The subnets in RNN-LSTM are known as memory units. Every memory unit has one or more memory cells and three units known as input, output, and forget gates. These three gates are affected by x(t) and h(t-1).

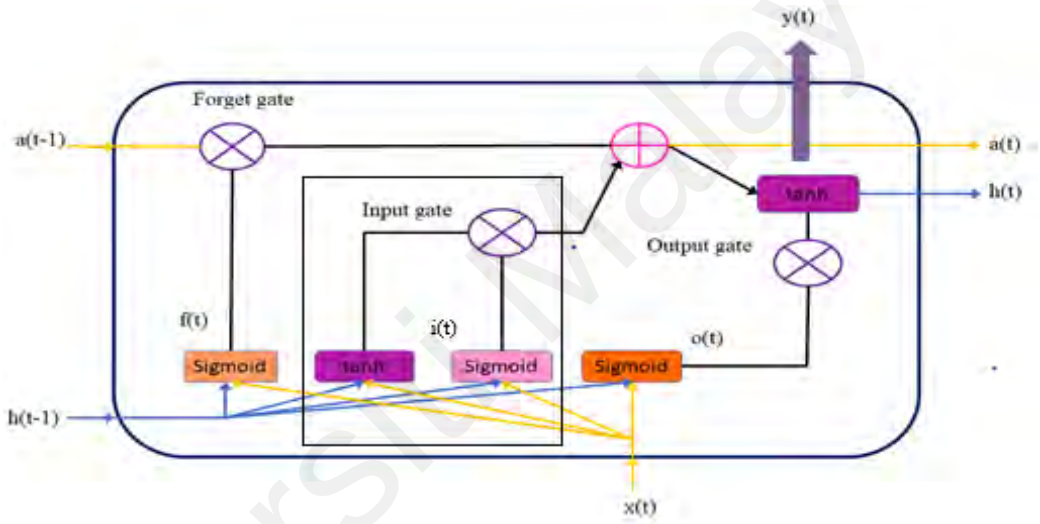

Figure 3.8: **A basic LSTM cell structure**

The output coefficient value of these gates varies between 0 and 1 by the activation function, known as the sigmoid function. This function controls the flow of information and is defined as:

$$\sigma = \frac{1}{1 + e^{-x}} \tag{3.56}$$

The following steps describe the functionality of the basic LSTM cell.

i. The elimination of the stored information from the last cell state a(t-1) is decided by the LSTM cell. The forget gate takes x(t) and h(t-1) on its

activation and generated output for the last cell state a(t-1). The output is zero (delete the information) and 1 (keep the information) totally in the memory cell. The f(t) is determined in the following equation

$$f(t) = \sigma[w_{xf}.X(t) + W_{hf}.h(t-1) + b_f] \tag{3.57}$$

ii. The information to be stored in the cell has two parts. The input x(t) and previous state h(t-1) are transformed into new information $\overline{a(t)}$ by the activation function (tanh). Second, the input gate gives the values between 0 and 1 to decide part of new information. These two pieces of information are mixed to decide about the upcoming state.

$$\tanh(x) = \frac{e^{x} - e^{-x}}{e^{x} + e^{-x}} \tag{3.58}$$

$$\overline{a(t)} = \tanh(w_{xc}.X(t) + W_{hf}.h(t-1) + b_c) \tag{3.59}$$

$$\mathrm{i(t)} = \sigma(W_{xi}.X(t) + W_{hi}.h(t-1) + b_i) \tag{3.60}$$

iii. In this step, the new cell state is updated using the information from the previous steps. The f(t) is multiplied with the previous state a(t-1) by losing the information in the first step. The resultant information is multiplied with input. Both components are added to decide the next state a(t), as shown in eq (3.61)

$$a(t) = f(t) * a(t-1) + i(t) * \overline{a(t)} \tag{3.61}$$

iv. This step decodes the final output. The hidden state h(t) is found by multiplying the combination of a(t)*tanh and o(t) to store the valuable information. The output is decided by the output gate. The equation for o(t), h(t), and y(t) are described as follows:

$$o(t) = \sigma\left(W_{xo}.X(t) + W_{ho}.h(t-1) + b_o\right) \quad (3.62)$$

$$h(t) = o(t) * \tanh\left[a(t)\right] \quad (3.63)$$

$$y(t) = \sigma\left(W_{hy}.h(t) + b_y\right) \quad (3.64)$$

W_{xf}, W_{xi}, W_{xo}, W_{xc} and W_{hf}, W_{hi}, W_{ho}, W_{hc} are the matrices which represent inputs recurrent weights, respectively. While W_{hy} is the weight bias for hidden output. The relevant bias vectors are b_f, b_i, b_o, b_c and b_y. The training of LSTM neurons is also performed by forward and backward passes. The BPTT method is used for updating the neuron weight. In this method, x(t) is the input data, and y(t) is PV power output.

3.4.5.2 Multilayered LSTM Structures

In basic LSTM, one hidden layer is used like ANN. In that hidden layer, a certain number of hidden units are incorporated. Following the theme of deep learning, more than one layer is added to observe the behavior of different LSTM structures to select the best one with the highest prediction accuracy. Figure 3.9 elaborates a two-layered LSTM structure. The first layer output behaves as the next layer input for the same moment. The information is transferred in the forward direction only in these multi-layered LSTM structures.

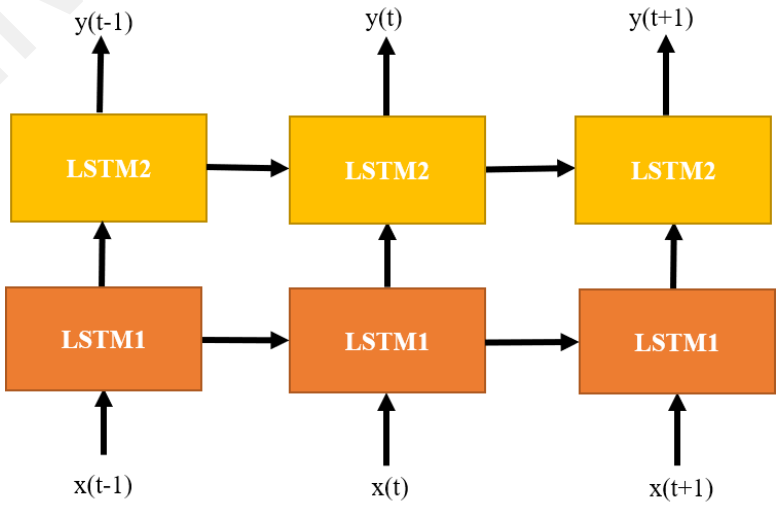

Figure 3.9: Double layered LSTM

Figure 3.10 describes bi-directional LSTM, which represents both forward and backward transmission of information connected with the output layer. With the help of bi-LSTM, the whole previous and incoming information for each input sequence can be delivered to the output layer.

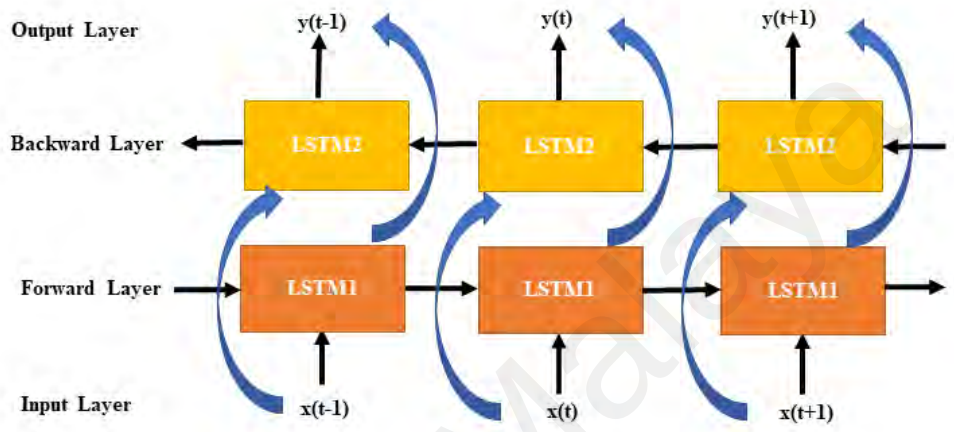

Figure 3.10: Single layered Bi-LSTM

3.4.6 Measurement indices for the evaluation of model performance

The measurement indices used for the evaluation of the prediction model are given as follows:

a) Root mean square error (RMSE)

$$RMSE = \sqrt{\frac{1}{N}\sum_{i=1}^{N}(X-Y)^2} \tag{3.65}$$

b) Mean square error (MSE)

$$MSE = \frac{1}{N}\sum_{i=1}^{N}(X-Y)^2 \tag{3.66}$$

c) Mean absolute error (MAE)

$$MAE = \frac{1}{N}\sum_{i=1}^{N}|(X - Y)| \tag{3.67}$$

d) Correlation coefficient (r)

$$r = \frac{\sum_{i=1}^{N}\left[\left(X - X_{avg}\right) * \left(Y - Y_{avg}\right)\right]}{\sqrt{\sum_{i=1}^{N}(X - X_{avg})^2 * \sum_{i=1}^{N}(Y - Y_{avg})^2}} \tag{3.68}$$

e) Coefficient of determination (R^2)

$$R^2 = 1 - \frac{\sum_{i=1}^{N}(X - Y)^2}{\sum_{i=1}^{N}(Y - Y_{avg})^2} \tag{3.69}$$

Where X and Y are the predicted and actual values, respectively, while X_{avg} and Y_{avg} are the average of predicted and actual values, respectively. RMSE indicates the deviation of the predicted value from the actual value. The MSE elaborates the mean square deviation between predicted and actual values. The MAE is the mean absolute error which indicates the absolute value of the average difference between predicted and actual values. The correlation coefficient (r) provides the strength and the direction of the linear relationship between two variables. It ranges between -1 and +1. A value of +1 indicates a strong correlation, while -1 shows a weak correlation. A value of r=0 provides no correlation between two variables. The coefficient of determination (R^2) provides the percentage deviation in Y, which is explained by all the X variables together. It ranges between 0 and 1. It shows the strength of the linear regression model. It is equivalent to the square of the correlation coefficient. Higher the value of R^2, data points are less scattered along the regression line. For the optimum performance model, higher the values of r and R^2 and lower the values of RMSE, MAE, MSE, MBE.

3.4.7 Optimization algorithms

In this research, three optimization algorithms are used to optimize the hyperparameters of the proposed deep learning method (RNN-LSTM) for an hour ahead

forecasting of PV power output to enhance its forecasting performance. The applied optimization algorithms are Genetic Algorithm (GA), Particle swarm optimization (PSO), and Salp swarm algorithm (SSA). Two and three months data is considered to optimize the hyperparameters but it has given inferior results and also increased the computational burden. The data in three different quarters of the year is also experimented to optimize the hyperparameters, but it has shown almost similar results. Therefore, the January data of each year is used to optimize the hyperparameters of the deep learning method (RNN-LSTM) for proper comparison of all three optimization algorithms. The remaining eleven months data is used for the optimal LSTM model to predict the PV power out. This remaining data is further divided into training (70%) and testing sets (30%).

The optimized hyperparameters extracted from GA, PSO, and SSA algorithms are used by the remaining data for training, validation, and testing purpose to evaluate the performance of optimization algorithms. The performance of these optimization algorithms is evaluated on annual data for four years (2016-2019) duration, based on improved forecasting accuracy and fast convergence speed. The population size and number of iterations are 5 and 40 in all three optimization algorithms to compare their performance equally. The selection of these two parameters is also based on higher forecasting accuracy and less computational burden.

The hyperparameters (decision variables), their constraints, and the objective function are described as follows:

$$Decision\ variables = [x_1, x_2, x_3, x_4, x_5] \tag{3.70}$$

Where

$$x_1 = \text{N}umber\ of\ hidden\ units \tag{3.71}$$

$$x_2 = \text{Maximum number of epochs} \tag{3.72}$$

$$x_3 = Learn\ rate\ drop\ period \tag{3.73}$$

$$x_4 = Initial\ learn\ rate \tag{3.74}$$

$$x_5 = Learn\ rate\ drop\ factor \tag{3.75}$$

The constraints of the hyperparameters for all three optimization algorithms are given as follows:

$$80 < x_1 < 250 \tag{3.76}$$

$$200 < x_2 < 400 \tag{3.77}$$

$$50 < x_3 < 200 \tag{3.78}$$

$$0.0001 < x_4 < 0.01 \tag{3.79}$$

$$0.002 < x_5 < 1 \tag{3.80}$$

$$\text{Objective function} = \text{Minimize}\ \{\text{RMSE in (Eq. 3.65)}\} \tag{3.81}$$

3.4.7.1 Genetic Algorithm (GA)

In this study, GA is used to choose the optimum hyperparameters for the best LSTM structure. Table 3.7 shows the parameters selected for the operation of GA. Figure 3.11 describes the flowchart of GA for this purpose. The main steps of GA are described as follows:

Table 3.7:Parameters for GA

Genetic operator	Selection pressure	Crossover percentage	No. of offspring	Mutation percentage	Number of mutants	Mutation rate
Roulette wheel	8	0.7	4	0.3	2	0.1

(a) ***Population Initialization***

The generation of the initial population is random, which allows the whole range of possible solutions in search space. All the solutions in the search space are transformed into binary strings. The size of the population is also dependent on the nature of the

problem. In this research, every individual of the population has five hyperparameters which need to be optimized. The objective function is to minimize the testing RMSE.

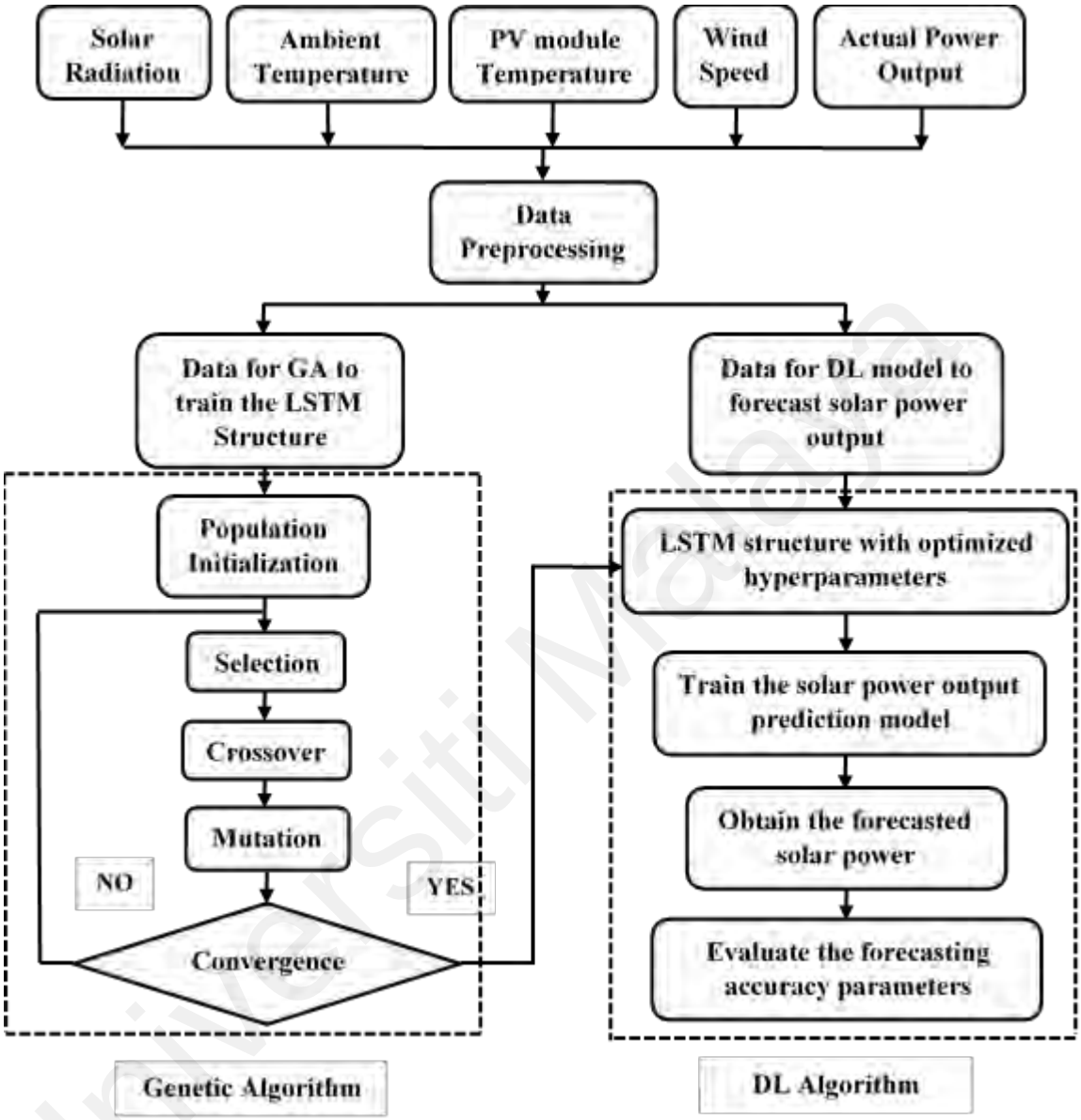

Figure 3.11: The GA flowchart

(b) ***Selection***

The selection operator is based on the survival of the fittest principle to find the best chromosomes to be transferred to the next stage. The selection chances for individuals with better fitness are higher than those with poor fitness. The GA evolves from generation to generation.

(c) ***Crossover***

Crossover is a genetic operator which generates new children based on the recombination of two parents. There are different types of crossovers: single point, two-point and uniform crossover. In a single-point crossover, the portions to the right side of the crossover point are exchanged with each other. Two-point and k-point crossovers are equivalent to two single point and k single point crossovers. While, in the uniform crossover, the probability of choosing each binary bit from either parent is equal.

(d) ***Mutation***

The mutation changes one or more binary values in a chromosome from its initial state. As a result, the new solution becomes entirely different from the previous solution. The mutation probability is kept low to avoid the random search. Based on the mutation rate, the binary values are changed from 1 to 0 or 0 to 1. It maintains the genetic diversity from one generation to the next.

(e) ***Convergence***

The GA continues in the loop until when an optimal solution is found, or a maximum number of iterations are exceeded. The best position will provide the optimum parameters for LSTM structures. The best cost will converge to the optimal value.

3.4.7.2 Particle Swarm Optimization (PSO)

In this research, PSO is also used to find the optimal hyperparameters for developed deep learning technique. The objective function is testing RMSE. The process is described as follows.

(a) ***Initialization***

In this first step, the size of the population (swarm size) is finalized. After that, first-generation is formed from the generation of several particles. The swarm size considered

is 5. Each candidate of the first generation has five hyperparameters information: hidden units, epochs, initial learn rate, learn rate drop period, and learn rate drop factor. Each particle has its own specific position and velocity.

(b) ***Fitness estimation***

The purpose of the PSO application is to reduce the training loss of the objective function (testing RMSE) to enhance the forecasting accuracy of the deep learning technique. Therefore, the training loss of each particle is evaluated for the PSO-RNN-LSTM model.

(c) ***Optimal values***

Two optimal values are evaluated in each iteration, one for the individual and the other for the population. Based on this optimal information, the particles are updated. The optimal values are dependent directly on training loss. The minimum value of training loss relates to optimal values.

(d) ***Position and velocity update***

The position and velocity of each particle are updated by having the information of two optimal values of the individual and population. As a result, a new generation is produced.

(e) ***Termination***

A certain minimum number of iterations are compulsory to find the optimal position. The best particle position is obtained by increasing the number of iterations. However, it also increases the computational burden. Therefore, a tradeoff is required between the number of iterations and convergence of particle position. At the end, finding the optimal individual value, the hyperparameters of the RNN-LSTM are deduced from it. Table 3.8

shows the parameters of the PSO algorithm. Figure 3.12 describes the flowchart of the PSO algorithm.

Table 3.8: The Parameters of PSO

Inertia weight (w)	Inertia weight damping ratio (w_{damp})	Personal learning coefficient (c_1)	Global learning coefficient (c_2)
1	0.99	1.5	2

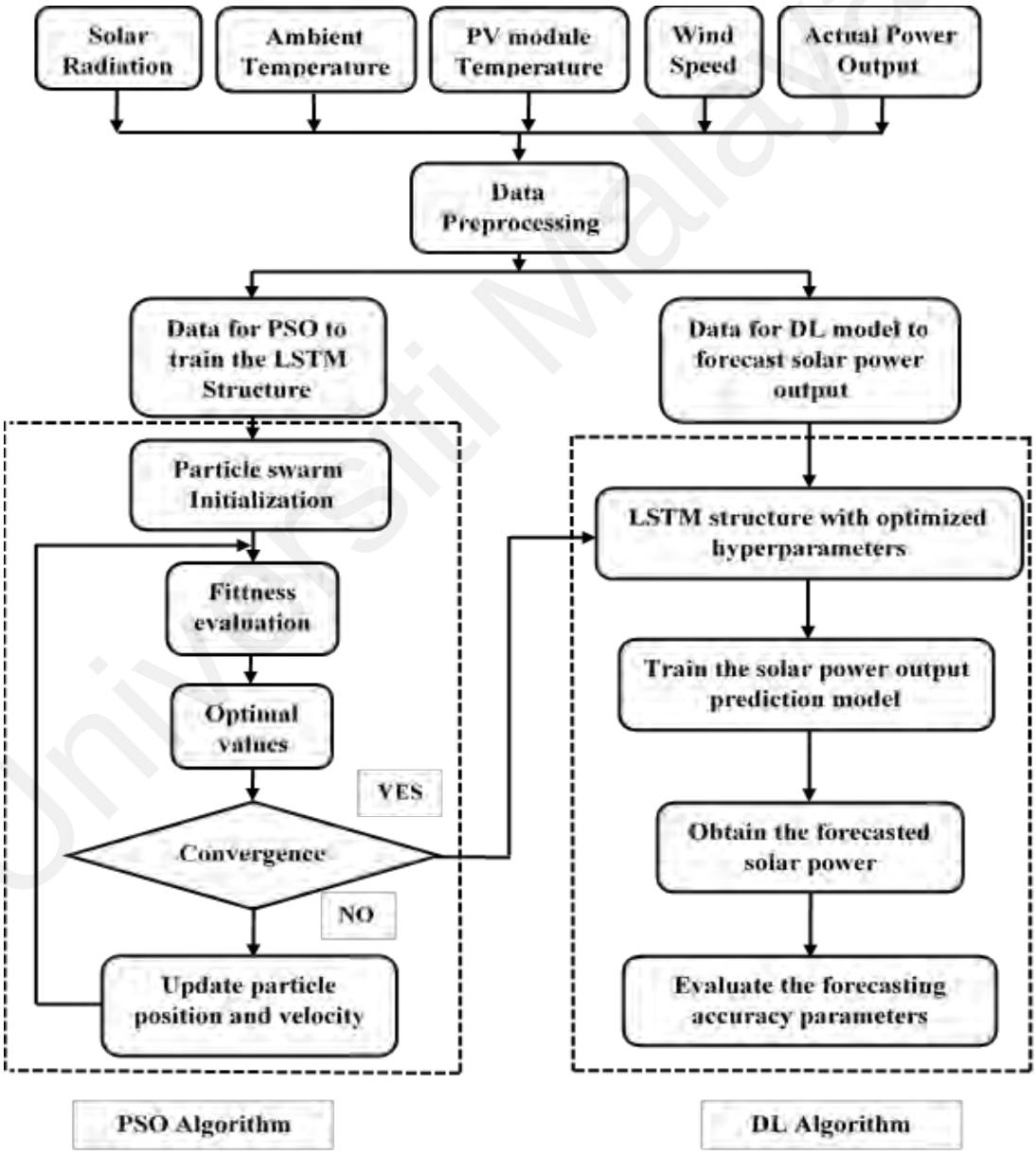

Figure 3.12: The PSO flowchart

3.4.7.3 Salp Swarm Algorithm (SSA)

The Salp swarm algorithm is an advanced optimization algorithm based on the salp population developed in 2017 (Mirjalili et al., 2017). The movement of salp is similar to jellyfish in which water is injected through the body as propulsion to proceed ahead. The salp population is partitioned into two groups. In one group, the salp individual that leads the whole swarm population is known as the leader, while the remaining salps are deemed as followers. It is the sole responsibility of the leader to guide the followers to a better position with its successive move. The leader updates its position by using the following equation,

$$T_j^1 = \begin{cases} K_j + b_1\left(\left(ub_{j\_} - lb_j\right)b_2 + lb_j\right) & b_3 \geq 0 \\ K_j - b_1\left(\left(ub_{j\_} - lb_j\right)b_2 + lb_j\right) & b_3 < 0 \end{cases} \quad (3.82)$$

Where T_j^1 and K_j indicates the leader and food source position in j^{th} direction, the upper and lower dimensions are shown by ub_j and lb_j, while b_1, b_2 and b_3 are random numbers. b_1 is the key parameter in SSA that makes the follower salps able to grab the food source efficiently.

$$b_1 = 2e^{(\frac{-4m}{M})^2} \quad (3.83)$$

where $\frac{m}{M}$ is the ratio of recent iteration to the total number of iterations. The random numbers generated between 0 and 1 are allocated to b_2 and b_3 to decide the next position in the j^{th} dimension along with the step size. The position of the salp followers is updated by using the following equation

$$T_j^i = \frac{1}{2}at^2 + v_0t \quad (3.84)$$

where $i \geq 2$ and T_j^i shows the follower's position. While t and v_0 are the time and initial velocity of the salp follower. The simplest form of the above equation is as follows

$$T_j^i = \frac{T_j^i + T_j^{i-1}}{2} \tag{3.85}$$

By exploration and exploitation of the defined search space, the follower salp chases the leader salp to retrieve the global optimum, which is the actual food source traced by the leader salp. The key features of SSA are described as follows (Mirjalili et al., 2017):

1. After each iteration, the algorithm retains the best solution and allocates it to the accessible food source. Therefore, it is not be erased even if the entire population gets worse.
2. This algorithm updates the leading salp position with respect to the food source only, which is the best solution; therefore, the leader salp discovers and utilizes the search space around it.
3. It renews the status of the follower salps with respect to each other, so they move gradually towards the leading salp.
4. The SSA avoids the local minima problem due to the slow movement of the follower salps.
5. At the start of the iteration, the parameter b_1 is decreased adaptively, which copes with the algorithm to discover the search space at the start phase and use at the finishing phase.
6. The SSA is less complex because it has only one main control parameter (b_1) and can be executed efficiently.

In this research, the SSA is used to give the best solution about five hyperparameters (hidden units, epochs, initial learn rate, learn rate drop period, and learn rate drop factor) of developed deep learning technique and a best optimal value of the objective function (testing RMSE). The adaptive nature of SSA ensures to avoid local minima problems and

allows to find the global solution. The parameters of SSA are given in Table 3.9. Figure 3.13 elaborates the flowchart of the SSA algorithm.

Table 3.9: The Parameters of SSA

Search Agents	No of variables	Objective function	No of iteration
5	5	Testing RMSE	40

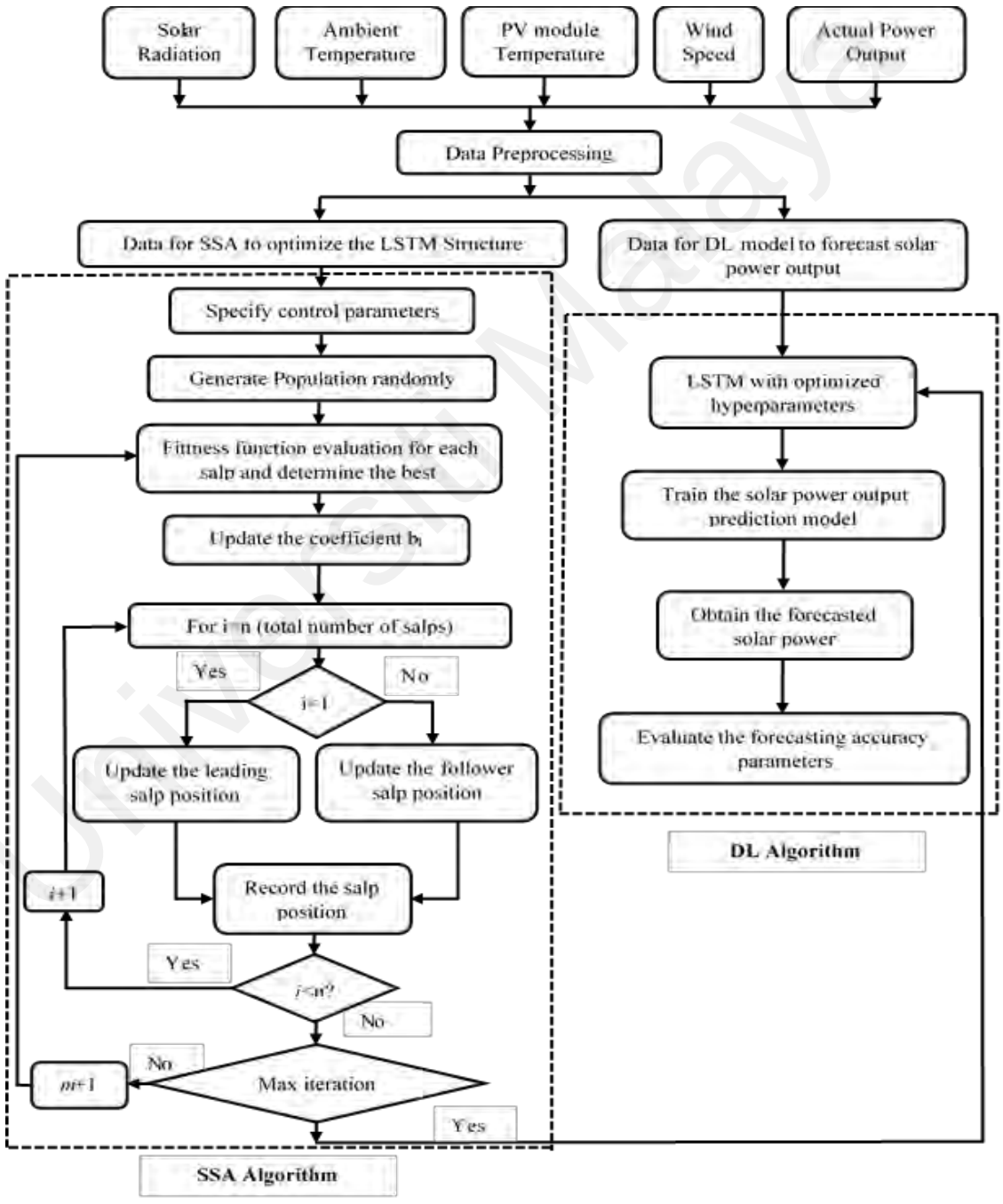

Figure 3.13: The flow chart for SSA

3.5 Summary

This chapter begins with the description of the three different grid-connected PV systems installed at the rooftop of the engineering tower UM followed by the data collection. The performance parameters, such as AC energy output, system yields, capacity factor, system efficiencies, PV array losses, PV system losses, and performance ratio, are illustrated to evaluate the performance of three grid-connected PV systems. Moreover, the methodology for forecasting the PV power output is elaborated in the next section. Data is preprocessed prior to be used for forecasting purpose. The forecasting methods such as regression [GPR, SVR, GPR(PCA) and SVR(PCA)], artificial neural network, ANFIS (grid partitioning, subtractive clustering, and FCM) are presented along with the proposed deep learning method (RNN-LSTM) for an hour ahead forecasting of PV power output on an annual basis for three PV systems over the duration (2016-2019). Furthermore, the performance parameters used for the evaluation of forecasting accuracy are mentioned. These performance parameters assess the accuracy of forecasting techniques by evaluating the difference between predicted and actual value. In addition, the methodology for three optimization algorithms (GA, PSO, and SSA) is described in detail to tune the parameters of the developed deep learning technique (RNN-LSTM) to improve its forecasting accuracy.

CHAPTER 4: RESULTS AND DISCUSSIONS

4.1 Introduction

This chapter presents the implementation of the proposed methodology on three grid-connected PV systems and discusses their results according to the research objectives. Monthly and annual performance analysis based on eleven performance parameters is executed for three different PV systems over four years of recorded data to decide about the most feasible PV system for the tropical climate of Kuala Lumpur, Malaysia. Moreover, the environmental impact of the composite PV system by avoiding CO_2 emission is also elaborated. An hour ahead forecasting of power output for three PV systems based on the proposed deep learning (RNN-LSTM) method is performed on an annual basis for four years data period. The forecasting results of the proposed method are also compared with regression (GPR, GPR (PCA)), machine learning (SVR, SVR (PCA)), ANN, and hybrid (ANFIS (GP, SC, FCM)) techniques. Moreover, the forecasting results of the developed deep learning method are further optimized on an annual basis using SSA and other optimization algorithms such as GA and PSO for three PV systems over the duration (2016-2019). These optimization algorithms are compared based on forecasting accuracy measurement parameters (RMSE, MAE, MSE, and R^2), convergence speed. In addition, the prediction results of three hybrid deep learning algorithms along with the basic proposed method (RNN-LSTM) are presented for all three different PV systems over four years period.

4.2 Performance analysis results for three different PV systems

The performance of the three different grid-connected PV systems is analyzed over four years recorded data period (2016-2019) based on eleven parameters. These parameters are total AC (E_{AC}) and DC energy (E_{DC}) outputs (kWh), performance yields [reference yield (Y_R), array yield (Y_A), and final yield (Y_F)] (kWh/kWp), system efficiencies [inverter efficiency, array efficiency, and system efficiency] (%), CF (%),

system losses [(array losses, system losses, and overall losses) (L_s)] (kWh/kWp) and PR (%).

4.2.1 Temperature effects on PV current and voltage

Figure 4.1 and Figure 4.2 describe the module temperature effects on PV voltage and current for one type of PV module at several intensities of solar irradiances. The maximum module temperature was 61.36 ℃, which occurred at solar irradiance of 884.8 W/m^2. The maximum difference between a module and ambient temperatures was 22.58℃. In Kuala Lumpur, the average daily ambient and module temperatures were 31.3℃ and 37.2℃, respectively, for the examined period. The monthly average module temperature changed from 33.7 ℃ in November to 40.7 ℃ in March. While the monthly average ambient temperature changed from 29.8 ℃ in November to 33.1 ℃ in March.

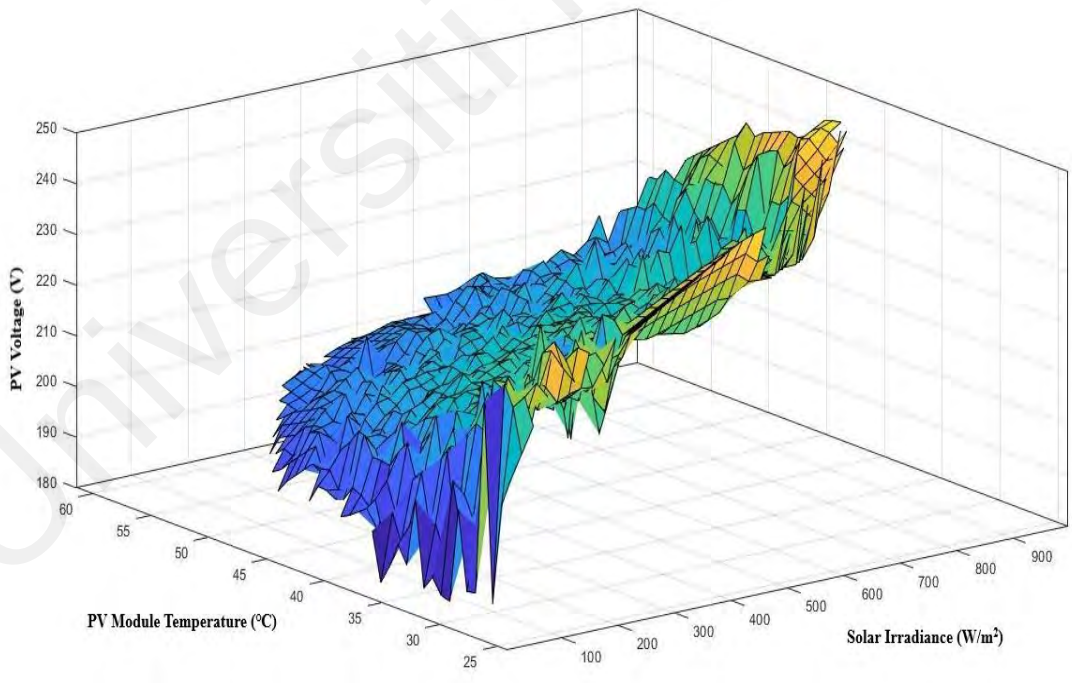

Figure 4.1: The module temperature effects on PV voltage at several intensities of solar irradiances

It can be perceived from Figure 4.1 that the PV voltage decreases slightly with the rise of module temperature at a certain solar irradiance level. The PV current is observed to

increase with the increase in module temperature at the same solar irradiance level, as revealed in Figure 4.2. At solar irradiance of 700W/m^2, the PV voltage decreases from 218.3 V to 209.5 V, and PV current rises from 9.38 A to 9.94 A as module temperature rises from 41.2 ℃ to 55.3 ℃. It indicates almost no power loss due to a rise in temperature.

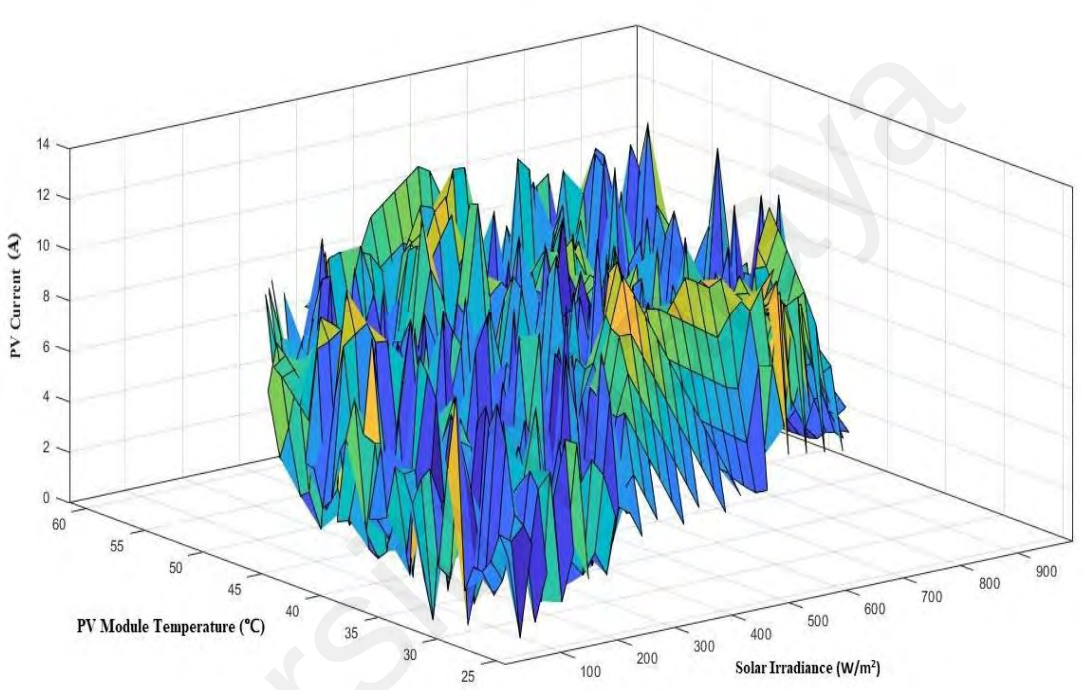

Figure 4.2: The module temperature effects on PV current at several intensities of solar irradiances

The PV voltage is decreased from 221.4 V to 206.8 V, and PV current has a rise from 2.02 A to 12.4 A at solar irradiance levels ranging from 100 W/m^2 to 900 W/m^2, respectively. An increase in PV module temperature is observed at solar irradiance levels between 600 W/m^2 and 900 W/m^2. 75 % of overall in-plane solar irradiance is below 600 W/m^2 with the highest module temperature of 42.4 ℃, which indicates a little effect of high module temperature on PV voltages and currents to acquire the maximum output power. The MPPT is also available in each inverter to track the maximum power point throughout the entire monitored period.

4.2.2 AC energy output

The monthly average AC energy output is depicted in Figure 4.3 for all PV systems over the observed period of four years. The solar radiation is ranging from 100.7 kWh/m^2 in November to 130.4 kWh/m^2 in March, showing a strong relationship with AC energy produced. The monthly average AC energy generated is ranging from (239.7-319.3) kWh, (181.3-229.6) kWh, (105.7-105.7) kWh, and (526.4-677.9) kWh, from November to March for a-s_i, p-s_i, m-s_i, and composite PV systems, respectively. The monthly average AC energy is perceived to be high for all three PV systems, from December to April, due to high solar radiation in these months. However, it is found low for all three PV systems, from May to November, due to less solar radiation in the rainy season.

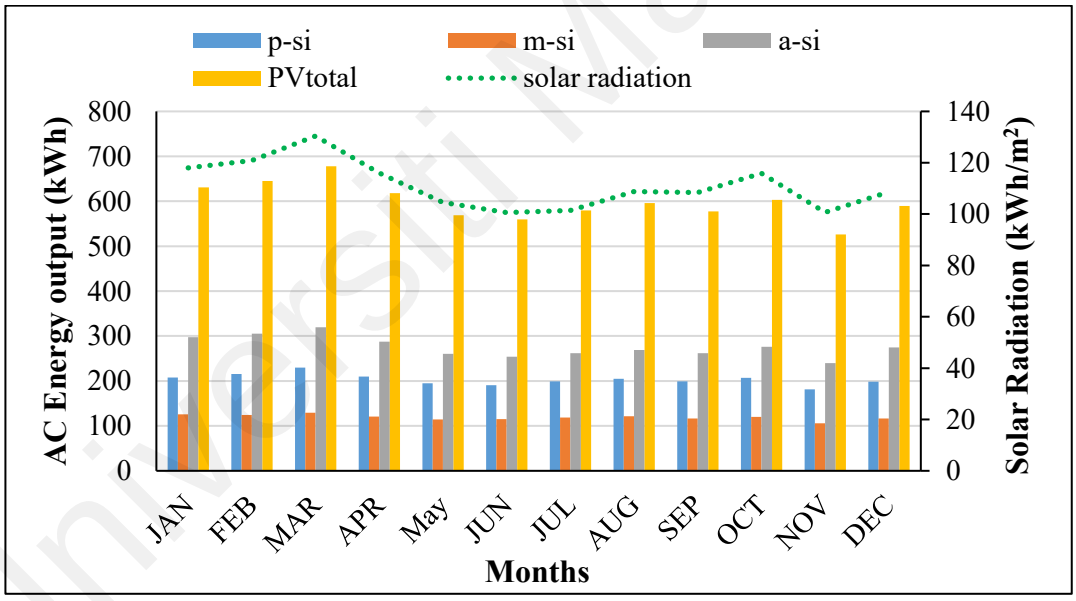

Figure 4.3: Monthly average AC Energy output and solar radiation for different PV systems over the period 2016-2019

Figure 4.4 describes the annual AC energy output for different PV systems over the period (2016-2019). The annual average AC energy generated is 3293.2 kWh, 2435.8 kWh, 1425.6 kWh, and 7179.5 kWh for a-s_i, p-s_i, m-s_i, and composite PV systems, respectively. The annual average AC energy of a-s_i based PV system (3293.2 kWh) is higher than yearly average AC energies of p-s_i (2435.8 kWh) and m-s_i (1425.6 kWh) PV

systems. The yearly average AC energy generated in m-s_i is about 56.7% and 41% less than that of a-s_i and p-s_i, respectively, because the array annual average array efficiency of m-s_i is 40% and 21.8% lower than that of p-s_i and a-s_i PV systems, respectively. The module hierarchy in the present study agrees with that reported in Penang, Malaysia (Yatim et al., 2017), in which a-s_i has also highest annual average AC energy (5179 kWh) followed by p-s_i (4999.6 kWh), m-s_i (4749.3 kWh) and HIT (4723 kWh).

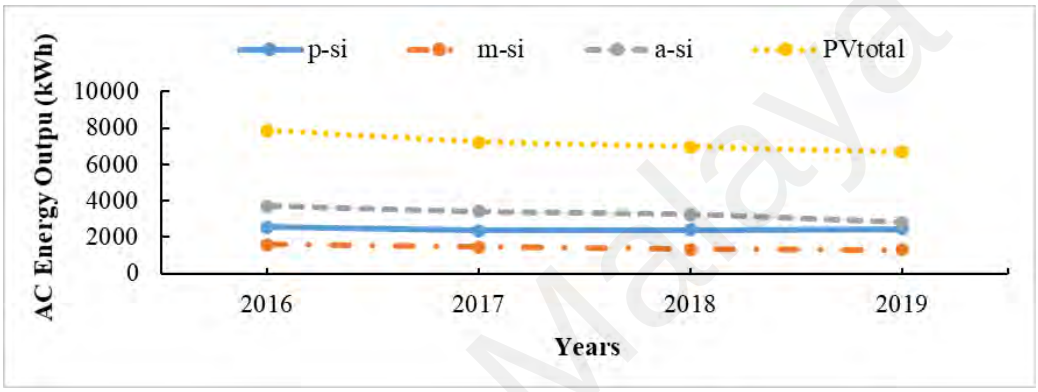

Figure 4.4: Annual AC energy output for different PV systems over the period 2016-2019

Figure 4.4 indicates that annual AC energy decreases slightly for the period (2016-2017), while it remains almost constant for the period (2017-2018) for all three PV systems. However, annual AC energy for a-s_i PV systems drops rapidly than the other two PV systems. The yearly AC energy has a variation of (3715-2808.9) kWh, (2547.6-2457.2) kWh, and (1600-1302.4) kWh during the monitored period (2016-2019) for a-s_i, p-s_i, and m-s_i PV systems, respectively. The difference between the maximum AC energy in 2016 and the minimum AC energy in 2019 provides the total degradation in AC energy for the whole monitored period. Therefore, the degradation calculated in AC energy is 906.1 kWh, 90.4 kWh, and 297.6 kWh for a-s_i, p-s_i, and m-s_i PV systems, respectively, over the monitored duration.

Hence, a-s_i modules-based PV system has a higher annual average AC energy generated than p-s_i and m-s_i PV systems, while the reduction in generated AC energy is found less for p-s_i (90.4kWh) than that for a-s_i (906.1kWh) and m-s_i (297.6kWh) over four years.

4.2.3 System yields

Figure 4.5 shows the monthly average array and reference yields of different PV systems for the given period. The monthly average array yield has a variation of (94.4-125.7) h, (97.5-123.8) h, (60.7-73.9) h, and (110.3-85.7) h, from November to March for a-s_i, p-s_i, m-s_i, and composite PV systems, respectively. The monthly array yield for all three PV systems is observed to increase slightly with reference yield from January to March, while a decreasing trend is observed from March to June due to reduced solar radiation. In July, the monthly array yield for p-s_i is slightly above the reference yield. It may happen due to improved array performance because of lower operating temperatures for this month. All three PV systems have followed the same trend as reference yield from August to December.

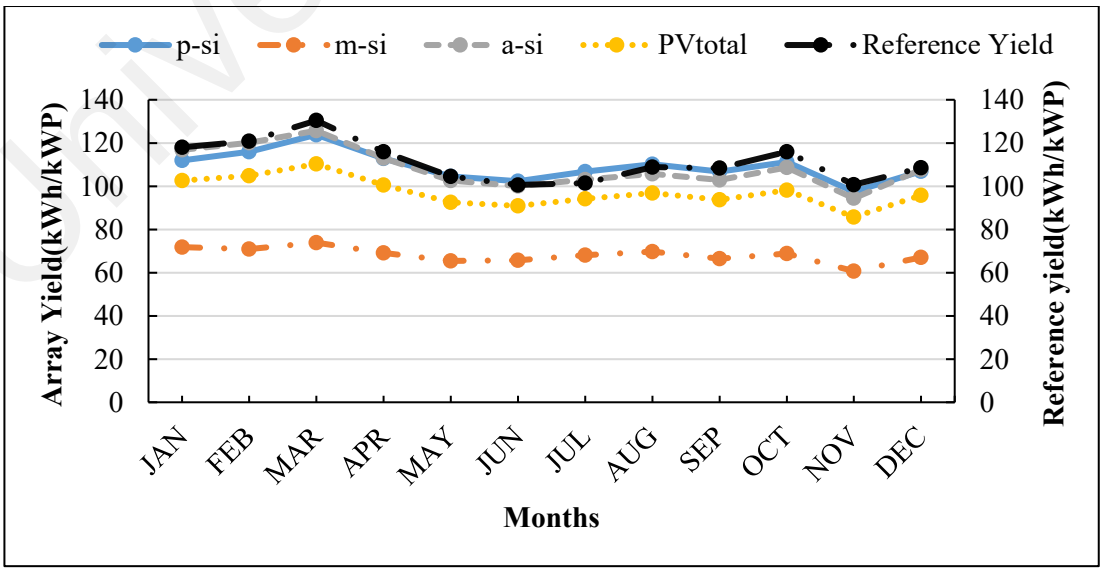

Figure 4.5: Monthly average array and reference yield for different PV systems over the period 2016-2019

The monthly array yield for all three PV systems is observed high in sunny season (December-April) due to high solar radiation, with maximum value in March, while it is found low during the rainy season (May-November) due to low solar radiation, with the minimum value in November.

The annual array yield has a variation of (1462.7-1104.2) h, (1369.6-1321.4) h, and (912.8-749) h for a-s_i, p-s_i, and m-s_i PV systems, respectively, for the duration (2016-2019). The difference between the maximum (2016) and minimum (2019) annual array yield gives the degradation in array yield over four years monitored period. Therefore, the degradation in array yield is 358.5 h, 48.2 h, and 163.8 h for a-s_i, p-s_i, and m-s_i modules PV systems, respectively. The degradation in array yield is higher for a-s_i (358.5 h) than p-s_i (48.2 h) and m-s_i (163.8 h) over four years period. Therefore, the p-s_i modules-based PV system has a high annual average array yield and less degradation compared to the other two systems.

Figure 4.6 and Figure 4.7 show the monthly average and annual final yield relative to reference yield for different PV systems, respectively, over the given data period. The a-s_i and p-s_i modules-based PV systems are generating the final yield close to the reference yield, as shown in Figure 4.6. The variation of monthly average final yield is (88.7-118.3) h, (90.6-114.8) h, (56.3-68.8) h, and (103.1-80.1) h, from November to March, for a-s_i, p-s_i, m-si, and composite PV systems, respectively. The monthly average final yield of a-s_i modules is higher than that of the other two modules from January to April due to high solar radiation, while from May to December, it is almost the same for both p-s_i and a-s_i PV systems. However, m-s_i modules have the lowest monthly average final yield for all months due to poor array performance. For all three PV systems, the monthly average final yield is observed high in the sunny season due to high solar radiation, while it is found low due to less solar radiation in the rainy season.

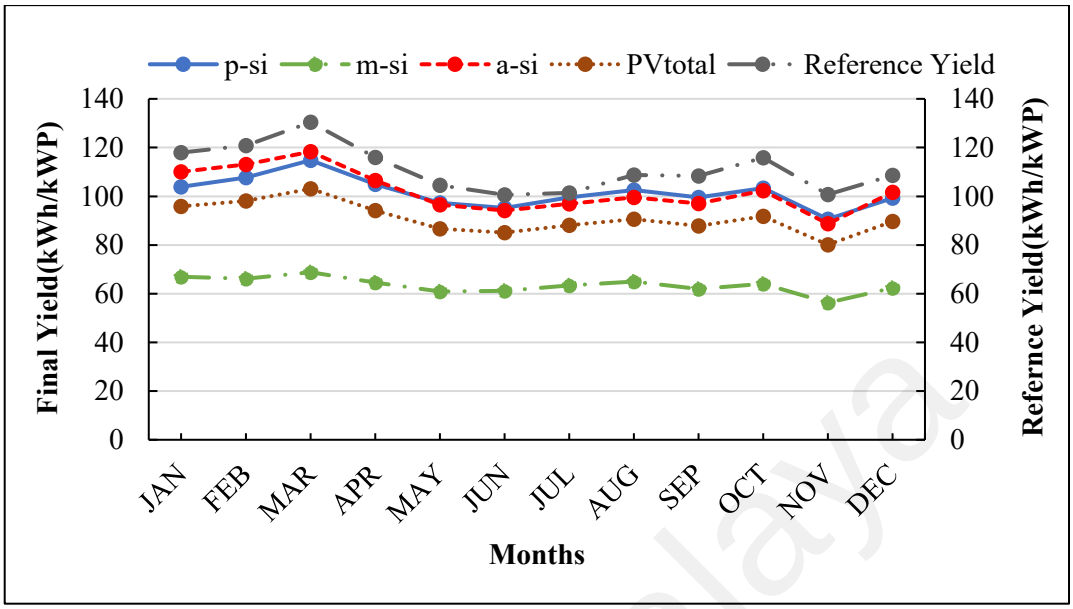

Figure 4.6: Monthly average final and reference yield for different PV systems over the period 2016-2019

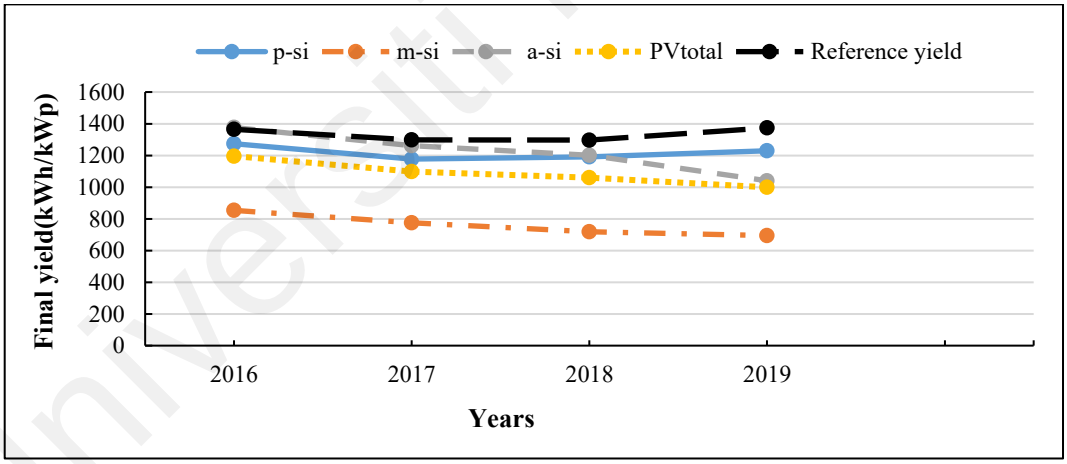

Figure 4.7: Annual final and reference Yield for different PV systems over the period 2016-2019

The annual average final yield is 1219.7 h, 1217.9 h, 760.3 h, and 1088.1 h for a-s_i, p-s_i, m-s_i, and composite PV systems, respectively. The results demonstrate that the annual average final yield for a-s_i modules system is almost equal to p-s_i and higher than m-s_i modules-based PV systems for a given period. The final yield for a-s_i modules is better than p-s_i and m-s_i from 2016 to 2018, but it is inferior to p-s_i modules for 2019. The annual

average final yield for m-s_i is low because the yearly average AC energy generated in m-s_i is about 56.7% and 41% less than that in a-s_i and p-s_i modules, respectively, due to poor PV array performance. The degradations in final yields are 335.6 h, 45.2 h, 158.75 h, and 196.8 h for a-s_i, p-s_i, m-s_i, and composite PV systems, respectively, over four years. Based on these statistics, p-s_i is better than the other two PV systems with less degradation in the final yield over four years.

Moreover, the daily average final yields of a-s_i (3.34 h) and p-s_i (3.34 h) based PV systems in the present study are better than daily final yields of a-s_i (3.08 h), p-s_i (3.1 h) in Ghana (Quansah et al., 2017) and p-s_i (3.12 h) in Singapore (Wittkopf et al., 2012), which have a similar tropical humid climate like Malaysia. In (Wittkopf et al., 2012), p-s_i modules have the same manufacturer (Mitsubishi) as p-s_i modules in the present study. When compared with different climate studies, p-s_i modules have a daily average final yield (3.34 h) better than 3.32 h in India (Pundir et al., 2016), 2.55 h in Norway (Adaramola et al., 2015), and 1.45-2.44 h in India (Sharma and Chandel, 2013).

4.2.4 Capacity factor

The monthly average CF for three PV systems, together with a composite system over the period (2016-2019), is described in Figure 4.8. The monthly average CF has variation of (12.6-15.5) %, (7.9-9.6) %, (12.3-16.5) % and (14.3-11.1) %, from November to February for p-s_i, m-s_i, a-s_i, and composite PV systems, respectively. Figure 4.8 shows that the CF for a-s_i modules is better than the other two types of modules from December to April, while from May to November, p-s_i has higher CF than the other two systems. For all PV systems, the monthly average CF is observed to be high from December to April due to high solar radiation in the sunny season, while it is found low from May to November due to low solar radiation in the rainy season.

Figure 4.9 shows the annual capacity factor for three PV systems along with the composite system over the period (2016-2019). The annual average CF is 13.9 %, 13.88 %, 8.7 % and 12.4% for a-s_i, p-s_i, m-s_i and composite PV systems, respectively. The a-s_i and p-s_i modules have equal annual average CF, which is better than the CF of m-s_i modules (8.7 %) based PV systems over the period (2016-2019).

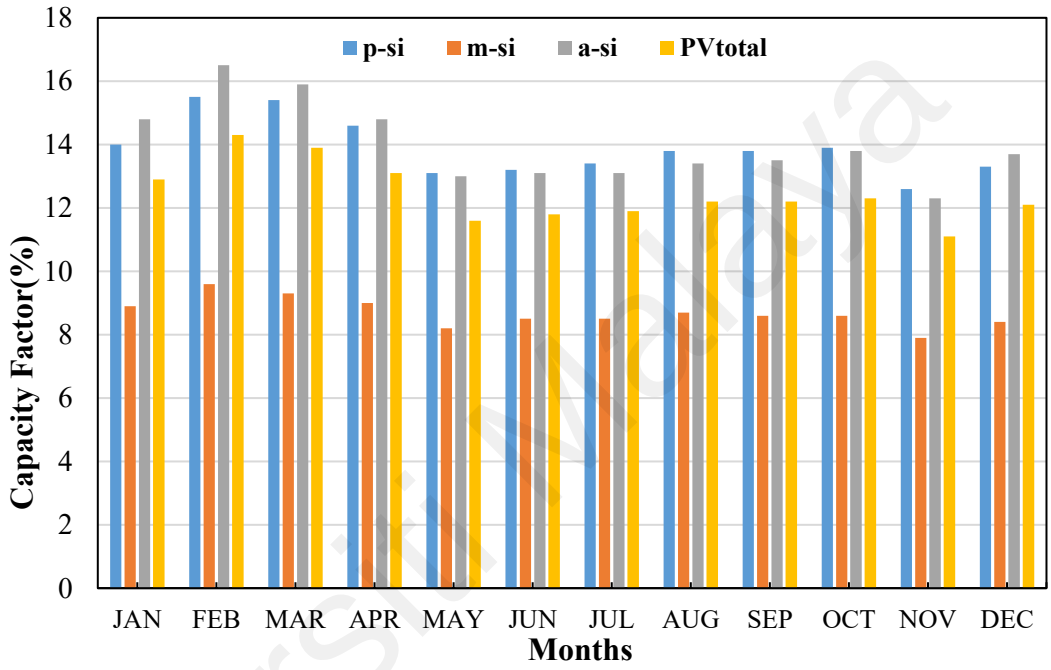

Figure 4.8: Monthly average capacity factor for different PV systems over the period 2016-2019

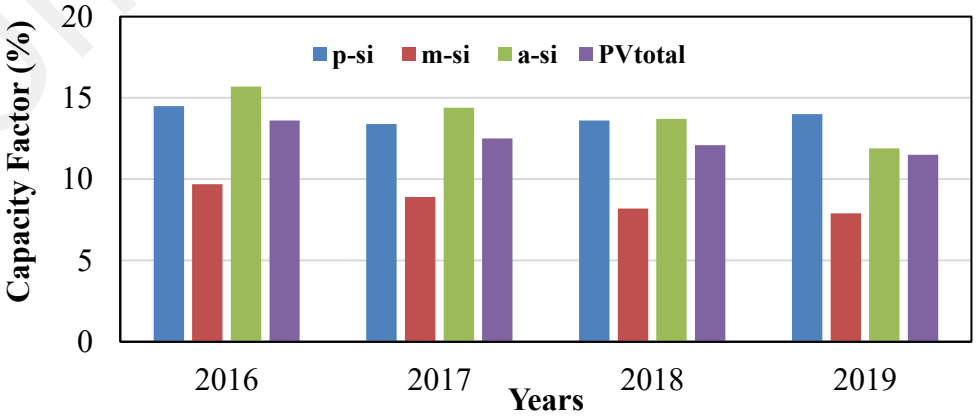

Figure 4.9: Annual capacity factor for different PV systems over the period 2016-2019

The a-s_i modules have better annual CF than p-s_i and m-s_i for the period 2016 to 2018. However, the CF in a-s_i modules is found lower than CF in p-s_i modules for 2019 due to less amount of generated AC energy this year. The degradation in annual CF is 3.8 %, 0.5 %, and 1.8 % for a-s_i, p-s_i and m-s_i modules respectively, over the monitored period (2016-2019). Therefore, the p-s_i is superior to both a-s_i and m-s_i PV systems due to less degradation (0.5 %) in CF.

In comparison with similar climate studies, it is found that the annual average CF of a-s_i (13.9 %) and p-s_i (13.9 %) modules in the present study is better than CF of a-s_i (12.8 %) and p-s_i (12.9 %) in Ghana (Quansah et al., 2017). While p-s_i modules in the present study have CF (13.9 %), which is almost the same as CF for p-s_i (14 %) in Thailand (Chimtavee and Ketjoy, 2012). In Singapore (Wittkopf et al., 2012), p-s_i modules (Mitsubishi) have better CF (15.7 %) than p-s_i modules (Mitsubishi) (12.9 %) in the present study. While, in comparison with different climate studies, p-s_i modules in this study have CF (13.9 %) better than 13.85 % in India (Pundir et al., 2016), 10.56 % in Norway (Adaramola et al., 2015), and 9.27 % in India (Sharma and Chandel, 2013).

4.2.5 System efficiencies

The monthly average array efficiency for three PV systems, together with a composite system for the recorded period, is shown in Figure 4.10. The array efficiency varies from 11.9 % in February, March, October, and November to 13 % in July for the p-s_i modules system, while it varies from 6.8 % in March to 7.9 % in July for the m-s_i modules system. For the a-s_i modules system, array efficiency varies from 9.3% in October and November to 9.8 % in July. For all three PV systems, the monthly average array efficiency is found to increase gradually from January to July, while it has a gradual decrease from July to December. However, it is found at its peak in July due to a higher array yield. The monthly average array efficiency is seen better in the showery season than that in the sunny season

due to better array performance as a result of low operating temperature (Adaramola et al., 2015). The monthly average array efficiency for p-s_i modules is found higher compared to the other two modules for the whole period.

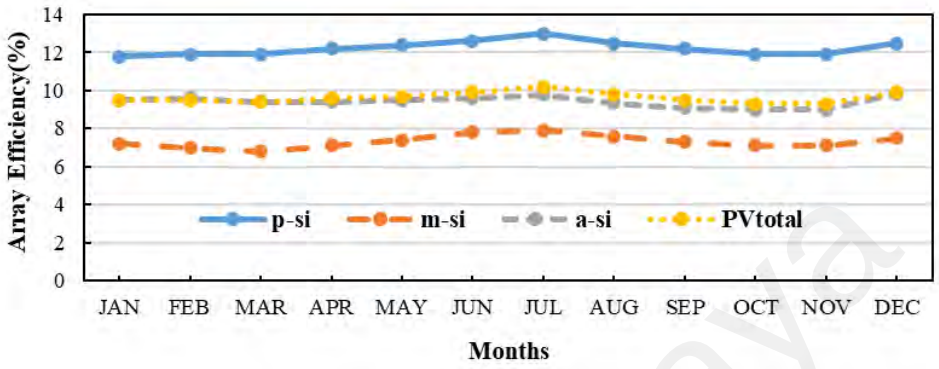

Figure 4.10: Monthly average array efficiency for different PV systems over the period 2016-2019

Figure 4.11 elaborates the annual array efficiency for three PV systems, along with a composite system for the recorded period. The annual average array efficiency is 12.17%, 9.34 %, 7.3 %, 9.6 % for p-s_i, a-s_i, m-s_i and composite PV systems, respectively. P-s_i modules system has higher annual average array efficiency than a-s_i and m-s_i modules system for the whole monitoring period. The degradations in array efficiencies are 1.46%, 1.94 %, 1.44 % for p-s_i, m-s_i, and a-s_i, respectively, over the monitored period (2016-2019). Degradation in array efficiency for p-s_i is almost the same as in a-s_i but lower than m-s_i.

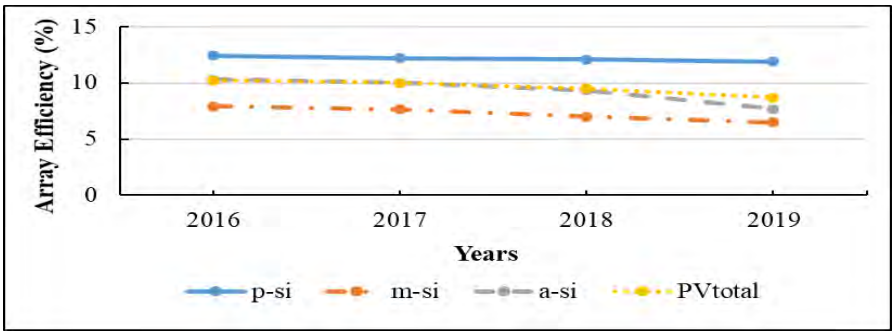

Figure 4.11: Annual array efficiency for different PV systems over the period 2016-2019

Furthermore, the annual average array efficiency of the p-s_i modules (12.17 %) based PV system is better than the p-s_i array efficiency (11.5%) found in a study at Kuala Lumpur (Zain et al., 2013). While, in comparison with different climate studies around the world, the annual average array efficiency of p-s_i (12.17 %) modules in the present study is better than 11.07 % in India (Tripathi et al., 2014), (9.5-10.8) % in Japan (Tahri et al., 2018), 12.7 % in Norway (Quansah et al., 2017), 11.34 % in India (Yadav and Bajpai, 2018), 10.93 % in Lesotho (Mpholo et al., 2015) and 9.45 % in Turkey (Eke et al., 2013), for the same p-s_i module. The a-s_i modules have better annual average efficiency (9.34 %) than 6.56 % in India.

The monthly average and annual system efficiencies for three types of PV systems, together with the composite system for the observed period (2016-2019), are shown in Figure 4.12 and Figure 4.13, respectively. The system efficiency fluctuates from 10.9 % in January and March to 12.2 % in July for p-s_i, while it varies from 6.3 % in March to 7.4 % in July for the m-s_i modules system. For the a-s_i modules system, the system efficiency varies from 8.5 % in September and October to 9.1 % in July. In the rainy season, the monthly average system efficiency is found higher than that in the sunny season for all three PV systems due to better array performance as a result of low operating temperature (Adaramola et al., 2015). The monthly average system efficiency for p-s_i modules is higher than the other two systems for the whole period.

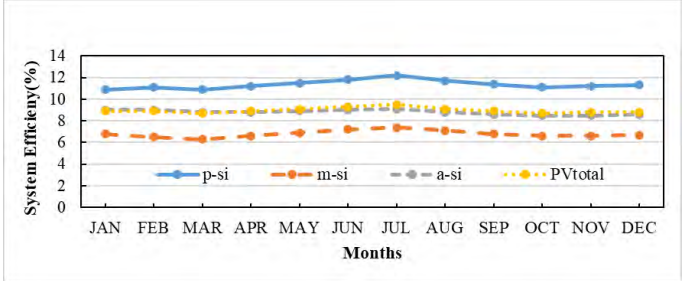

Figure 4.12: Monthly average System efficiency for different PV systems over the period 2016-2019

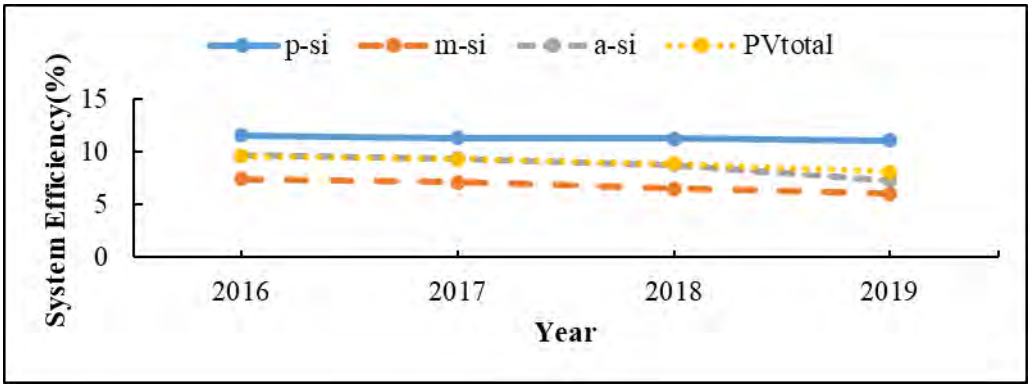

Figure 4.13: Annual system efficiency for different PV systems over the period 2016-2019

Figure 4.13 indicates that the annual average system efficiency is 11.33 %, 8.8 %, 6.8%, and 9 % for p-s_i, a-s_i, m-s_i, and composite PV systems, respectively. The annual average system efficiency for m-s_i is lower than that in p-s_i because the AC energy generated in m-s_i is about 41% less than AC energy in p-s_i due to the poor array performance of m-s_i. The annual average system efficiency depends on AC energy, in-plane solar radiation, and the area of the PV module. Solar radiation is the same for all types of PV systems, and the area is fixed for each PV array. Therefore, the AC energy generated is the key factor that affects system efficiency. The degradation in system efficiency is 0.5 %, 1.42 %, and 2.42 % for p-s_i, m-s_i, and a-s_i, respectively, over the monitored period. Therefore, p-s_i is superior to both a-s_i and m-s_i systems with a high yearly average value and less degradation in system efficiency for the recorded period (2016-2019).

Moreover, the p-s_i modules in the current study have annual average system efficiency (11.33 %) better than 11.2 % in Singapore (Wittkopf et al., 2012) and 10.41 % in Thailand (Chimtavee and Ketjoy, 2012). In (Wittkopf et al., 2012), p-s_i modules have the same manufacturer (Mitsubishi) as p-s_i modules in the present study. While, in comparison with different climate studies around the world, the annual average system efficiency of p-s_i (11.33 %) modules in the present study is found better than 10.52 % in India (Tripathi et

al., 2014), (10.24-10.7) % in Japan (Tahri et al., 2018), 8.7 % in India (Pundir et al., 2016), 10.02 % in India (Yadav and Bajpai, 2018) and 9.58 % in Lesotho (Mpholo et al., 2015), for the same p-s_i module. The a-s_i modules also have better annual average system efficiency (8.8 %) than 6.06 % in India (Tripathi et al., 2014).

Figure 4.14 shows the monthly average inverter efficiency for three PV systems together with a composite system over the monitored period (2016-2019). The inverter efficiency of a-s_i is found better compared to the inverter efficiencies of the other two PV systems. The inverter efficiency varies from 94 % in May and June to 94.3 % in September and December for the a-s_i modules system, while it varies from 92.8 % in November to 93.3 % in February for the m-s_i modules system and from 92.7 % in March to 93.2% in July for the p-s_i modules system.

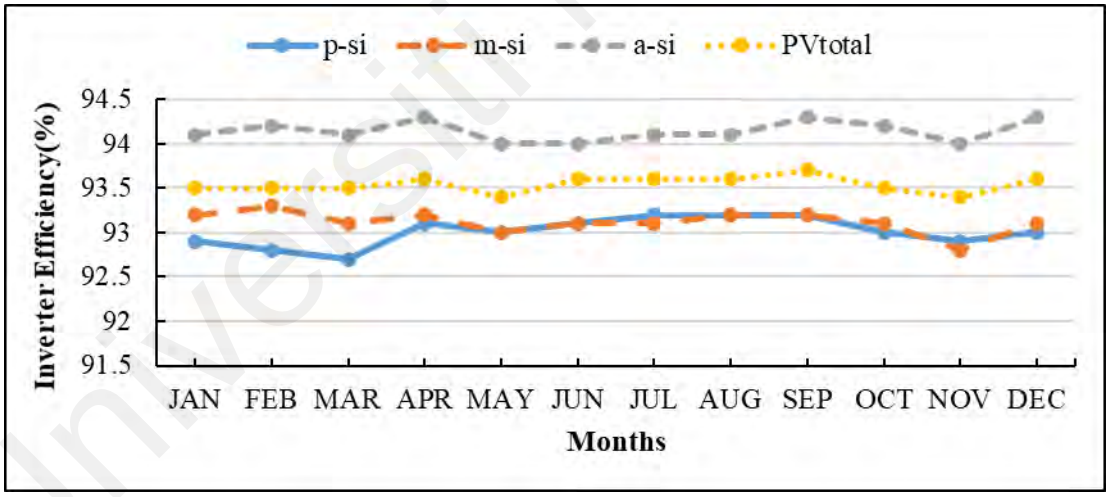

Figure 4.14: Monthly average Inverter efficiency for different PV systems over the period 2016- 2019

Figure 4.15 and Figure 4.16 reveal the variation of inverter efficiency with inverter power output or inverter loading for (p-s_i, m-s_i) and a-s_i PV modules, respectively. The inverters for three PV modules achieve maximum efficiency at about 30 % loading, and it remains relatively constant until 80 % loading. A slight dip is observed in inverter efficiencies between 80 % and 100 % inverter loading. The inverters for p-s_i, m-s_i, and a-

s_i PV systems have performed at maximum loading of 100 %, 70 %, and 100 %, respectively.

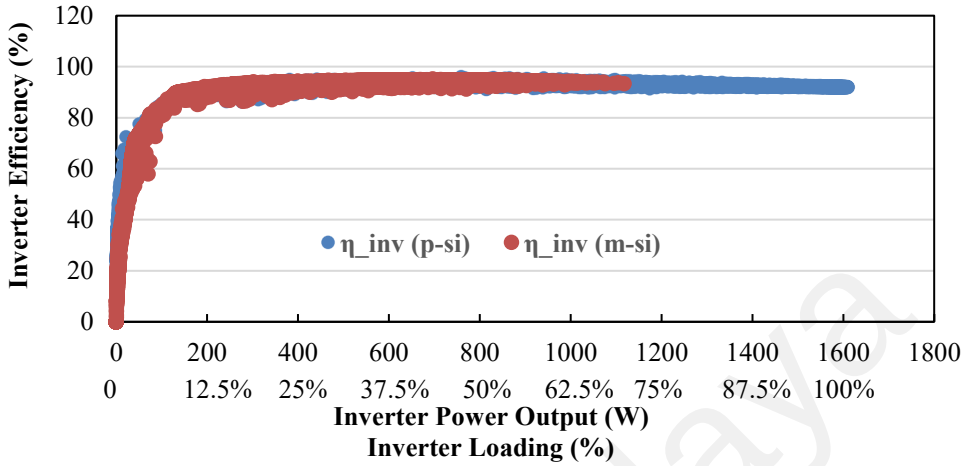

Figure 4.15: Inverter efficiency and inverter power output for p-s_i and m-s_i PV systems

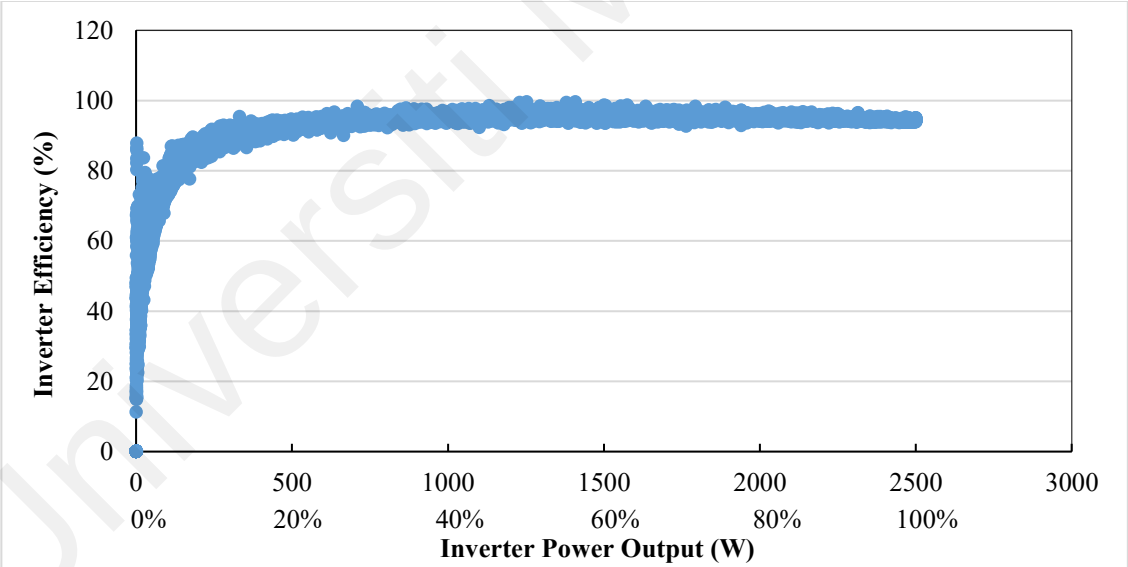

Figure 4.16: Inverter efficiency and inverter power output for a-s_i PV system

The annual average inverter efficiencies are 93 %, 93.1 %, 94.1 %, 93.5 % for p-s_i, m-s_i, a-s_i modules and composite PV systems, respectively. The annual average inverter efficiency for a-s_i modules PV system is greater than that for the other two PV systems over the whole period. In comparison with similar climate studies, the p-s_i modules in the present study have an annual average inverter efficiency (93%), equal to 93 % (Chimtavee

and Ketjoy, 2012) and better than (87.9-89.2)% (Chimtavee et al., 2011), both in Thailand. While comparing with different climate studies around the world, the annual average inverter efficiency of p-s_i (93 %) modules in the present study is better than (89.1-89.2) % in Japan (Tahri et al., 2018), 89.8 % in India (Sharma and Goel, 2017), 8.7 % in India (Pundir et al., 2016), 88.8 % in Norway (Quansah et al., 2017), 88.4 % in India (Yadav and Bajpai, 2018), 87.8 % in Lesotho (Mpholo et al., 2015) and 88.1 % in South Africa (Okello et al., 2015), for the same p-s_i module.

4.2.6 Array and system losses

The monthly average array and system losses for three types of PV systems, along with the composite system for the observed duration (2016-2019), are displayed in Figure 4.17. The array losses vary from -5.3 h in July to 4.9 h in February for p-s_i and from 33.3 h in July to 56.5 h in March for the m-s_i PV system, while they vary from -1.6 h in July to 7.3 h in October for a-s_i PV systems. For all three PV systems, a gradual decrease in annual array losses is observed from March to July due to the decline in solar radiation and an increase in PV array efficiency during these months. Array losses are increased gradually from July to October due to the decrease in PV array efficiency. However, monthly average array losses are found higher in a sunny season than in the rainy season due to poor array performance for all three PV systems.

The annual average array losses are 24.7 h, 517.8 h, 38.7 h, and 171.7 h for p-s_i, m-s_i, a-s_i, and composite PV systems. The annual average array losses for m-s_i PV systems are higher than the other two PV systems. The reason is that the yearly average array yield of m-s_i PV systems is 37.6% and 37% lower than p-s_i and a-s_i, respectively, due to poor m-s_i array performance. The annual average array efficiency of m-s_i PV systems is also 40% and 21.8% lower than that of p-s_i and a-s_i PV systems, respectively.

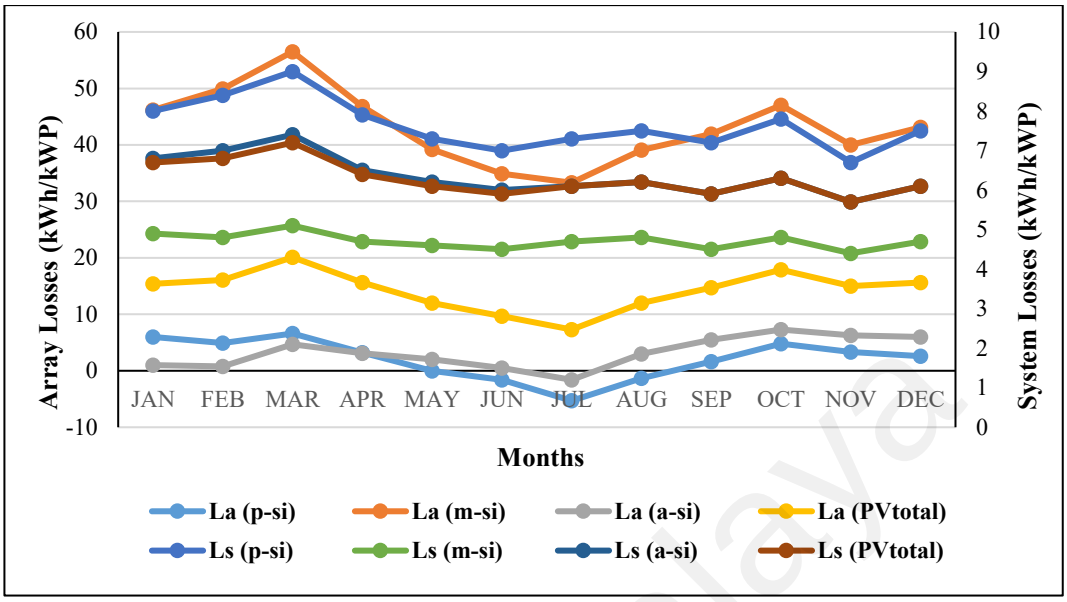

Figure 4.17: Monthly average array and system losses for different PV systems over the period 2016-2019

The negative values of array losses (array capture gain) in a few months for the p-s_i and a-s_i modules PV system caused higher PR and array efficiency. The reason is that solar radiation is lowest with high humidity in June and July due to heavy rains. The drops of water remain on the PV module due to heavy rains and humid environments, which keep the module cool by transferring its heat into the ambient by evaporation. The array performance is enhanced as a result of this cooling effect due to high humidity in these rainy months (June and July) (Adaramola et al., 2015). The annual average array losses for p-s_i modules-based PV systems are lower than those for the other two PV systems.

The monthly system losses have variations of (6.7-9) h, (4.4-5.1) h, and (5.7-7.4) h, from November to March, for p-s_i, m-s_i, and a-s_i modules, respectively. The system losses are higher in the sunny season than in the rainy season due to poor array performance and lower system efficiency. The annual average system losses are 91.7 h, 56.1 h, 76 h, and 75.1 h for p-s_i, m-s_i, a-s_i, and composite PV systems, respectively. The m-s_i modules-based PV systems have lower yearly system losses than the other two PV systems.

The overall annual losses (array losses + system losses) for three types of PV systems, along with the composite system, are depicted in Figure 4.18. The overall annual average losses 116.4 h, 574 h, 115.3 h, 246.15 h for p-s_i, m-s_i, a-s_i, and composite PV systems, respectively. The overall annual losses for a-s_i based PV system are negative in 2016 due to enhanced array performance in rainy months as a result of low operating temperatures (Adaramola et al., 2015). The annual average overall losses of a-s_i and p-s_i modules are almost the same and less than the m-s_i PV system over the monitored period (2016-2019).

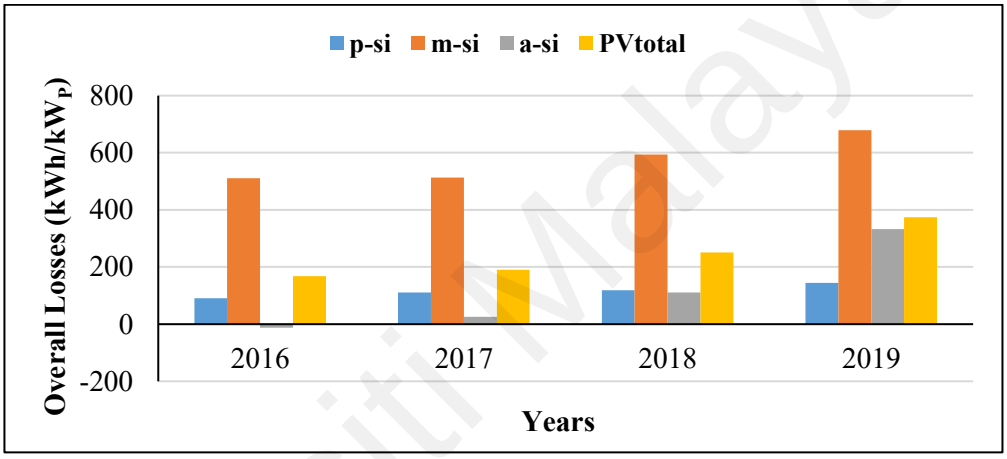

Figure 4.18: Annual overall losses (array +system) for different PV systems over the period 2016-2019

4.2.7 Performance ratio

The monthly average and annual PRs for three types of PV systems along with composite PV systems over the observed duration (2016-2019) are revealed in Figure 4.19 and Figure 4.20, respectively. The average monthly PR varies from 88 % in January and March to 98.1 % in July for p-s_i modules, while it varies from 53 % in March to 62.8 % in July for m-s_i modules. However, for a-s_i modules, the average monthly PR is ranged from 88 % in October to 95.7 % in July. The a-s_i modules have better PR than the other two PV systems from January to April, while for the remaining eight months, p-s_i has higher PR than the other two. For all three PV systems, the average monthly PR is observed low from December to April due to high reference yield and overall losses

during the sunny season. However, it is found high from May to November during the rainy season due to low reference yield and overall losses.

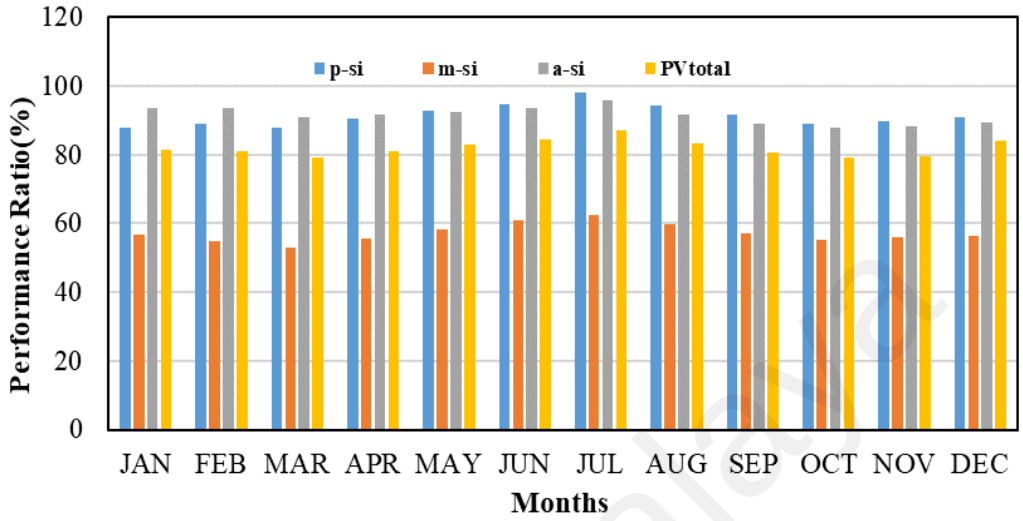

Figure 4.19: Monthly average PR for different PV systems over the period 2016-2019

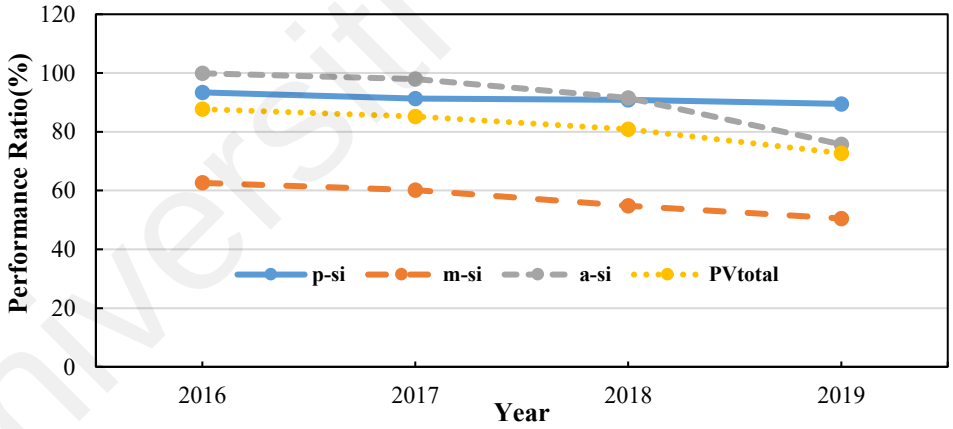

Figure 4.20: Annual performance ratio for different PV systems over the period 2016-2019

The annual average PR is 91.3 %, 91.3 %, 57.2 % and 81.6 % for p-s_i, a-s_i, m-s_i and composite PV systems, respectively. The annual PR is found to drop rapidly for a-s_i than p-s_i and m-s_i PV systems over the duration (2017-2019). It is due to high overall losses in a-s_i during that period. While the m-s_i PV system is observed to have a lower average yearly PR than a-s_i and p-s_i because the yearly average final yield of m-s_i modules is about

37.6% and 37.7% lower than that of p-s_i and a-s_i modules, respectively. The PR degradation for a-s_i modules (24.2 %) is higher than p-s_i (3.9 %) and m-s_i modules (12.1 %) for the monitored period. Therefore, the p-s_i modules-based PV system is superior to both a-s_i and m-s_i modules-based PV systems due to less PR degradation, even though the PR of p-s_i and a-s_i is equal.

Table 4.1 elaborates the comparison of the present study with similar and different climate studies in the world. In comparison with similar studies, the annual average PR of a-s_i (91.3 %) and p-s_i (91.3 %) based PV systems in the present study is better than PR of a-s_i (75.8 %) in Ghana (Quansah et al., 2017), p-s_i (76.3 %) in Ghana (Quansah et al., 2017), p-s_i (80 %) in Kuala Lumpur (Zain et al., 2013), p-s_i (84 %) in Singapore (Wittkopf et al., 2012) and p-s_i (73.45 %) in Thailand (Chimtavee and Ketjoy, 2012). In (Wittkopf et al., 2012), p-s_i modules have the same manufacturer (Mitsubishi) as p-s_i modules in the present study. The m-s_i has comparatively less annual average PR (57.2 %) than (59.9 % -79.1 %) (Humada et al., 2016) and 77.28 % (Farhoodnea et al., 2015) in Malaysia.

Comparing with different climate studies, p-s_i modules in the present study have annual average PR (91.3 %) better than (80.8 % - 86.5 %) in Japan (Tahri et al., 2018), 78.48 % in India (Ramanan and Karthick, 2019), 78 % in India (Sharma and Goel, 2017), 63.7 % in India (Pundir et al., 2016), 83.03 % in Norway (Adaramola et al., 2015), 74 % in India (Sharma and Chandel, 2013), 77 % in India (Yadav and Bajpai, 2018), 70 % in Lesotho (Mpholo et al., 2015), 72 % in Turkey (Eke et al., 2013), 84.3 % in South Africa (Okello et al., 2015), 85 % in India (Vasisht et al., 2016) and 67.36 % in Greece (Kymakis et al., 2009). While, a-s_i modules have PR (91.3 %) better than 70.8 % in India (Tripathi et al., 2014), (68 % - 75 %) in Mauritania (Sidi et al., 2016), and 79.5 % in India (Shukla et al., 2016).

Table 4.1:Comparison of performance parameters with other installed PV systems at various world locations

Reference	year	Location	PV type	System size	Y_F (kWh/kW_P/d)	η_{PV} (%)	η_{inv} (%)	η_{sys} (%)	CF (%)	PR(%)
Present study	**2019**	**Malaysia**	**a-s_i**	**2.7 kW_P**	**3.34**	**9.34**	**94.14**	**8.8**	**13.9**	**91.3**
			p-s_i	**2 kW_P**	**3.34**	**12.17**	**93**	**11.33**	**13.9**	**91.3**
			m-s_i	**1.875 kW_P**	**2.08**	**7.3**	**93.1**	**6.8**	**8.7**	**57.2**
(Ramanan and Karthick, 2019)	2019	India	p-s_i CIS	1 kW_P 1.36 kW_P	4.21 4.65	14.19 12.19	-	13 10.85	17.99 19.57	78.48 86.73
(Seme et al., 2019)	2019	Slovenia	-	25 MW_P	2.84	-	-	-	11.85	68.84
(Tahri et al., 2018)	2018	Japan	p-s_i 1 p-s_i 2	4.26 kW_P	4.05 3.85	10.8 9.5	89.1 89.2	10.69 10.24	-	80.81 86.50
			CIS 1 CIS 2	2.25 kW_P	3.95 3.90	10.1 9.3	85.1 85.3	10.17 9.93		76.06 74.69
(Quansah et al., 2017)	2017	Ghana	HIT	4 kW_P	3	-	-	-	12.6	74.8
			m-s_i	4 kW_P	2.8	-	-	-	11.47	67.9
			p-s_i	4 kW_P	3.10	-	-	-	12.9	76.3
			a-s_i	4 kW_P	3.08	-	-	-	12.8	75.8
			CIS	4 kW_P	2.12	-	-	-	8.8	52.3
(Yadav and Bajpai, 2018)	2017	Lucknow	p-s_i	5 kW_P	3.99	11.34	88.38	10.02	16.39	76.97
(Sharma and Goel, 2017)	2017	India	p-s_i	11.2 kW_P	3.67	13.42	89.83	12.5	15.27	78
(Sidi et al., 2016)	2016	Mauritania	a-s_i/ µa-s_i	15 MW_P					17.7/19.5	68/75.25
(Shukla et al., 2016)	2016	Bhopal, India	c-s_i/ a-s_i/CdTe/CIS	-	-	-	-	-	-	71/79.5/ 77/73.1
(Humada et al., 2016)	2016	Malaysia	m-s_i		2.92-4.14				14.4-20.2	59.9-79.1
			CIS		2.98-4.31	-	-	-	15.6-21.1	63.8-84.1

Table 4.1 continued

Reference	year	Location	PV type	System size	Y_F (kWh/kW_P/d)	η_{PV} (%)	η_{inv} (%)	η_{sys} (%)	CF (%)	PR(%)
(Vasisht et al., 2016)	2016	India	p-s_i	20 kW_P	4.1	13.71	-	-		85
(Pundir et al., 2016)	2016	Roorkee	p-s_i	1816 kW_P	3.32	-	97	8.7	13.85	63.68
(Kumar and Systems, 2016)	2016	India	m-s_i	80 kW_P	4.45	15.53	-	-	-	83.2
(Adaramola et al., 2015)	2015	Norway	p-s_i	2.07 kW_P	2.55	12.7	88.8	11.6	10.56	83.03
(Okello et al., 2015)	2015	S. Africa	p-s_i	3.2 kW_P	4.9	13.72	88.1	-	20.41	84.3
(Mpholo et al., 2015)	2015	Lesotho	p-s_i	281 kW_P	4.15	10.93	87.75	9.58	17.20	70%
(Farhoodnea et al., 2015)	2015	Malaysia	m-s_i	3 kW_P	3.8	10.11	95.15	-	15.7	77.28
(Sundaram et al., 2015)	2015	India	-	11 MW_P	4.81	6.08	88.2	5.08	-	85.8-92.3
(Tripathi et al., 2014)	2014	India	p-s_i a-s_i	500 kW_P 500 kW_P	2.79-5.14 2.62-4.84	11.07 6.56	-	10.52 6.06	-	75.3 70.8
(Tahri et al., 2013)	2013	Algeria	m-s_i CIS	4.27 kW_P 2.25 kW_P	-	-	-	-	-	79%
(Eke et al., 2013)	2013	Turkey	p-s_i	2.73 kW_P	3.87	9.54	-	-	23.2	72
(Padmavathi and Daniel, 2013)	2013	Karnataka	m-s_i	3 MW_P	3.73	10.1-13.25	-	-	15.69	72
(Sharma and Chandel, 2013)	2013	India	p-s_i	190 kW_P	1.45-2.44	-	-	8.3	9.27	74
(Chimtavee and Ketjoy, 2012)	2012	Thailand	p-s_i	11 kW_P	3.84	11.2	93	10.41	14	73.45
(Wittkopf et al., 2012)	2012	Singapore	p-s_i	142.5 kW_P	3.12	13.7	94.8	11.2	15.7	84
(Kymakis et al., 2009)	2009	Greece	p-s_i	171.4 kW_P	1.96-5.07	-	-	-	15.26	67.36

4.2.8 Environmental impacts of composite PV power system

The clean energy generated by the PV has a favorable impression on the atmosphere. A considerable amount of greenhouse gases (CO_2, SO_2, NO_x, and Ash) are released by the coal thermal power plants. It is estimated that composite PV system has caused a total reduction of 28143.7 kg CO_2 (Kumar and Systems, 2016; Sharma and Goel, 2017), 35.64 kg SO_2, 74.4 kg NO_x, and 1952.9 kg Ash (Tarigan and Kartikasari, 2015) in four years. The annual average reduction is 7035.9 kg CO_2, 8.9 kg SO_2, 18.6 kg NO_x, and 488.2 kg Ash. The annual reduction of GHG emissions by composite (6.575 kW_P) PV system is presented in Table 4.2. The formula for calculating GHG (CO_2, SO_2, NO_x, Ash) emission reduction is given as follows:

[Produced electricity (kWh)] X [Factor for GHG (CO_2, SO_2, NO_x, Ash) avoided (kg/kWh)] = avoided (CO_2, SO_2, NO_x, Ash) in kg. For example,

The avoided CO_2 (kg) for 2016 = [7862.6 (kWh)] X [0.980 (kg/kWh)] = 7705.35 kg.

Table 4.2: The annual reduction of GHG emissions by composite (6.575 kW_P) PV system

Reference	GHG	Emission (kg/kWh)	Annual reduction (KG) every year			
			7862.6 kWh	7216 kWh	6971 kWh	6668.5 kWh
			2016	2017	2018	2019
(Kumar and Systems, 2016; Sharma and Goel, 2017)	CO_2	0.980	7705.35	7071.7	6831.6	6535.1
(Tarigan and Kartikasari, 2015)	SO_2	0.0124	9.75	8.95	8.6	8.3
(Tarigan and Kartikasari, 2015)	NO_X	0.0259	20.4	18.7	18.05	17.3
(Tarigan and Kartikasari, 2015)	Ash	0.068	534.7	490.7	474.03	453.46

4.2.9 Summary of performance analysis work

The a-s_i modules-based PV system has shown better annual performance parameters than the other two PV systems except for the array efficiency, system efficiency, and array yield over three- years period (2016-2018). However, in 2019, the performance of a-s_i becomes worse than p-s_i due to less value of generated DC and AC energies because

of poor array performance. The m-s_i PV system is observed to have a lower annual average PR than the a-s_i and p-s_i PV systems because the yearly average final yield of the m-s_i PV system is about 37.6% and 37.7% lower than that of p-s_i and a-s_i PV systems, respectively. The annual average final yield and CF for m-s_i are lowest because the yearly average AC energy generated in m-s_i is about 56.7% and 41% less than that in a-s_i and p-s_i, respectively. It is due to the poor array annual average array efficiency of m-s_i, which is 40% and 21.8% lower than that of p-s_i and a-s_i PV systems, respectively. The yearly average array yield of m-s_i PV systems is also 37.6% and 37% lower than p-s_i and a-s_i, respectively, due to poor array performance. Therefore, the overall annual losses (array + system) of m-s_i are found higher than that of a-s_i and p-s_i PV systems, respectively. However, the m-s_i modules have less annual average system losses (56.1 h) than the p-s_i (91.3 h) and a-s_i (76 h) PV systems. While the yearly average inverter efficiency of m-s_i (93.1 %) modules is slightly better than that of p-s_i (93 %) but less than that of a-s_i (94.1 %).

The monthly average (PR, array, and system efficiencies) are found lower in the sunny season (November-April) than in the rainy season (May-October) due to poor array performance and higher overall losses for all three PV systems. In contrast, the monthly average (DC energy, AC energy, array yield, final yield, CF, and overall losses) are found higher in the sunny season than in the rainy season due to higher solar radiation. However, monthly average inverter efficiency is observed almost equal in both seasons.

The PV systems based on p-s_i and a-s_i modules have an equal annual average (PR, CF, final yield, and overall losses). However, the yearly average (array yield, array, and system efficiency) of p-s_i based PV system is better compared to the other two PV systems for the monitored period (2016-2019). The degradations in almost all these performance parameters are found less in p-s_i than a-s_i and m-s_i modules-based PV systems for the

entire monitored period. Therefore, poly-crystalline based PV systems are the more suitable choice for the site considered due to high (array yield, array, and system efficiencies) along with less degradation in almost all the considered performance parameters in comparison with the other two (a-s_i, m-s_i) PV systems for the monitored period (2016-2019). It is also estimated that the composite PV system has caused a total reduction of 28143.7 kg CO_2, 35.64 kg SO_2, 74.4 kg NO_x, and 1952.9 kg Ash in four years. The performance of the composite PV system is significant in this research because it gives the environment cleaning impact and can be compared with other composite systems in similar and different climates in literature.

4.3 Solar power output forecasting results for three different PV systems

The prediction results of the proposed deep learning and hybrid technique for an hour ahead forecasting of solar power output are discussed in this section. The proposed deep learning method (RNN-LSTM) is compared with other techniques such as GPR, SVR, GPR(PCA), SVR(PCA), ANN, ANFIS(GP), ANFIS(SC), and ANFIS(FCM). The comparison is performed based on the same recorded data (2016-2019) on an annual basis for each of three different PV systems. Every year data is divided into two segments; 70% for training and 30% for testing purpose, to compare all techniques on equal grounds. The input parameters considered are solar radiation, ambient temperature, PV module temperature, and wind speed. While the output parameter is the solar power output for each PV system. In addition, SSA optimization is used to optimize the hyperparameters of developed deep learning technique for an hour ahead forecasting of solar power output. The proposed hybrid method is also compared with RNN-LSTM, GA-RNN-LSTM and PSO-RNN-LSTM. The measurement indices considered for evaluating the forecasting accuracy of the developed deep learning and hybrid methods are root mean square error (RMSE), mean square error (MSE), mean absolute error (MAE), correlation coefficient (r), and coefficient of determination (R^2).

4.3.1 LSTM structures comparison

Table 4.3 shows the comparison of different LSTM structures based on 2019 data to show the supremacy of the proposed method (RNN-LSTM). Some missing data is incorporated in each year due to non-functioning of recording sensors as a result of power failure. The reason for choosing 2019 data to compare LSTM structures, is that it is more cleaned compared to other years data. It is clear from the table that single-layered LSTM has performed better compared to double-layered LSTM and single-layered biLSTM structures. The proposed technique RNN-LSTM (single-layered) has shown the lowest testing RMSE, MAE, and R^2 for three PV systems compared to other LSTM structures. This indicates that RNN-LSTM (single-layered) architecture is more feasible to be implemented in predicting the PV power output for all three PV systems (p-si, m-si, and a-si) over four years data period (2016-2019).

Table 4.3: Comparison of different LSTM structures for power output prediction for three different PV plants based on 2019 data

LSTM Structures	P-si			M-si			Thin film		
	RMSE	MAE	R^2	RMSE	MAE	R^2	RMSE	MAE	R^2
RNN-LSTM (single layered)	24.25	17.46	0.9971	19.4	13.88	0.994	65.03	50.92	0.9855
RNN-LSTM (double layered)	30.97	22.1	0.9952	23	16	0.968	69.3	54	0.9835
RNN-Bi LSTM (single layered)	33.82	24.92	0.9943	27.03	20.61	0.9855	71	58.25	0.9826

4.3.2 Forecasting of solar power output for polycrystalline PV system

Figure 4.21 and Figure 4.22 elaborates on the training (RMSE and MSE) and training (R^2 and r) respectively, for an hour ahead forecasting of the solar power output of p-si PV system on an annual basis over the period (2016-2019). It is obvious from Figure 4.21 that the proposed deep learning technique (RNN-LSTM) has shown the lowest training RMSE and MSE values of 16.5, 14.3, 104.78, 18.58, and 272, 204.3, 10978.8, 345.12

respectively over the four years period in comparison with other techniques. ANFIS(GP) and ANN have shown second and third best lowest RMSE and MSE.

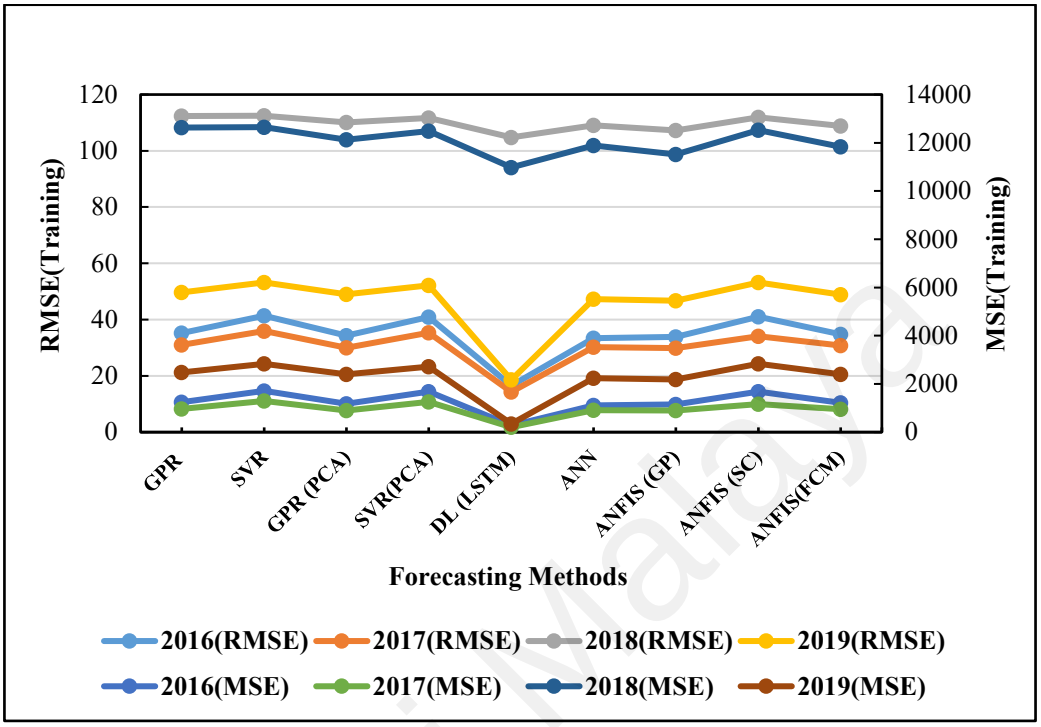

Figure 4.21:Training RMSE and MSE for p-si over period (2016-2019)

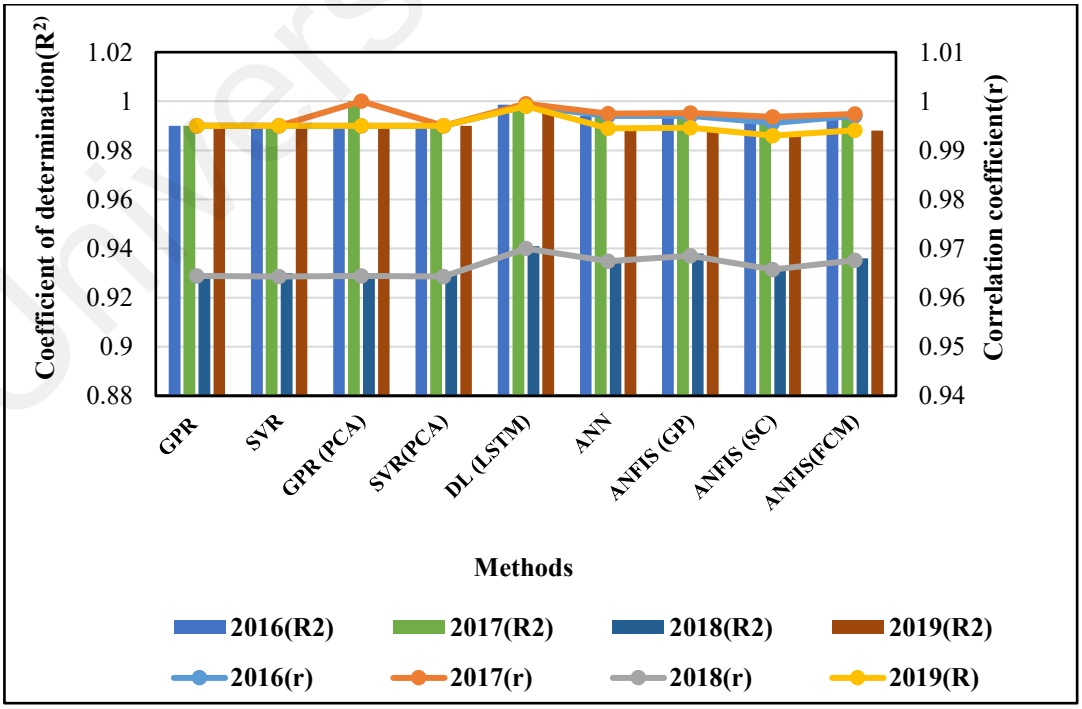

Figure 4.22:Training R^2 and r for p-si over period (2016-2019)

While in Figure 4.22, the training R^2 and r of RNN-LSTM for a p-si module are also found highest, which are 0.9986, 0.999, 0.941, 0.9982, and 0.999, 0.9995, 0.97, 0.999 over the period (2016-2019) respectively, in comparison with other applied techniques.

Figure 4.23 and Figure 4.24 explain the testing (RMSE and MSE) and testing (R^2 and r) respectively, for hourly ahead forecasting of solar power output for a p-si module on an annual basis over the period (2016-2019). Figure 4.23 shows that the deep learning technique (RNN-LSTM) has the lowest testing RMSE and MSE values of 30.25, 27.25, 44.06, 24.25 and 915.1, 742.5, 1941.2, 588.07 respectively over the period (2016-2019) in comparison with all other presented techniques.

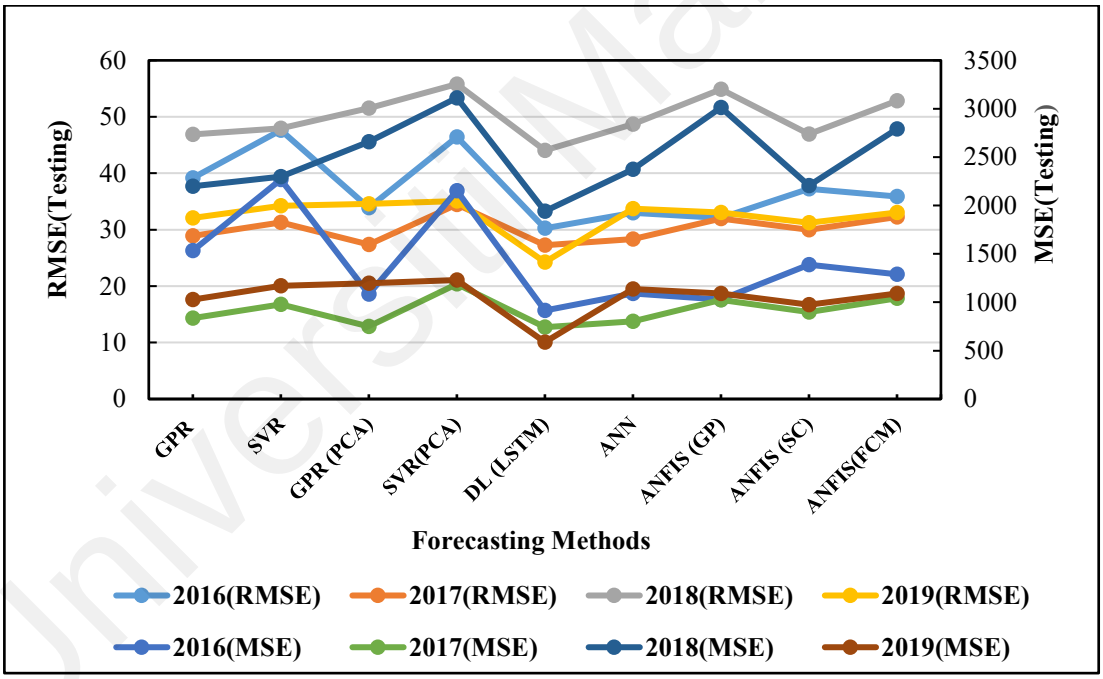

Figure 4.23:Testing RMSE and MSE for p-si over period (2016-2019)

Figure 4.24 indicates that the RNN-LSTM for the p-si module has exhibited the highest testing R^2 and r values of 0.995, 0.996, 0.9893,0.9971, and 0.9975, 0.998, 0.9946, 0.9985 respectively, over the duration (2016-2019), compared to other techniques.

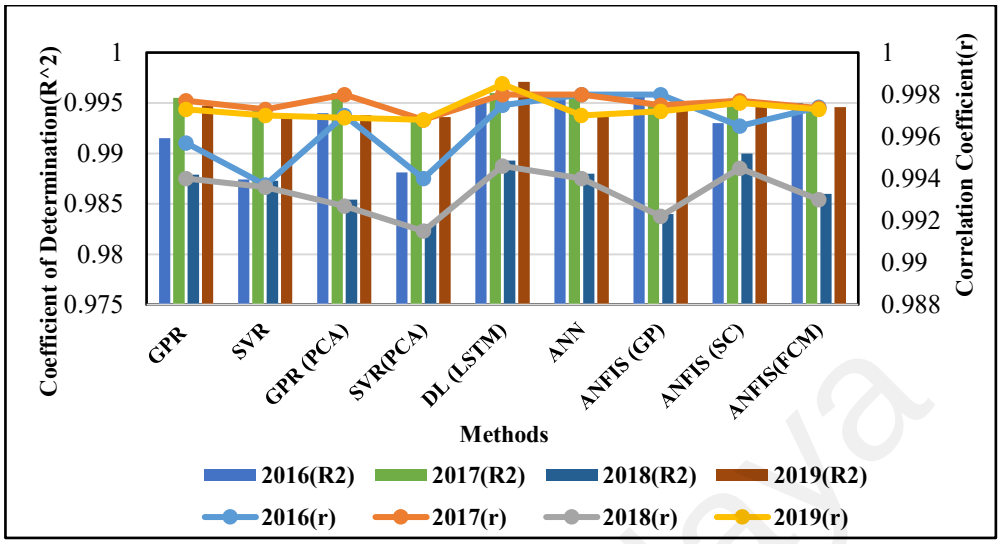

Figure 4.24:Testing R^2 and r for p-si over period (2016-2019)

4.3.3 Forecasting of solar power output for monocrystalline PV system

Figure 4.25 and Figure 4.26 exhibit the training (RMSE and MSE) and training (R^2 and r) respectively for an hour ahead forecasting of solar power output for the m-si module on an annual basis over the period (2016-2019). It is clear from Figure 4.25 that the deep learning technique (RNN-LSTM) has presented the lowest training RMSE and MSE values of 12.28, 12.81, 47.84, 13.32, and 150.86, 164.3, 2288.6, 177.55 respectively over the four years period in comparison with other techniques.

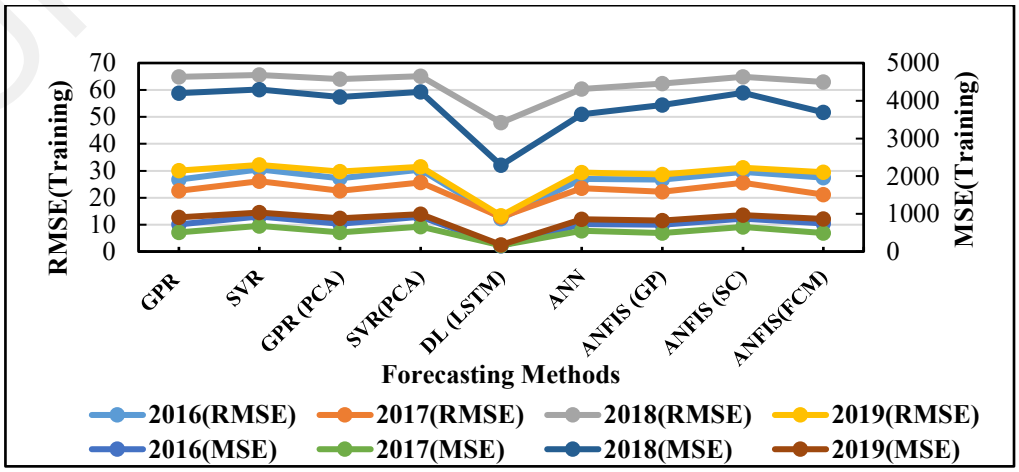

Figure 4.25:Training RMSE and MSE for m-si over period (2016-2019)

While in Figure 4.26, the RNN-LSTM for the m-si module has shown the highest training R^2 and r values of 0.998, 0.9976, 0.9617, 0.9963, and 0.999, 0.9988, 0.9807, 0.9981 over the period (2016-2019) respectively, compared to other techniques.

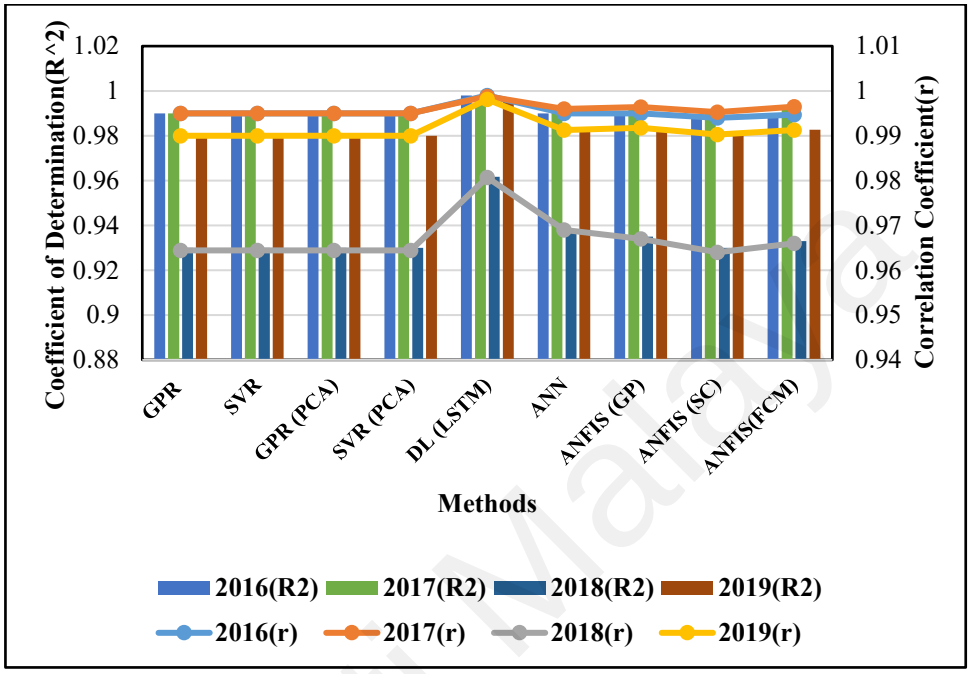

Figure 4.26:Training R^2 and r for m-si over period (2016-2019)

Figure 4.27 and Figure 4.28 presents the testing (RMSE and MSE) and testing (R^2 and r) respectively, for an hour ahead forecasting of solar power output for the m-si module on an annual basis over the period (2016-2019). The deep learning technique (RNN-LSTM) has exhibited the lowest testing RMSE and MSE values of 24.94, 29.04, 31.5, 19.4 and 621.65, 843.22, 991.9, 376.36 respectively over the period (2016-2019) in comparison with all other techniques as shown in Figure 4.27. While in Figure 4.28, the RNN-LSTM for the m-si modules have displayed the highest testing R^2 and r values of 0.991, 0.987,0.9832, 0.994 and 0.9954, 0.993, 0.9915, 0.997 over the period (2016-2019) respectively, in comparison with the testing results shown by other techniques. The RMSE and (r, R^2) are inversely related to each other. As RMSE is decreased, the correspond r and R^2 values are increased showing strong correlation.

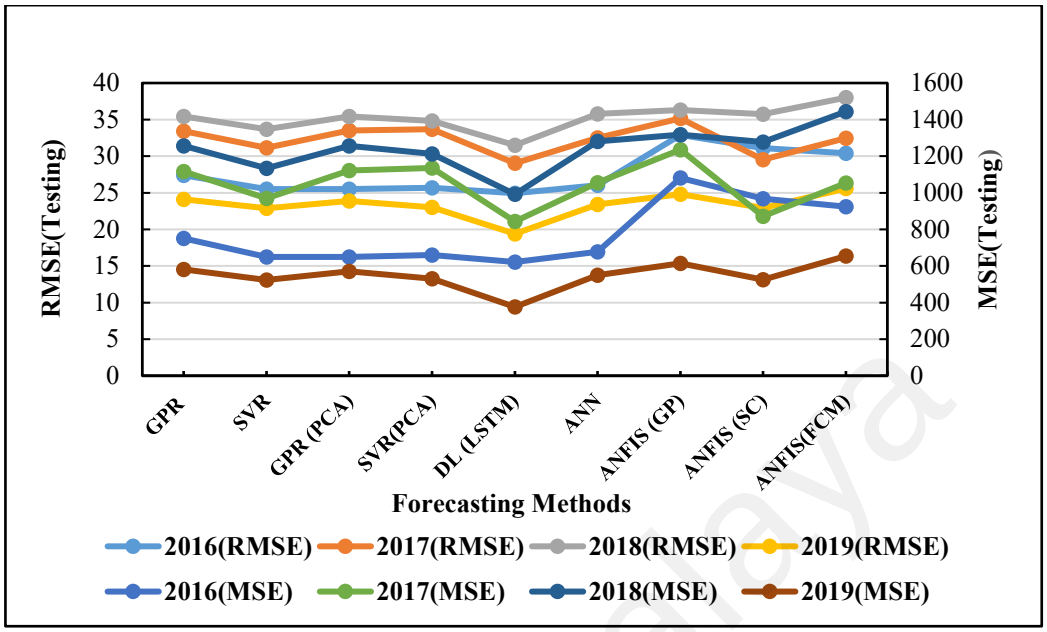

Figure 4.27:Testing RMSE and MSE for m-si over period (2016-2019)

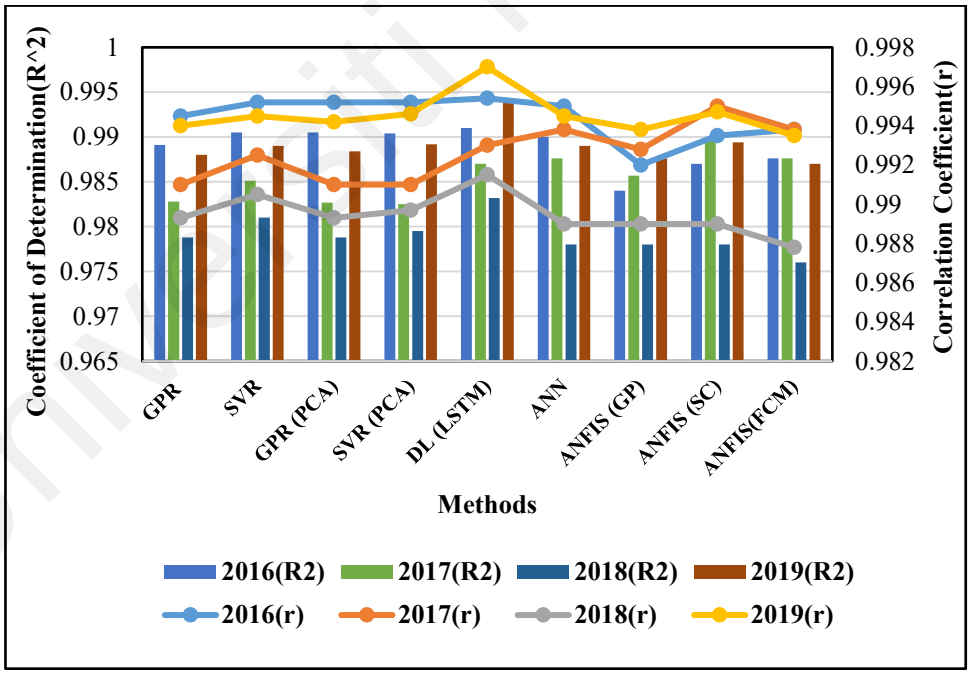

Figure 4.28:Testing R^2 and r for m-si over period (2016-2019)

4.3.4 Forecasting of solar power output for thin-film PV system

Figure 4.29 and Figure 4.30 illustrate the training (RMSE and MSE) and training (R^2 and r) respectively, for an hour ahead forecasting of solar power output for a a-si PV

system on an annual basis over the period (2016-2019). Figure 4.29 shows that that the proposed deep learning technique (RNN-LSTM) has proved the lowest training RMSE and MSE values of 38.06, 35.16, 130.44, 26.42, and 1448.4, 1236.4, 17015, 698.2 respectively over the four years period, in comparison with other techniques. While, the RNN-LSTM has also revealed the highest training R^2 and r values of 0.9967, 0.997, 0.957, 0.9978, and 0.998, 0.9985, 0.9782, 0.9989 over the period (2016-2019) respectively, compared to other techniques as indicated in Figure 4.30.

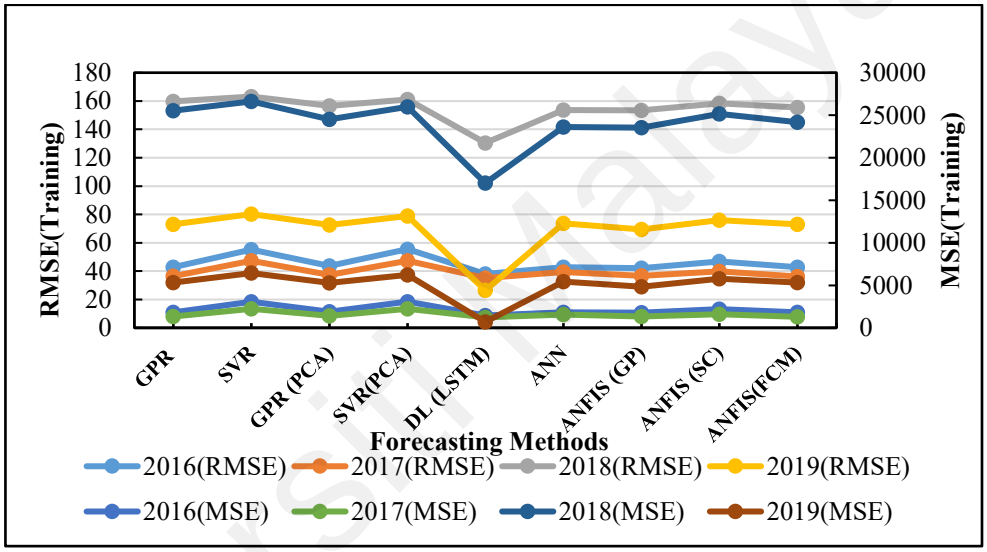

Figure 4.29:Training RMSE and MSE for a-si over period (2016-2019)

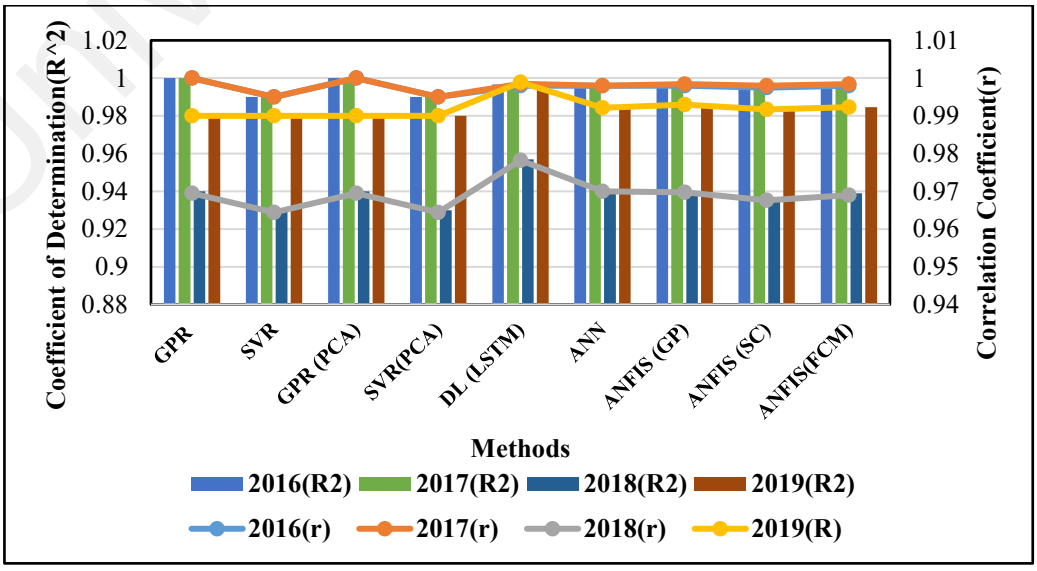

Figure 4.30:Training R^2 and r for a-si over period (2016-2019)

Figure 4.31 and Figure 4.32 describe the testing (RMSE and MSE) and testing (R^2 and r) respectively, for an hour ahead forecasting of solar power output for a a-si PV system on an annual basis over the period (2016-2019). The deep learning technique (RNN-LSTM) has illustrated the lowest testing RMSE and MSE values of 43.37, 39.2, 78.25, 65.03, and 1881.3, 1561, 6123.7, 4228.9 over four years (2016-2019) respectively, in comparison with all other techniques as shown in Figure 4.31.

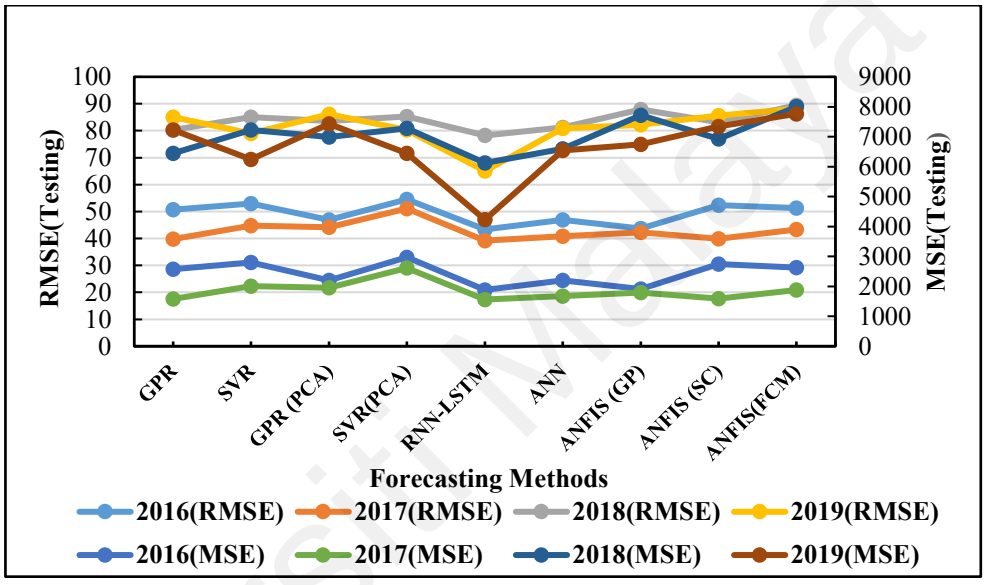

Figure 4.31:Testing RMSE and MSE for a-si over period (2016-2019)

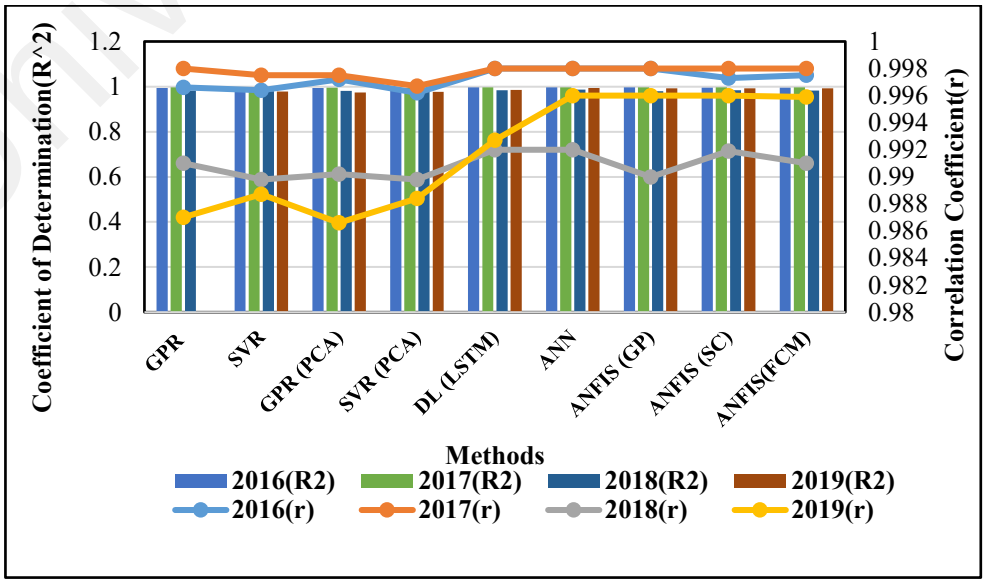

Figure 4.32:Testing R^2 and r for a-si over period (2016-2019)

Figure 4.32 indicates that the proposed (RNN-LSTM) have shown the highest testing R^2 and r values of 0.996, 0.9961, 0.984 and 0.998, 0.998, 0.992 over the period (2016-2018) respectively for a a-si PV system, compared to forecasting results presented by other regression, machine learning, and hybrid methods. However, for the year 2019, the ANN and ANFIS has shown better R^2 and r values than the proposed method.

4.3.5 Comparative study

PV power output forecasting for an hour ahead is performed for three different types of PV systems on an annual basis over four years of data recorded period (2016-2019). The proposed deep learning technique (RNN-LSTM) is compared with other forecasting methods such as GPR, SVR, GPR(PCA), SVR(PCA), ANN, ANFIS(GP), ANFIS(SC), and ANFIS(FCM).

The forecasting accuracy is evaluated based on the parameters such as RMSE, MSE, MAE, r, and R^2. Initially, the comparison of different LSTM structures is performed for 2019 data only to show the dominance of the single layered LSTM structure used in the proposed deep learning method (RNN-LSTM). The 2019 data is more clean and accurate compared with other three years data, because there is no missing data incorporated in it due to power failure of data recording sensors. Moreover, it is shown that the proposed technique (RNN-LSTM) has presented the lowest testing (RMSE, MSE) and highest (r, R^2) in comparison with other eight benchmark methods for an hour ahead prediction of output PV power for all three different PV systems on an annual basis during the observed data period (2016-2019). The exception is that for a-si PV system, the ANFIS and ANN have shown better testing r and R^2 than the proposed method for 2019 data only.

Furthermore, the p-si, m-si, and a-si PV systems have presented the lowest RMSE values of 24.25 W/m^2 in 2019, 19.4 W/m^2 in 2016, and 39.2 W/m^2 W/m^2 in 2017, respectively compared to the results in the other three years. On the other hand, all PV

systems have the highest values of RMSE for the year 2018. This may happen due to some missing input data incorporated because of the power failure of recording sensors. It can be observed that the proposed method has exhibited better forecasting accuracy for three different PV systems on an annual basis over four years of data duration. The three different PV systems are based on p-si, m-si and a-si technologies. The proposed deep learning method can also work with other PV systems in similar and different climates. The data over four years (2016-2019) is recorded on a practical system. Due to power failure, the recording sensors could not record the input parameters for some days. The missing data is swapped with the actual data from previous or next year. Robustness is defined as an ability of the system to function properly despite of the faults in the system. Despite of some missing data incorporated, the proposed deep learning method has functioned properly over four years of data for three different PV systems. The proposed method has shown lower RMSE for all PV systems than the RMSE presented by LSTM in other commercialized systems (Qing & Niu, 2018; Srivastava & Lessmann, 2018; Zhang, Verschae, Nobuhara, & Lalonde, 2018). Therefore, it can be stated that the proposed deep learning method (RNN-LSTM) is robust for an hour ahead forecasting of power output for three different PV systems.

In addition, Table 4.4 presents the prediction accuracy comparison of the proposed method (RNN-LSTM) and related benchmark methods used in this research with the similar forecasting methods used in (Hossain, Mekhilef, Danesh, et al., 2017) for similar site data of 2016. The proposed (RNN-LSTM) and benchmark methods used in this research have shown better forecasting results than those shown by the given methods in (Hossain, Mekhilef, Danesh, et al., 2017).

4.3.6 Forecasting results of optimized deep learning methods

In this section, the hyperparameters of proposed deep learning model are further tuned using three different optimization algorithms such as GA, PSO, and SSA, to enhance

Table 4.4: Forecasting accuracy comparison of the proposed and benchmark methods (ANN, SVR) in this research with the results in existing literature for similar 2016 data

Parameters	PV Systems	Predicted Results			(Hossain, Mekhilef, Danesh, et al., 2017)		
		Proposed (RNN-LSTM)	ANN	SVR	ELM	ANN	SVR
RMSE	p-si	30.25	33	47.63	54.96	60.27	71.92
	m-si	24.94	26.03	25.49	59.93	101.23	103.61
	a-si	43.37	46.9	52.92	90.41	101.99	145.38
R^2	p-si	0.995	0.996	0.9874	0.9809	0.9798	0.9750
	m-si	0.991	0.99	0.9905	0.8675	0.8647	0.8618
	a-si	0.996	0.996	0.9928	0.9783	0.9754	0.9704

the forecasting accuracy of the developed model for all three PV systems over the data period (2016-2019). The optimized forecasting accuracy measurement parameters (RMSE, MAE, MSE and R^2), tuned hyperparameters, convergence speed, and prediction plots of optimized deep learning methods are presented and discussed separately for all three PV systems over the duration (2016-2019).

4.3.6.1 Optimized forecasting accuracy measurement parameters

Table 4.5 - Table 4.8 elaborate the optimized forecasting accuracy measurement parameters of deep learning algorithm hybridized with three different optimization algorithms, which are GA, PSO, and SSA in comparison with (RNN-LSTM) method for three different PV system based on 2016, 2017, 2018 and 2019 data respectively. Table 4.5 shows that for the year 2016, the proposed hybrid (SSA-RNN-LSTM) method has exhibited the lowest testing RMSE of 24.46, 21.1, and 35.77 for p-si, m-si, and a-si PV systems, respectively in comparison with the results shown by GA and PSO hybridized deep learning methods. For the year 2017, the proposed method has also presented the lowest testing RMSE values of 26.74, 26.29, and 38.79 for all three PV systems, respectively, in Table 4.6.

Table 4.5: The Optimized forecasting accuracy measurement parameters of three PV systems for 2016 data

Methods	p-si				m-si				a-si			
	RMSE	**MAE**	**MSE**	**R^2**	**RMSE**	**MAE**	**MSE**	**R^2**	**RMSE**	**MAE**	**MSE**	**R^2**
RNN- LSTM	30.25	20.43	915.1	0.995	24.94	18.04	621.65	0.991	43.37	29.74	1881.3	0.996
GA- RNN- LSTM	28.46	20.14	810	0.9955	22.65	16.93	513.6	0.9925	38.28	27.14	1465.1	0.9962
PSO-RNN-LSTM	26.87	19.59	722.08	0.996	22.07	16.73	486.97	0.993	37.4	26.55	1398.76	0.9964
SSA-RNN-LSTM	**24.46**	**17.95**	**598.42**	**0.9967**	**21.1**	**16.09**	**445.6**	**0.9935**	**35.77**	**25.58**	**1279.8**	**0.9967**

Table 4.6: The Optimized forecasting accuracy measurement parameters of three PV systems for 2017 data

Methods	p-si				m-si				a-si			
	RMSE	**MAE**	**MSE**	**R^2**	**RMSE**	**MAE**	**MSE**	**R^2**	**RMSE**	**MAE**	**MSE**	**R^2**
RNN- LSTM	27.25	15.14	742.5	0.996	29.04	20.02	843.22	0.987	39.2	21.98	1561	0.9961
GA- RNN- LSTM	27.04	15.2	731.6	0.9961	28.46	19.47	810.07	0.9875	39	21.65	1521.6	0.9962
PSO-RNN-LSTM	26.78	14.72	717.38	0.9961	27.93	19.2	779.9	0.988	38.88	21.63	1511.9	0.9962
SSA-RNN-LSTM	**26.74**	**14.34**	**715.1**	**0.9961**	**26.29**	**18.23**	**691**	**0.9894**	**38.79**	**21.52**	**1505.2**	**0.9963**

Table 4.7: The Optimized forecasting accuracy measurement parameters of three PV systems for 2018 data

Methods	p-si				m-si				a-si			
	RMSE	**MAE**	**MSE**	**R^2**	**RMSE**	**MAE**	**MSE**	**R^2**	**RMSE**	**MAE**	**MSE**	**R^2**
RNN- LSTM	44.06	24.02	1941.2	0.9893	31.5	17.8	991.9	0.9832	78.25	44.93	6123.7	0.9829
GA- RNN- LSTM	41.58	20.1	1728.9	0.9905	29.77	17	886.33	0.9850	75.76	44.49	5740.2	0.984
PSO-RNN-LSTM	40.53	19.56	1643.1	0.991	28.72	16.87	825	0.9861	72.43	39.56	5246.6	0.9854
SSA-RNN-LSTM	**39.2**	**18.84**	**1537.5**	**0.9915**	**28.4**	**16.29**	**806.34**	**0.9864**	**72.15**	**38.47**	**5206.5**	**0.9855**

Table 4.8: The Optimized forecasting accuracy measurement parameters of three PV systems for 2019 data

Methods	p-si				m-si				a-si			
	RMSE	**MAE**	**MSE**	**R^2**	**RMSE**	**MAE**	**MSE**	**R^2**	**RMSE**	**MAE**	**MSE**	**R^2**
RNN- LSTM	24.25	17.46	588.07	0.9971	19.4	13.88	376.36	0.994	65.03	50.92	4228.9	0.9855
GA- RNN- LSTM	23.93	17.13	572.85	0.9971	18.92	13.78	357.97	0.9935	59.9	45.44	3587.8	0.9877
PSO-RNN-LSTM	22.93	16.53	525.9	0.9974	18.51	13.63	342.61	0.9932	53.49	41.35	2861.1	0.9902
SSA-RNN-LSTM	**22.21**	**16.1**	**493.2**	**0.9975**	**18.46**	**13.31**	**340.82**	**0.9932**	**50.14**	**38.09**	**2514.3**	**0.9991**

Results in Table 4.7 and Table 4.8 also indicate that the proposed hybrid (SSA-RNN-LSTM) method is superior to conventional (RNN-LSTM) and other hybrid methods such as GA-RNN-LSTM and PSO-RNN-LSTM in terms of having the lowest testing RMSE, MAE, MSE, and highest testing R^2 values for all three different PV systems for 2018 and 2019 respectively. The reason is that the SSA always looks for global optima due to the gradual movement of the follower salp. The leader salp discovers and utilizes the search space around it. It is also less complex due to one controlling parameter. The (PSO-RNN-LSTM) has demonstrated the second lowest forecasting accuracy measurement parameters for all three PV systems over the four years data duration (2016-2019) in comparison with GA-RNN-LSTM because the PSO has fewer parameters and can deal with continuous problems of optimization like LSTM. While GA is more feasible for the optimization of discrete problems.

4.3.6.2 Tuned hyperparameters and convergence speed

The optimized hyperparameters and convergence time of three hybrid deep learning methods for three PV systems based on 2016 data are presented in Table 4.9. It can be observed that the proposed (SSA-RNN-LSTM) method has shown less convergence time for all three PV systems compared to other optimized deep learning methods. The convergence time of (PSO-RNN-LSTM) is between GA-RNN-LSTM and SSA-RNN-LSTM for m-si and a-si PV systems; while, GA has the second lowest convergence time for the p-si PV system.

Table 4.10 indicates the optimized hyperparameters and convergence time of three hybrid deep learning methods for three PV systems based on 2017 data. It can be observed that the proposed (SSA-RNN-LSTM) method has shown the lowest convergence time of 1160.64 and 1115.77 seconds for m-si and a-si PV systems, respectively compared to other optimized deep learning methods. For the p-si PV system, the convergence time of

the proposed (SSA-RNN-LSTM) is a little inferior and comparable to (PSO-RNN-LSTM), while GA-RNN-LSTM has shown the second lowest convergence time for a-si PV systems.

Table 4.9: Optimized hyperparameters of hybrid deep learning methods for three PV systems based on 2016 data

Methods	PV Systems	Hidden units	Epochs	Learn rate drop period	Learning rate	Learn rate drop factor	Convergence time (sec)
GA-RNN-LSTM	p-si	120	400	125	0.005	0.1	1334.9
	m-si	150	399	140	0.0097	1	1631.5
	a-si	102	279	127	0.0022	0.5152	1637.9
PSO-RNN-LSTM	p-si	102	340	54	0.01	0.3883	1576.5
	m-si	83	302	158	0.00099	0.5575	1306.8
	a-si	90	292	111	0.0025	0.2954	1226.5
SSA-RNN-LSTM	p-si	200	257	75	0.001	0.68	1236.25
	m-si	105	201	111	0.0075	0.74	1189.48
	a-si	200	200	106	0.001	1	1180.16

Table 4.10: Optimized hyperparameters of hybrid deep learning methods for three PV systems based on 2017 data

Methods	PV Systems	Hidden units	Epochs	Learn rate drop period	Learning rate	Learn rate drop factor	Convergence time (sec)
GA-RNN-LSTM	p-si	166	364	146	0.007	0.3757	2081.5
	m-si	152	236	135	0.0072	0.0107	1602.8
	a-si	86	311	150	0.006	0.5898	1848.5
PSO-RNN-LSTM	p-si	127	319	84	0.0041	0.6835	1584.6
	m-si	181	231	98	0.0029	0.9	1285.3
	a-si	170	322	143	0.0038	0.7131	1869
SSA-RNN-LSTM	p-si	200	400	125	0.005	0.2	1740.22
	m-si	130	249	120	0.008	0.9	1160.64
	a-si	179	215	157	0.0051	0.68	1115.77

Table 4.11 specifies the optimized hyperparameters and convergence time of three hybrid deep learning methods for three PV systems based on 2018 data. It can be viewed that the proposed (SSA-RNN-LSTM) method has proven the lowest convergence time of 1218.53 and 1277.52 seconds for m-si and a-si PV systems, respectively compared to other optimized deep learning methods. However, the p-si PV system has developed the second lowest convergence time for the proposed method compared to other methods. The GA and PSO have comparable convergence performance for the other two PV systems.

Table 4.11: Optimized hyperparameters of hybrid deep learning methods for three PV systems based on 2018 data

Methods	PV Systems	Hidden units	Epochs	Learn rate drop period	Learning rate	Learn rate drop factor	Convergence time (sec)
GA-RNN-LSTM	p-si	148	359	70	0.0085	0.5975	1584.74
	m-si	200	400	125	0.005	0.2	1632.74
	a-si	147	272	130	0.008	0.806	1906.8
PSO-RNN-LSTM	p-si	119	295	103	0.0052	0.4863	1316
	m-si	135	327	187	0.0036	0.6948	1688.7
	a-si	140	314	122	0.0051	0.6791	3156.4
SSA-RNN-LSTM	p-si	194	200	84	0.006	0.76	1387.88
	m-si	191	200	200	0.0047	1	1218.53
	a-si	185	200	200	0.0055	0.85	1277.52

Table 4.12 denotes the optimized hyperparameters and convergence time of three hybrid deep learning methods for three PV systems based on 2019 data. It can be viewed that the proposed (SSA-RNN-LSTM) method has shown fast convergence speed with the lowest convergence time of 1195, 1279, and 1506.9 seconds for p-si, m-si, and a-si PV systems, respectively, compared to other optimized deep learning methods. The convergence speed of (PSO-RNN-LSTM) is almost in between GA and SSA for p-si and m-si PV systems; while, GA has the second lowest convergence time for a a-si PV system. The convergence plots of three hybrid algorithms for three PV systems over four years period (2016-2019) are given in Appendix A.

Table 4.12: Optimized hyperparameters of hybrid deep learning methods for three PV systems based on 2019 data

Methods	PV Systems	Hidden units	Epochs	Learn rate drop period	Learning rate	Learn rate drop factor	Convergence time (sec)
GA-RNN-LSTM	p-si	134	355	158	0.0047	0.4022	1914.8
	m-si	164	358	116	0.0077	0.8119	1628.2
	a-si	192	395	108	0.0032	0.3522	1520.1
PSO-RNN-LSTM	p-si	114	263	135	0.0027	0.6618	1354.8
	m-si	104	268	151	0.0058	0.7840	1396.3
	a-si	169	343	137	0.0055	0.6734	1713.9
SSA-RNN-LSTM	p-si	94	200	82	0.01	1	1195
	m-si	155	205	50	0.01	0.03	1279
	a-si	86	262	192	0.01	0.69	1506.9

4.3.6.3 Prediction results of optimized deep learning methods

To observe the difference between prediction results shown by different hybrid methods, only 25 predicted samples of the predicted data are plotted for all four years.

Figure 4.33, Figure 4.34, and Figure 4.35 describe the prediction results of the optimized deep learning methods for p-si, m-si, and a-si PV systems, respectively, based on 2016 data. The predicted results for the proposed hybrid method (SSA-RNN-LSTM) are following the actual power curve more closely as compared to other methods.

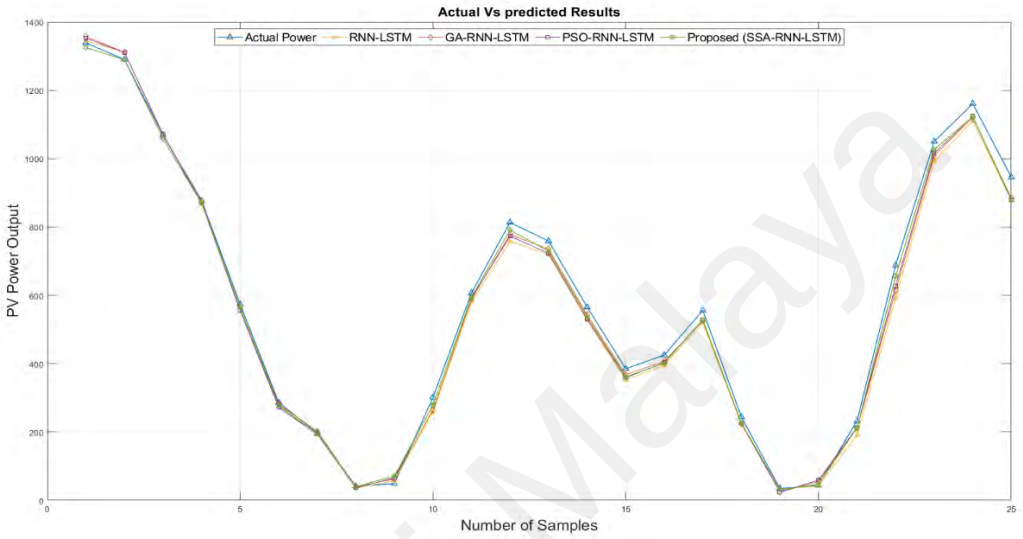

Figure 4.33: Prediction results of optimized deep learning methods for p-si PV system based on 2016 data

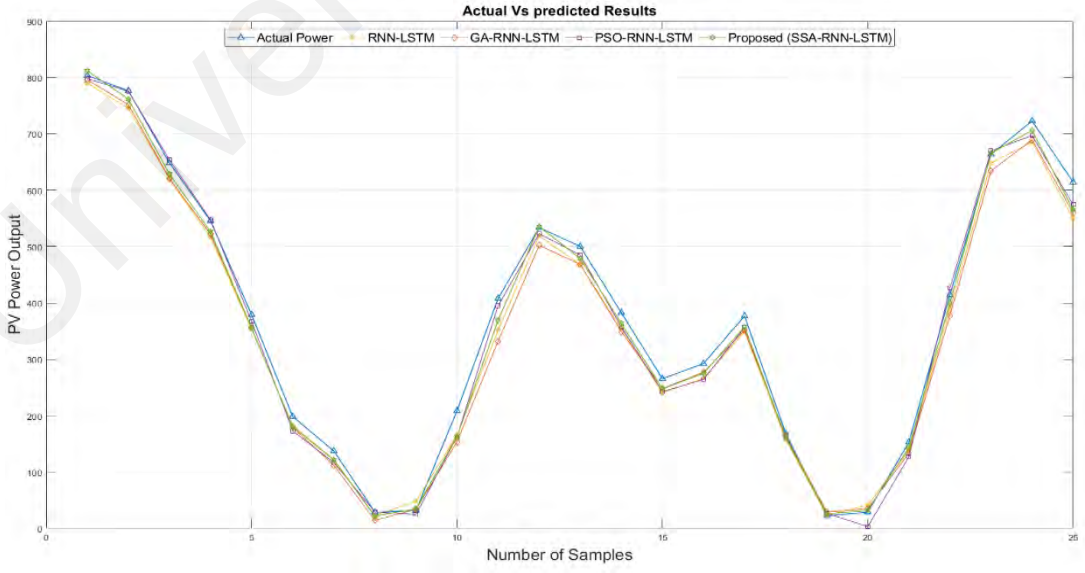

Figure 4.34: Prediction results of optimized deep learning methods for m-si PV system based on 2016 data

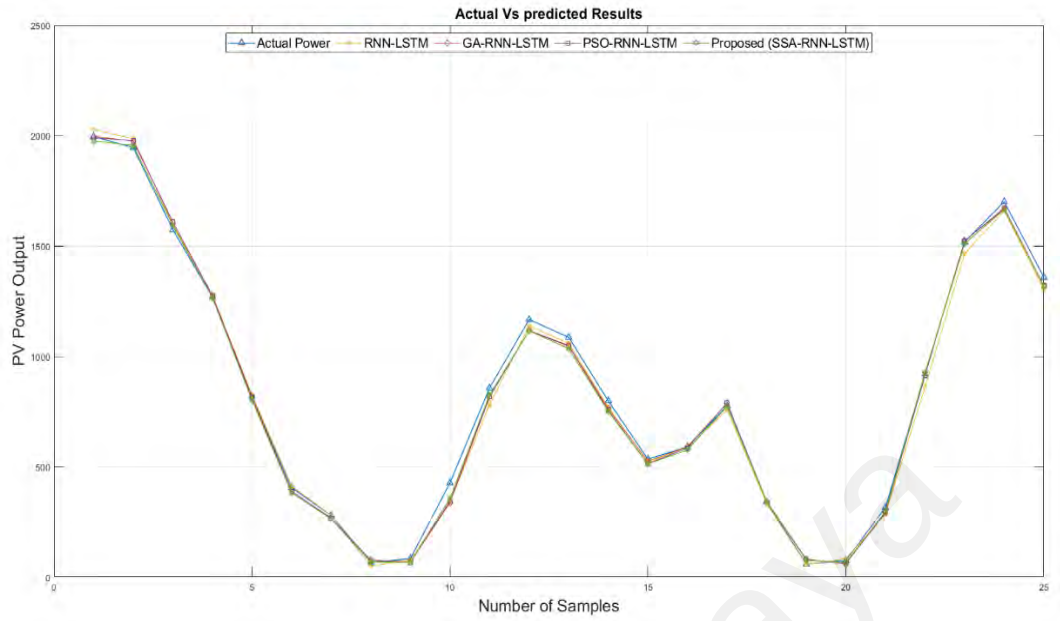

Figure 4.35: Prediction results of optimized deep learning methods for a-si PV system based on 2016 data

Figure 4.36, Figure 4.37, and Figure 4.38 show the prediction plots of the optimized deep learning methods for p-si, m-si, and a-si PV systems, respectively, based on 2017 data. The proposed hybrid method (SSA-RNN-LSTM) is closely tracking the actual power dotted line curve in comparison with other methods.

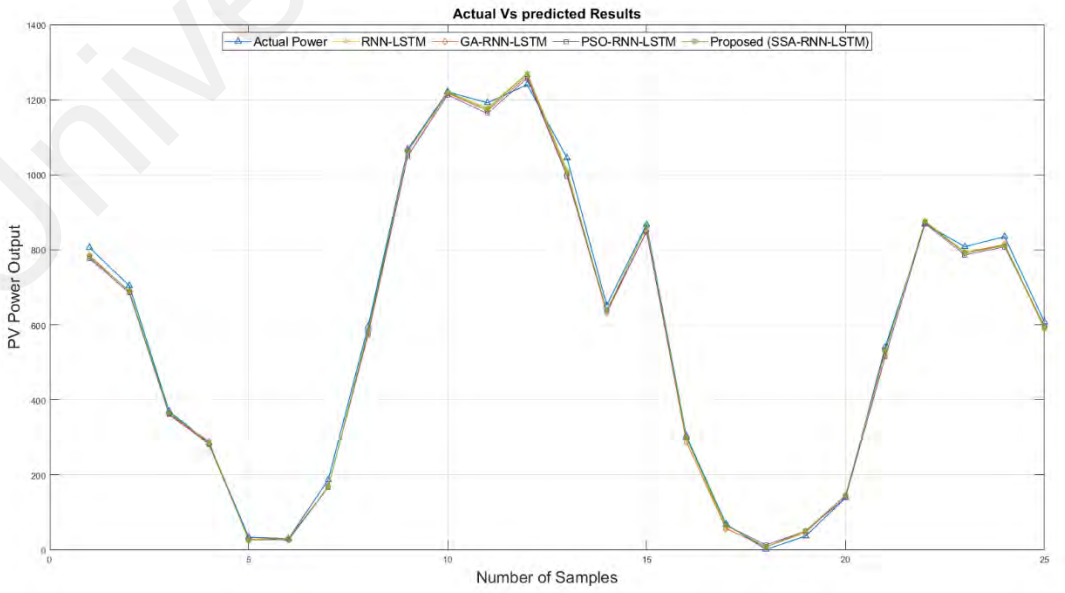

Figure 4.36: Prediction results of optimized deep learning methods for p-si PV system based on 2017 data

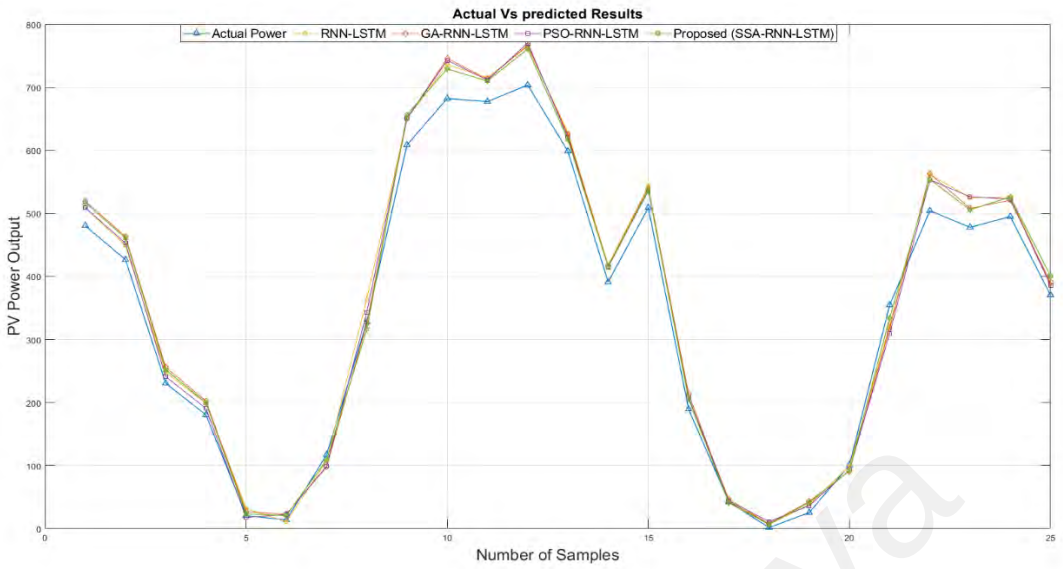

Figure 4.37: Prediction results of optimized deep learning methods for m-si PV system based on 2017 data

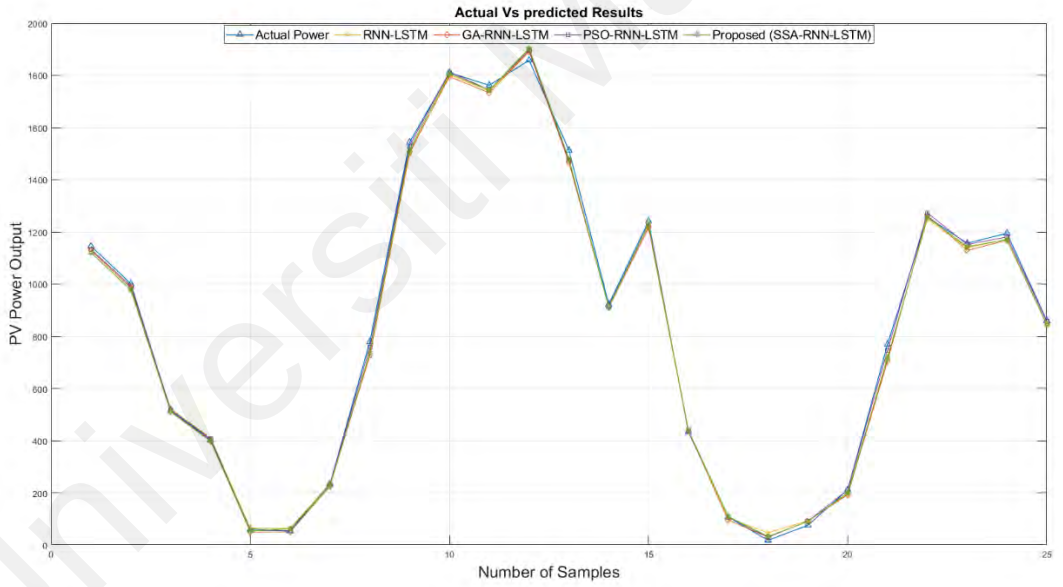

Figure 4.38: Prediction results of optimized deep learning methods for a-si PV system based on 2017 data

The proposed hybrid method (SSA-RNN-LSTM) is also following the actual power dotted line curve more closely than other methods for the prediction plots presented in Figure 4.39, Figure 4.40, and Figure 4.41 for p-si, m-si, and a-si PV systems, respectively, based on 2018 data.

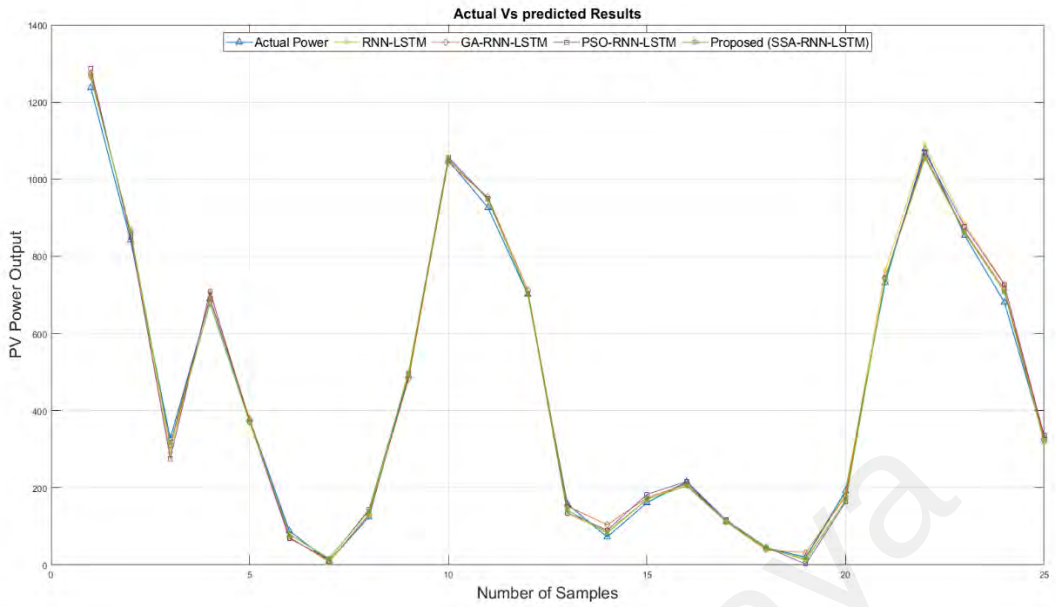

Figure 4.39: Prediction results of optimized deep learning methods for p-si PV system based on 2018 data

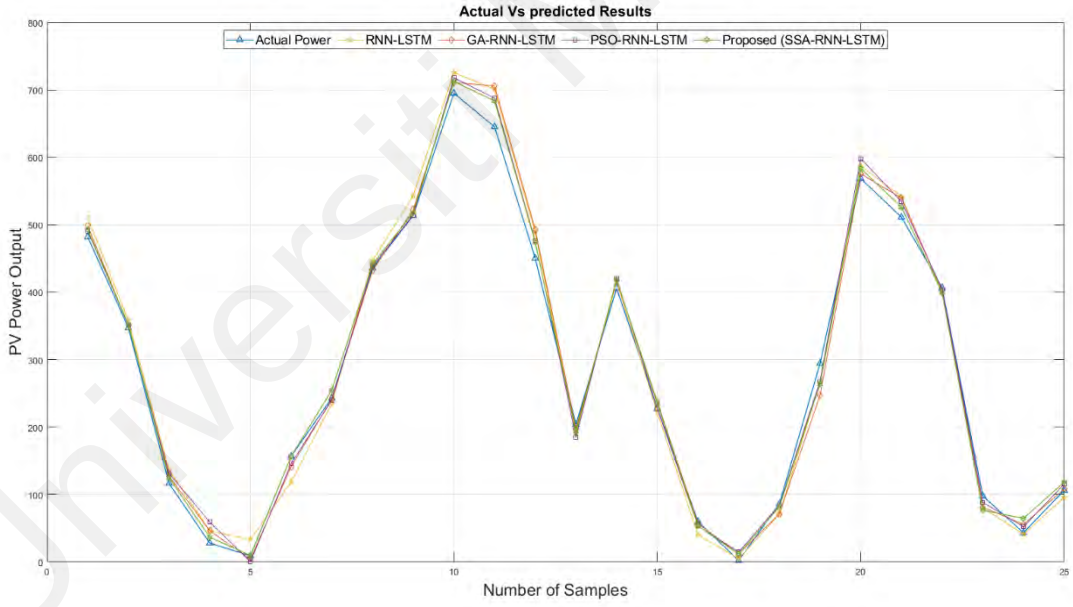

Figure 4.40: Prediction results of optimized deep learning methods for m-si PV system based on 2018 data

Figure 4.42, Figure 4.43, and Figure 4.44 show the prediction plots of the optimized deep learning methods for p-si, m-si, and a-si PV systems, respectively, based on 2019 data. The proposed hybrid method (SSA-RNN-LSTM) is closely following the actual power dotted line curve in comparison with other methods.

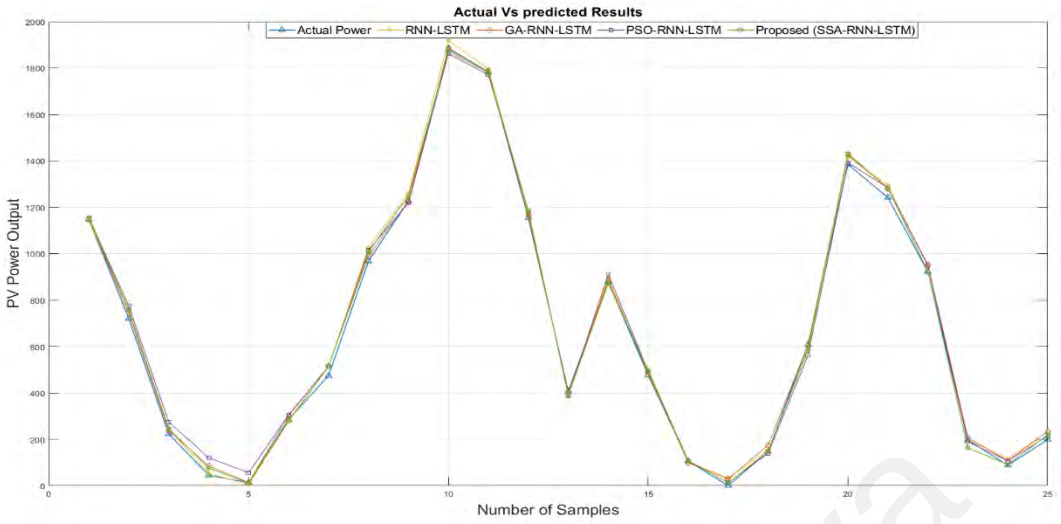

Figure 4.41: Prediction results of optimized deep learning methods for a-si PV system based on 2018 data

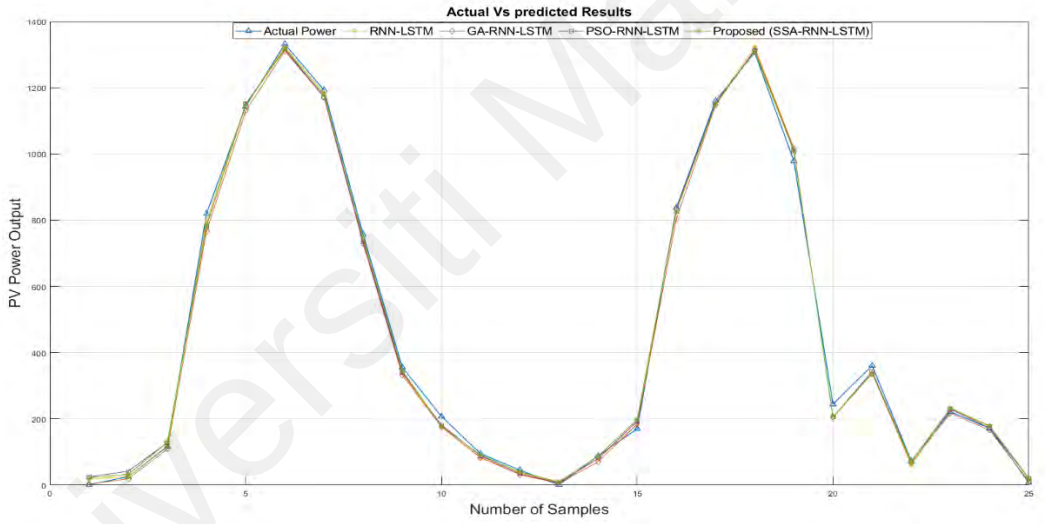

Figure 4.42: Prediction results of optimized deep learning methods for p-si PV system based on 2019 data

4.3.6.4 Comparative analysis

In this section, an hour ahead forecasting accuracy of the developed deep learning algorithm (RNN-LSTM) is enhanced by tuning its hyperparameters using three optimization algorithms, namely GA, PSO, and the SSA, on an annual basis over all four years data. It can be observed from the results that the proposed hybrid method (SSA-RNN-LSTM) has performed better compared to developed (RNN-LSTM) and other

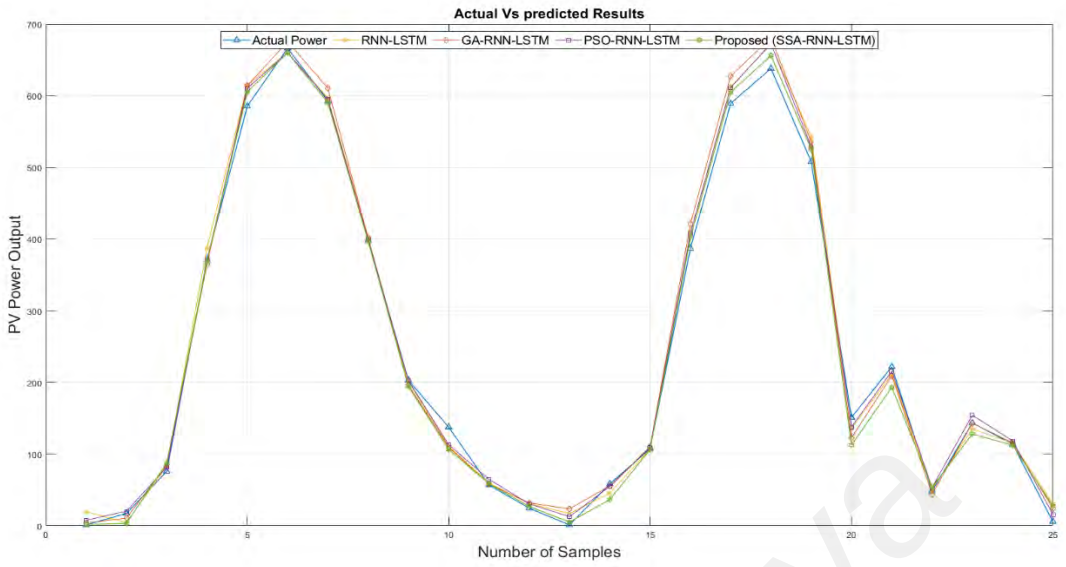

Figure 4.43:Prediction results of optimized deep learning methods for m-si PV system based on 2019 data

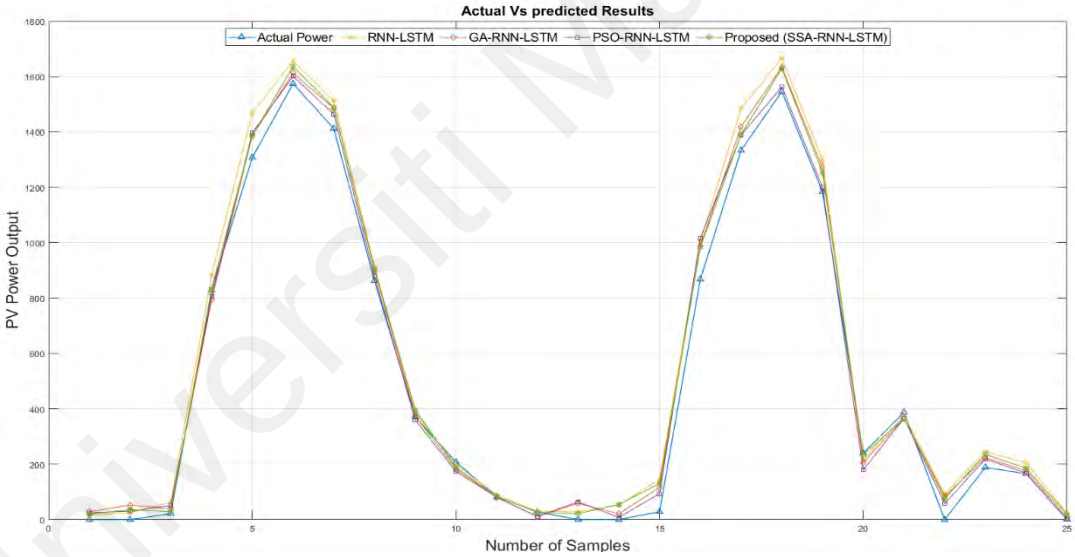

Figure 4.44:Prediction results of optimized deep learning methods for a-si PV system based on 2019 data

hybrid algorithms. It has shown the lowest (RMSE, MAE, and MSE) and highest R^2 in comparison to other methods for an hour ahead forecasting of PV power output for three different PV systems on an annual basis for four years of data.

Figure 4.45-Figure 4.48 elaborate the % reduction in testing RMSE and MAE with respect to the developed (RNN-LSTM) model by three hybrid algorithms for three PV

systems over the years 2016-2019, respectively. It can be observed that the proposed hybrid method (SSA-RNN-LSTM) has provided a higher % reduction in testing RMSE and MAE for all three PV systems for each year in comparison with the other two hybrid methods. For the p-si PV system, the % reduction in RMSE (19.14%) is found higher in 2016 than other three years, while the % reduction in MAE (21.57%) is observed higher in 2018 than in other years.

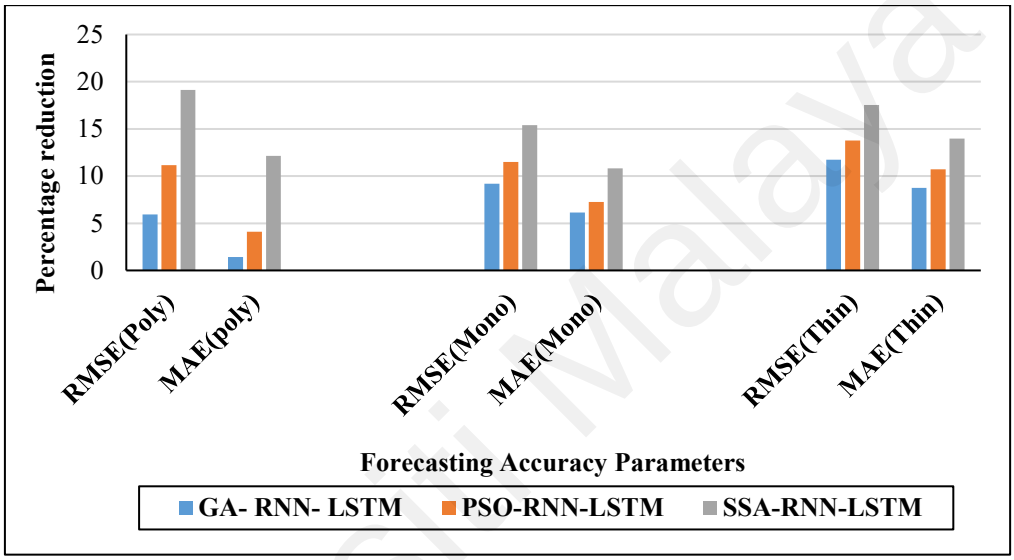

Figure 4.45: Percentage reduction in testing RMSE and MAE for three PV systems in 2016

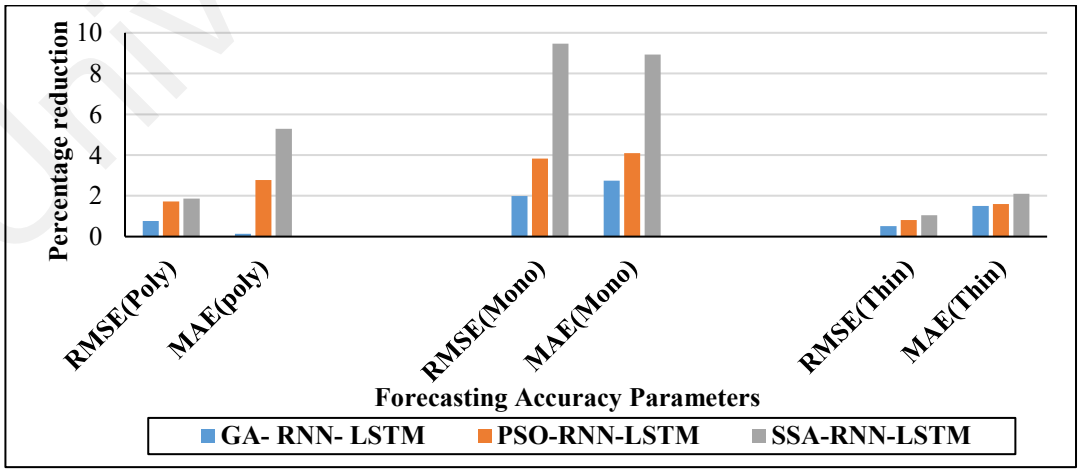

Figure 4.46: Percentage reduction in testing RMSE and MAE for three PV systems in 2017

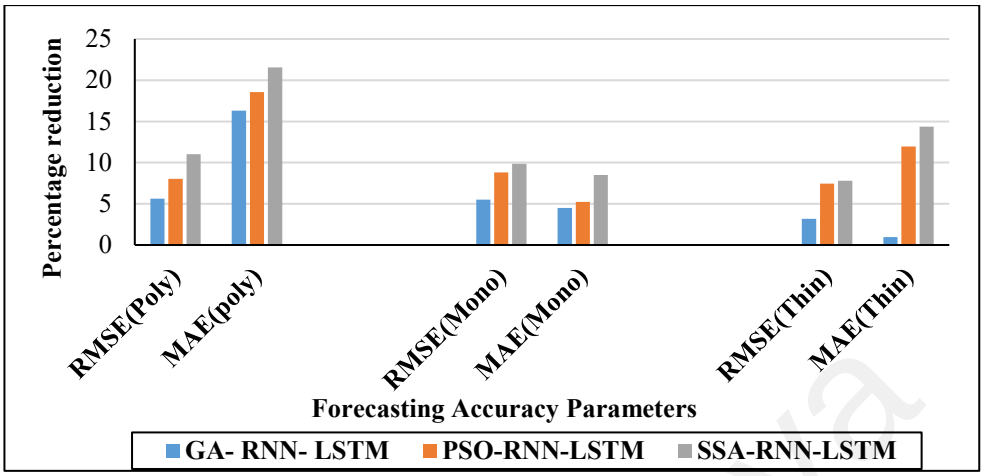

Figure 4.47: Percentage reduction in testing RMSE and MAE for three PV systems in 2018

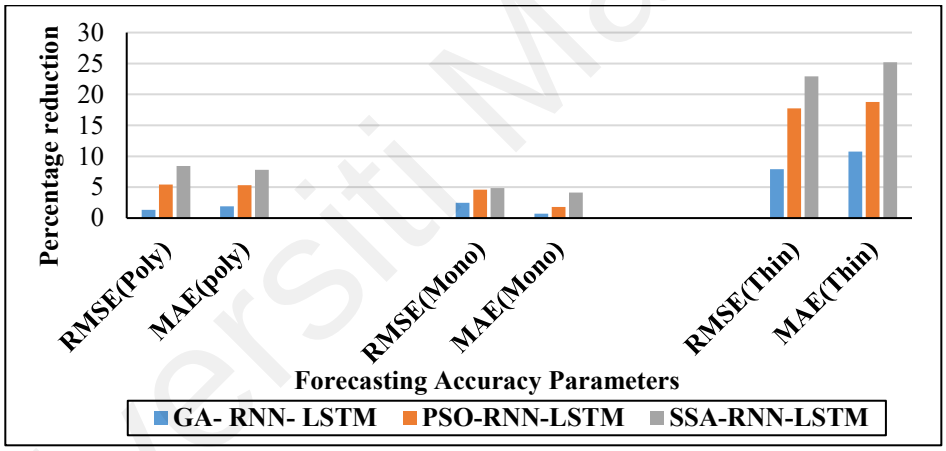

Figure 4.48: Percentage reduction in testing RMSE and MAE for three PV systems in 2019

For the m-si PV system, the % reduction in RMSE (15.4%) and MAE (10.81%) is higher for 2016 than other years. Moreover, the proposed hybrid method has presented a higher % reduction in RMSE (22.9%) and MAE (25.2%) for a-si PV systems compared to other hybrid methods based on 2019 data.

The convergence speed of the proposed hybrid algorithm (SSA-RNN-LSTM) is also higher than the other two optimization methods for the whole four years of data. Finally, the prediction results for the optimized deep learning method for all three PV systems

over four years period (2016-2019) have shown that the predicted data curves for the proposed (SSA-RNN-LSTM) are following the actual data curve more closely than other methods. Table 4.13 elaborates the forecasting accuracy comparison of the proposed hybrid (SSA-RNN-LSTM) method with the results given in the literature. The lowest testing RMSE and MAE values are selected among four years results. For p-si and m-si PV system, the testing RMSE and MAE are lowest for the year 2019. While, the year 2016 has shown lowest testing RMSE and MAE for thin film PV system. It can be observed that the proposed hybrid method has shown less testing RMSE and MAE compared to other deep learning and hybrid methods given in the literature.

Table 4.13:Forecasting accuracy comparison of proposed hybrid method with literature

Forecasting Method	Reference	Testing RMSE (W/m^2)	Testing MAE(W/m^2)
SSA-RNN-LSTM (p-si)	**Proposed study**	**22.1**	**16.1**
SSA-RNN-LSTM (m-si)	**Proposed study**	**18.41**	**13.31**
SSA-RNN-LSTM (a-si)	**Proposed study**	**35.77**	**25.58**
DPNN	(Zjavka, 2020)	52.8	-
K-means clustering-autoencoder-CNN-LSTM	(Zhen et al., 2020)	45.11	-
LSTM	(Zhang et al., 2018)	139.3	-
LSTM	(Qing & Niu, 2018)	122.7	-
LSTM	(Qing & Niu, 2018)	76.24	-
LSTM	(Srivastava & Lessmann, 2018)	<29.26	-
DCGSO-LASSO	(Jiang et al., 2017)	28.058	MAPE (13.247%)
K-means clustering-SVR	(Bae, Jang, & Sung, 2017)	99.95	-
ANN and KNN	(H. T. C. Pedro & Coimbra, 2015)	41.8	20
ST-ARX	(C. Yang et al., 2015)	154.5	111.4
SOM-LVQ-SVR	(H.-T. Yang et al., 2014)	350.2	-
TDNN -clustering algorithm	(J. Wu & Chan, 2013)	122	-

4.4 Summary

At the start of this chapter, the monthly and annual performance of three different PV systems is analyzed based on eleven performance parameters over the four years period to decide the most feasible PV system for the tropical climate of Kuala Lumpur, Malaysia. It is found that poly-crystalline based PV systems are the more suitable choice for the site considered due to higher (array yield, array, and system efficiencies) together with less degradation in almost all the considered performance parameters in comparison with the other two (a-s_i, m-s_i) PV systems for the monitored period (2016-2019). The results also indicate that environmentally the composite PV system has the potential to avoid 28143.7 kg of CO_2 emissions in four years.

Secondly, an hour ahead forecasting of solar power output is performed for three types of PV systems on an annual basis for the data recorded period (2016-2019). The deep learning technique (RNN-LSTM) is proposed to forecast the solar power output. The forecasting accuracy of the proposed deep learning method is compared with other methods, namely GPR, SVR, GPR(PCA), SVR(PCA), ANN, ANFIS(SC), ANFIS(FCM). The forecasting accuracy is evaluated based on the performance parameters such as RMSE, MAE, MSE, r, and R^2. It can be observed that the proposed method is found robust with better forecasting accuracy for three different PV systems on an annual basis over four years of data duration.

Finally, an hour ahead forecasting accuracy of the developed deep learning algorithm (RNN-LSTM) is enhanced further by tuning its hyperparameters using three optimization algorithms, GA, PSO, and SSA, on an annual basis for all four years data. The proposed hybrid (SSA-RNN-LSTM) method has performed better compared to other hybrid methods. It has shown the lowest (RMSE, MAE, and MSE) and highest R^2 in comparison to other methods for an hour ahead forecasting of PV power output on an annual basis for

three different PV systems over four years of data. The convergence speed of the proposed hybrid algorithm (SSA-RNN-LSTM) is also found higher than the other two hybrid methods for the whole four years duration. In addition, the tuned hyperparameters and prediction results are also presented for each year for three PV systems.

CHAPTER 5: CONCLUSIONS AND FUTURE WORK

5.1 Conclusions

This thesis focuses on the performance analysis and forecasting of solar power output for three grid-linked PV systems installed on the rooftop of the engineering tower at the Faculty of engineering, UM, Kuala Lumpur, Malaysia, over the monitored data period (2016-2019). The grid-connected PV systems are based on poly-crystalline (p-s_i), mono-crystalline (m-s_i), and a-si (amorphous silicon (a-s_i)) technologies. Firstly, the performance analysis of three PV systems along with the composite PV system is conducted based on eleven performance parameters, which are performance ratio, capacity factor, array yield, final yield, PV array efficiency, PV system efficiency, inverter efficiency, AC energy, array losses, system, and the overall losses.

Secondly, an hour ahead forecasting of solar power output for three PV systems is performed on an annual basis for actual data period (2016-2019) based on the proposed deep learning (RNN-LSTM) technique. The proposed technique (RNN-LSTM) is compared with other forecasting methods, which are GPR, SVR, GPR(PCA), SVR(PCA), ANN, ANFIS(GP), ANFIS(SC), and ANFIS(FCM). The performance parameters used to evaluate the forecasting accuracy of these techniques are root mean square error (RMSE), mean absolute error (MAE), mean square error (MSE), correlation coefficient (r), and coefficient of determination (R^2).

Moreover, the forecasting accuracy of the developed deep learning algorithm (RNN-LSTM) is enhanced further on an annual basis by tuning its hyperparameters using SSA optimization and is compared with other optimization algorithms such as GA and PSO for three PV systems over four years duration.

The findings of performance analysis of PV systems have shown that the p-s_i and a-s_i PV systems have an equal annual average (PR, CF, final yield, and overall losses);

while an annual average (array yield, array, and system efficiency) of p-s_i based PV system is better than those for other two PV systems for the monitored period (2016-2019). The degradations in almost all these performance parameters are found less for p-s_i than a-s_i, and m-s_i modules-based PV systems over the entire monitored period (2016-2019). Therefore, it is concluded that p-s_i based PV systems are the most suitable choice for the tropical climate of Kuala Lumpur. In contrast, m-s_i based PV system is the least appropriate choice for the site considered. It is also estimated that as a source of clean energy, the composite PV system (6.575kW_P) has significant potential to clean the environment from pollution by avoiding 28143.7 kg CO_2 in four years with an annual average of 7035.9 kg CO_2.

The results for an hour ahead PV power output forecasting showed that the proposed deep learning method (RNN-LSTM) has better hour ahead forecasting accuracy in terms of lower (RMSE and MSE) and higher (r and R^2) in both training and testing phases for all years over the duration (2016-2019), in comparison with regression [GPR, GPR(PCA)], machine learning [SVR, SVR(PCA), ANN] and hybrid [ANFIS(GP), ANFIS(SC), ANFIS(FCM)] methods. Furthermore, the p-si, m-si, and a-si PV systems have presented the lowest RMSE values of 24.25 W/m^2 in 2019, 19.4 W/m^2 in 2016, and 39.2 W/m^2 W/m^2 in 2017, respectively compared to the results in the other three years. On the other hand, all PV systems have the highest values of RMSE for the year 2018. This may happen due to some missing input data incorporated because of the power failure of recording sensors. Therefore, it is concluded that the proposed deep learning model (RNN-LSTM) is proved to be a robust model for an hour ahead forecasting of power output for three different PV systems.

Furthermore, the optimized forecasting results indicate that the proposed hybrid algorithm (SSA-RNN-LSTM) has performed better compared to developed algorithm (RNN-LSTM), (GA-RNN-LSTM) and (PSO-RNN-LSTM). The proposed hybrid method

has shown the lowest (RMSE, MAE, and MSE) and highest R^2 in comparison to other hybrid methods for an hour ahead forecasting of PV power output for three different PV systems on an annual basis over four years data duration (2016-2019). For the p-si PV system, the percent reduction in RMSE (19.14%) is found higher in 2016 compared to other three years, while the percent reduction in MAE (21.57%) is found higher in 2018 than in other years. For the m-si PV system, the percent reduction in RMSE (15.4%) and MAE (10.81%) is higher for 2016 than that for other years. Moreover, the proposed hybrid method has offered a higher percent reduction in RMSE (22.9%) and MAE (25.2%) for a-si PV systems based on 2019 data. The convergence speed of the proposed hybrid algorithm (SSA-RNN-LSTM) is also found higher than the other two hybrid methods for each year data over the duration (2016-2019). This research is helpful for installing high efficiency solar PV forms and enhance the grid reliability to meet the social demand for improving the life quality in Malaysia.

5.2 Recommendation for future works

Following are potential works that can be considered in the future:

- Further study can be conducted to analyze the performance of the PV systems from an economic perspective to determine the most cost-effective PV system for this tropical climate.
- A day ahead and month ahead forecasting of solar power output can also be performed for long-term planning to improve the stability and reliability of the grid.
- Different data preprocessing techniques can be incorporated to enhance the forecasting accuracy of proposed techniques.

- The forecasting accuracy of the proposed deep learning and optimized deep learning method (SSA-RNN-LSTM) can also be assessed over whole four years of data, instead of forecasting on an annual basis.

REFERENCES

Adaramola, M. S., Paul, S. S., & Oyewola, O. M. (2014). Assessment of decentralized hybrid PV solar-diesel power system for applications in Northern part of Nigeria. *Energy for Sustainable Development, 19*, 72-82.

Ağbulut, Ü., Gürel, A. E., & Biçen, Y. (2021). Prediction of daily global solar radiation using different machine learning algorithms: Evaluation and comparison. *Renewable and Sustainable Energy Reviews, 135*, 110114.

Ahmad, M. W., Mourshed, M., & Rezgui, Y. (2018). Tree-based ensemble methods for predicting PV power generation and their comparison with support vector regression. *Energy, 164*, 465-474.

Akarslan, E., & Hocaoglu, F. O. (2016). A novel adaptive approach for hourly solar radiation forecasting. *Renewable energy, 87*, 628-633.

AlHakeem, D., Mandal, P., Haque, A. U., Yona, A., Senjyu, T., & Tseng, T.-L. (2015). *A new strategy to quantify uncertainties of wavelet-GRNN-PSO based solar PV power forecasts using bootstrap confidence intervals.* Paper presented at the IEEE Power & Energy Society General Meeting, 2015.

Alzahrani, A., Shamsi, P., Dagli, C., & Ferdowsi, M. (2017). Solar Irradiance Forecasting Using Deep Neural Networks. *Procedia Computer Science, 114*, 304-313.

Antonanzas, J., Osorio, N., Escobar, R., Urraca, R., Martinez-de-Pison, F., & Antonanzas-Torres, F. (2016). Review of photovoltaic power forecasting. *Solar energy, 136*, 78-111.

Aslam, S., Herodotou, H., Mohsin, S. M., Javaid, N., Ashraf, N., & Aslam, S. (2021). A survey on deep learning methods for power load and renewable energy forecasting in smart microgrids. *Renewable and Sustainable Energy Reviews, 144*, 110992. doi:https://doi.org/10.1016/j.rser.2021.110992

Asrari, A., Wu, T. X., & Ramos, B. (2017). A hybrid algorithm for short-term solar power prediction—Sunshine state case study. *IEEE Transactions on Sustainable Energy, 8*(2), 582-591.

Azimi, R., Ghayekhloo, M., & Ghofrani, M. (2016). A hybrid method based on a new clustering technique and multilayer perceptron neural networks for hourly solar radiation forecasting. *Energy Conversion and Management, 118*, 331-344.

Bae, K. Y., Jang, H. S., & Sung, D. K. (2017). Hourly solar irradiance prediction based on support vector machine and its error analysis. *IEEE Transactions on power systems, 32*(2), 935-945.

Belaid, S., Mellit, A., Boualit, H., & Zaiani, M. (2020). Hourly global solar forecasting models based on a supervised machine learning algorithm and time series principle. *International Journal of Ambient Energy*, 1-12.

Benali, L., Notton, G., Fouilloy, A., Voyant, C., & Dizene, R. (2019). Solar radiation forecasting using artificial neural network and random forest methods: Application to normal beam, horizontal diffuse and global components. *Renewable energy, 132*, 871-884.

Besharat, F., Dehghan, A. A., & Faghih, A. R. (2013). Empirical models for estimating global solar radiation: A review and case study. *Renewable and Sustainable Energy Reviews, 21*, 798-821.

Bigdeli, N., Borujeni, M. S., & Afshar, K. (2017). Time series analysis and short-term forecasting of solar irradiation, a new hybrid approach. *Swarm and evolutionary computation, 34*, 75-88.

Blaga, R., Sabadus, A., Stefu, N., Dughir, C., Paulescu, M., & Badescu, V. (2019). A current perspective on the accuracy of incoming solar energy forecasting. *Progress in Energy and Combustion Science, 70*, 119-144.

Boland, J., David, M., & Lauret, P. (2016). Short term solar radiation forecasting: Island versus continental sites. *Energy, 113*, 186-192.

Bou-Rabee, M., Sulaiman, S. A., Saleh, M. S., & Marafi, S. (2017). Using artificial neural networks to estimate solar radiation in Kuwait. *Renewable and Sustainable Energy Reviews, 72*, 434-438.

Bouzerdoum, M., Mellit, A., & Pavan, A. M. (2013). A hybrid model (SARIMA–SVM) for short-term power forecasting of a small-scale grid-connected photovoltaic plant. *Solar energy, 98*, 226-235.

Bugała, A., Zaborowicz, M., Boniecki, P., Janczak, D., Koszela, K., Czekała, W., & Lewicki, A. (2018). Short-term forecast of generation of electric energy in photovoltaic systems. *Renewable and Sustainable Energy Reviews, 81*, 306-312.

Bulut, H., & Büyükalaca, O. (2007). Simple model for the generation of daily global solar-radiation data in Turkey. *Applied Energy, 84*(5), 477-491.

Capizzi, G., Napoli, C., & Bonanno, F. (2012). Innovative second-generation wavelets construction with recurrent neural networks for solar radiation forecasting. *IEEE Transactions on neural networks and learning systems, 23*(11), 1805-1815.

Chang, G. W., & Lu, H.-J. J. I. T. o. S. E. (2018). Integrating Gray Data Preprocessor and Deep Belief Network for Day-Ahead PV Power Output Forecast. *IEEE Transactions on Sustainable Energy, 11*(1), 185-194.

Chen, C., Duan, S., Cai, T., & Liu, B. (2011). Online 24-h solar power forecasting based on weather type classification using artificial neural network. *Solar energy, 85*(11), 2856-2870.

Cheng, H.-Y. (2017). Cloud tracking using clusters of feature points for accurate solar irradiance nowcasting. *Renewable energy, 104*, 281-289.

Cherkassky, V., & Ma, Y. (2004). Practical selection of SVM parameters and noise estimation for SVM regression. *Neural networks, 17*(1), 113-126.

Chiteka, K., & Enweremadu, C. (2016). Prediction of global horizontal solar irradiance in Zimbabwe using artificial neural networks. *Journal of cleaner production, 135*, 701-711.

Cristaldi, L., Leone, G., & Ottoboni, R. (2017). *A hybrid approach for solar radiation and photovoltaic power short-term forecast.* Paper presented at the IEEE International Instrumentation and Measurement Technology Conference (I2MTC), 2017.

Dairi, A., Harrou, F., Sun, Y., & Khadraoui, S. J. A. S. (2020). Short-term forecasting of photovoltaic solar power production using variational auto-encoder driven deep learning approach. *Applied Sciences, 10*(23), 8400.

Das, U. K., Tey, K. S., Seyedmahmoudian, M., Mekhilef, S., Idris, M. Y. I., Van Deventer, W., . . . Stojcevski, A. (2018). Forecasting of photovoltaic power generation and model optimization: A review. *Renewable and Sustainable Energy Reviews, 81*, 912-928.

David, M., Ramahatana, F., Trombe, P.-J., & Lauret, P. (2016). Probabilistic forecasting of the solar irradiance with recursive ARMA and GARCH models. *Solar energy, 133*, 55-72.

De Giorgi, M., Malvoni, M., & Congedo, P. (2016). Comparison of strategies for multi-step ahead photovoltaic power forecasting models based on hybrid group method of data handling networks and least square support vector machine. *Energy, 107*, 360-373.

Deo, R. C., Downs, N., Parisi, A. V., Adamowski, J. F., & Quilty, J. M. (2017). Very short-term reactive forecasting of the solar ultraviolet index using an extreme learning machine integrated with the solar zenith angle. *Environmental Research, 155*, 141-166.

Deo, R. C., Şahin, M., Adamowski, J. F., & Mi, J. (2019). Universally deployable extreme learning machines integrated with remotely sensed MODIS satellite predictors over Australia to forecast global solar radiation: A new approach. *Renewable and Sustainable Energy Reviews, 104*, 235-261.

Diagne, M., David, M., Lauret, P., Boland, J., & Schmutz, N. (2013). Review of solar irradiance forecasting methods and a proposition for small-scale insular grids. *Renewable and Sustainable Energy Reviews, 27*, 65-76.

Din, G. M. U., & Marnerides, A. K. (2017). *Short term power load forecasting using deep neural networks.* Paper presented at the International Conference on Computing, Networking and Communications (ICNC), 2017

Dolara, A., Grimaccia, F., Leva, S., Mussetta, M., & Ogliari, E. (2015). A physical hybrid artificial neural network for short term forecasting of PV plant power output. *Energies, 8*(2), 1138-1153.

dos Santos, C. M., Escobedo, J. F., Teramoto, É. T., & da Silva, S. H. M. G. (2016). Assessment of ANN and SVM models for estimating normal direct irradiation (Hb). *Energy Conversion and Management, 126*, 826-836.

Fan, J., Wu, L., Ma, X., Zhou, H., & Zhang, F. (2020). Hybrid support vector machines with heuristic algorithms for prediction of daily diffuse solar radiation in air-polluted regions. *Renewable energy, 145*, 2034-2045.

Fentis, A., Bahatti, L., Mestari, M., & Chouri, B. (2017). *Short-term solar power forecasting using Support Vector Regression and feed-forward NN.* Paper presented at the 15th IEEE International New Circuits and Systems Conference (NEWCAS), 2017

Fliess, M., Join, C., & Voyant, C. (2018). Prediction bands for solar energy: New short-term time series forecasting techniques. *Solar energy, 166*, 519-528.

Fouilloy, A., Voyant, C., Notton, G., Motte, F., Paoli, C., Nivet, M.-L., . . . Duchaud, J.-L. (2018). Solar irradiation prediction with machine learning: Forecasting models selection method depending on weather variability. *Energy, 165*, 620-629.

GhaffarianHoseini, A., Dahlan, N. D., Berardi, U., GhaffarianHoseini, A., Makaremi, N., & GhaffarianHoseini, M. (2013). Sustainable energy performances of green buildings: A review of current theories, implementations and challenges. *Renewable and Sustainable Energy Reviews, 25*, 1-17.

Ghayekhloo, M., Ghofrani, M., Menhaj, M., & Azimi, R. (2015). A novel clustering approach for short-term solar radiation forecasting. *Solar energy, 122*, 1371-1383.

Ghimire, S., Deo, R. C., Downs, N. J., & Raj, N. (2018). Self-adaptive differential evolutionary extreme learning machines for long-term solar radiation prediction with remotely-sensed MODIS satellite and Reanalysis atmospheric products in solar-rich cities. *Remote Sensing of Environment, 212*, 176-198.

Ghofrani, M., Ghayekhloo, M., & Azimi, R. (2016). A novel soft computing framework for solar radiation forecasting. *Applied Soft Computing, 48*, 207-216.

Gorunescu, F. (2011). *Data Mining: Concepts, models and techniques* (Vol. 12): Springer Science & Business Media.

Guermoui, M., Rabehi, A., Gairaa, K., & Benkaciali, S. J. T. E. P. J. P. (2018). Support vector regression methodology for estimating global solar radiation in Algeria. *The European Physical Journal Plus, 133*(1), 1-9.

Gueymard, C. A. (2004). The sun's total and spectral irradiance for solar energy applications and solar radiation models. *Solar energy, 76*(4), 423-453.

Guo, J., You, S., Huang, C., Liu, H., Zhou, D., Chai, J., . . . Gardner, M. (2016). *An ensemble solar power output forecasting model through statistical learning of historical weather dataset.* Paper presented at the Power and Energy Society General Meeting (PESGM), 2016.

Gupta, M., Jin, L., & Homma, N. (2004). *Static and dynamic neural networks: from fundamentals to advanced theory*: John Wiley & Sons.

Halawa, E., GhaffarianHoseini, A., & Li, D. H. W. (2014). Empirical correlations as a means for estimating monthly average daily global radiation: a critical overview. *Renewable energy, 72*, 149-153.

Hamilton, J. D. (1994). *Time series analysis* (Vol. 2): Princeton university press Princeton.

Hepbasli, A., & Alsuhaibani, Z. (2011). A key review on present status and future directions of solar energy studies and applications in Saudi Arabia. *Renewable and Sustainable Energy Reviews, 15*(9), 5021-5050.

Hossain, M., Mekhilef, S., Danesh, M., Olatomiwa, L., & Shamshirband, S. (2017). Application of extreme learning machine for short term output power forecasting of three grid-connected PV systems. *Journal of cleaner production, 167*, 395-405.

Hossain, M., Mekhilef, S., & Olatomiwa, L. (2017). Performance evaluation of a stand-alone PV-wind-diesel-battery hybrid system feasible for a large resort center in South China Sea, Malaysia. *Sustainable cities and society, 28*, 358-366.

Hou, M., Zhang, T., Weng, F., Ali, M., Al-Ansari, N., & Yaseen, Z. M. (2018). Global Solar Radiation Prediction Using Hybrid Online Sequential Extreme Learning Machine Model. *Energies, 11*(12), 3415.

Huang, G.-B., Zhu, Q.-Y., & Siew, C.-K. (2004). *Extreme learning machine: a new learning scheme of feedforward neural networks.* Paper presented at the IEEE International Joint Conference Proceedings on Neural Networks, 2004.

Huang, G.-B., Zhu, Q.-Y., & Siew, C.-K. (2006). Extreme learning machine: theory and applications. *Neurocomputing, 70*(1-3), 489-501.

Huang, J., Korolkiewicz, M., Agrawal, M., & Boland, J. (2013). Forecasting solar radiation on an hourly time scale using a Coupled AutoRegressive and Dynamical System (CARDS) model. *Solar energy, 87*, 136-149.

Huang, J., & Perry, M. (2016). A semi-empirical approach using gradient boosting and k-nearest neighbors regression for GEFCom2014 probabilistic solar power forecasting. *International Journal of Forecasting, 32*(3), 1081-1086.

Huang, R., Huang, T., Gadh, R., & Li, N. (2012). *Solar generation prediction using the ARMA model in a laboratory-level micro-grid.* Paper presented at the IEEE Third International Conference on Smart Grid Communications (SmartGridComm), 2012.

Hussain, S., & Al Alili, A. (2016). *Day ahead hourly forecast of solar irradiance for Abu Dhabi, UAE.* Paper presented at the IEEE Smart Energy Grid Engineering (SEGE), 2016

Hussain, S., & AlAlili, A. (2017). A hybrid solar radiation modeling approach using wavelet multiresolution analysis and artificial neural networks. *Applied Energy, 208*, 540-550.

Ibrahim, I. A., & Khatib, T. (2017). A novel hybrid model for hourly global solar radiation prediction using random forests technique and firefly algorithm. *Energy Conversion and Management, 138*, 413-425.

Jäger-Waldau, A. J. E. (2020). Snapshot of Photovoltaics—February 2020. *13*(4), 930.

Jaidee, S., & Pora, W. (2019). *Very Short-Term Solar Power Forecasting Using Genetic Algorithm Based Deep Neural Network.* Paper presented at the 4th International Conference on Information Technology (InCIT), 2019.

Jang, H. S., Bae, K. Y., Park, H.-S., & Sung, D. K. (2016). Solar power prediction based on satellite images and support vector machine. *IEEE Transactions on Sustainable Energy, 7*(3), 1255-1263.

Jang, J.-S. R., Sun, C.-T., Mizutani, E., & Computing, S. J. I. T. o. a. c. (1997). A computational approach to learning and machine intelligence. *IEEE Transactions on automatic control, 42*(10), 1482-1484.

Ji, W., & Chee, K. C. (2011). Prediction of hourly solar radiation using a novel hybrid model of ARMA and TDNN. *Solar energy, 85*(5), 808-817.

Jiang, H., Dong, Y., & Xiao, L. (2017). A multi-stage intelligent approach based on an ensemble of two-way interaction model for forecasting the global horizontal radiation of India. *Energy Conversion and Management, 137*, 142-154.

Jiménez-Pérez, P. F., & Mora-López, L. (2016). Modeling and forecasting hourly global solar radiation using clustering and classification techniques. *Solar energy, 135*, 682-691.

Junior, J. G. d. S. F., Oozeki, T., Ohtake, H., Shimose, K.-i., Takashima, T., & Ogimoto, K. (2014). Forecasting regional photovoltaic power generation-a comparison of strategies to obtain one-day-ahead data. *Energy Procedia, 57*, 1337-1345.

Keshtegar, B., Mert, C., & Kisi, O. (2018). Comparison of four heuristic regression techniques in solar radiation modeling: Kriging method vs RSM, MARS and M5 model tree. *Renewable and Sustainable Energy Reviews, 81*, 330-341.

Kisi, O., Heddam, S., & Yaseen, Z. M. (2019). The implementation of univariable scheme-based air temperature for solar radiation prediction: New development of dynamic evolving neural-fuzzy inference system model. *Applied Energy, 241*, 184-195.

Kostylev, V., & Pavlovski, A. (2011). *Solar power forecasting performance–towards industry standards.* Paper presented at the 1st international workshop on the integration of solar power into power systems, Aarhus, Denmark, 2011.

Lauret, P., Voyant, C., Soubdhan, T., David, M., & Poggi, P. (2015). A benchmarking of machine learning techniques for solar radiation forecasting in an insular context. *Solar energy, 112*, 446-457.

LeCun, Y., Bengio, Y., & Hinton, G. (2015). Deep learning. *Nature, 521*(7553), 436-444.

Lee, W., Kim, K., Park, J., Kim, J., & Kim, Y. J. I. A. (2018). Forecasting solar power using long-short term memory and convolutional neural networks. *IEEE Access, 6*, 73068-73080.

Leva, S., Dolara, A., Grimaccia, F., Mussetta, M., & Ogliari, E. (2017). Analysis and validation of 24 hours ahead neural network forecasting of photovoltaic output power. *Mathematics and Computers in Simulation, 131*, 88-100.

Li, Y., Su, Y., & Shu, L. (2014). An ARMAX model for forecasting the power output of a grid connected photovoltaic system. *Renewable energy, 66*, 78-89.

Li, Z., Zang, C., Zeng, P., Yu, H., & Li, H. (2015). *Day-ahead hourly photovoltaic generation forecasting using extreme learning machine.* Paper presented at the IEEE International Conference on Cyber Technology in Automation, Control, and Intelligent Systems (CYBER), 2015.

Lima, F. J. L., Martins, F. R., Pereira, E. B., Lorenz, E., & Heinemann, D. (2016). Forecast for surface solar irradiance at the Brazilian Northeastern region using NWP model and artificial neural networks. *Renewable energy, 87*, 807-818.

Lin, K.-P., & Pai, P.-F. (2016). Solar power output forecasting using evolutionary seasonal decomposition least-square support vector regression. *Journal of cleaner production, 134*, 456-462.

Lipperheide, M., Bosch, J., & Kleissl, J. (2015). Embedded nowcasting method using cloud speed persistence for a photovoltaic power plant. *Solar energy, 112*, 232-238.

Lu, H., & Chang, G. J. I.-P. (2018). A hybrid approach for day-ahead forecast of PV power generation. *IFAC-Papers OnLine, 51*(28), 634-638.

Lucheroni, C. (2009). *A resonating model for the power market and its calibration.* Paper presented at the 6th International Conference on the European Energy Market (EEM), 2009.

Mandal, P., Madhira, S. T. S., Meng, J., & Pineda, R. L. (2012). Forecasting power output of solar photovoltaic system using wavelet transform and artificial intelligence techniques. *Procedia Computer Science, 12*, 332-337.

Mao, M., Gong, W., & Chang, L. (2013). *Short-term photovoltaic output forecasting model for economic dispatch of power system incorporating large-scale photovoltaic plant.* Paper presented at the IEEE Energy Conversion Congress and Exposition (ECCE), 2013.

Massidda, L., & Marrocu, M. (2017). Use of Multilinear Adaptive Regression Splines and numerical weather prediction to forecast the power output of a PV plant in Borkum, Germany. *Solar energy, 146*, 141-149.

Mathiesen, P., Collier, C., & Kleissl, J. (2013). A high-resolution, cloud-assimilating numerical weather prediction model for solar irradiance forecasting. *Solar energy, 92*, 47-61.

Mellit, A., Kalogirou, S. A., & Drif, M. (2010). Application of neural networks and genetic algorithms for sizing of photovoltaic systems. *Renewable energy, 35*(12), 2881-2893.

Mellit, A., Kalogirou, S. A., Hontoria, L., & Shaari, S. (2009). Artificial intelligence techniques for sizing photovoltaic systems: A review. *Renewable and Sustainable Energy Reviews, 13*(2), 406-419.

Mellit, A., & Pavan, A. M. (2010). A 24-h forecast of solar irradiance using artificial neural network: Application for performance prediction of a grid-connected PV plant at Trieste, Italy. *Solar energy, 84*(5), 807-821.

Mellit, A., Pavan, A. M., & Lughi, V. (2014). Short-term forecasting of power production in a large-scale photovoltaic plant. *Solar energy, 105*, 401-413.

Memon, M. A., Mekhilef, S., Mubin, M., & Aamir, M. (2018). Selective harmonic elimination in inverters using bio-inspired intelligent algorithms for renewable energy conversion applications: A review. *Renewable and Sustainable Energy Reviews, 82*, 2235-2253.

Mirjalili, S., Gandomi, A. H., Mirjalili, S. Z., Saremi, S., Faris, H., & Mirjalili, S. M. J. A. i. E. S. (2017). Salp Swarm Algorithm: A bio-inspired optimizer for engineering design problems. *Advances in Engineering Software, 114*, 163-191.

Mohammadi, B., & Aghashariatmadari, Z. J. A. J. o. G. (2020). Estimation of solar radiation using neighboring stations through hybrid support vector regression boosted by Krill Herd algorithm. *Arabian Journal of Geosciences, 13*, 1-16.

Mohammadi, K., Shamshirband, S., Tong, C. W., Arif, M., Petković, D., & Ch, S. (2015). A new hybrid support vector machine–wavelet transform approach for estimation of horizontal global solar radiation. *Energy Conversion and Management, 92*, 162-171.

Mojumder, J. C., Ong, H. C., Chong, W. T., & Shamshirband, S. (2016). Application of support vector machine for prediction of electrical and thermal performance in PV/T system. *Energy and Buildings, 111*, 267-277.

Mori, H., & Takahashi, M. (2012). *Development of GRBFN with global structure for PV generation output forecasting.* Paper presented at the IEEE Power and Energy Society General Meeting, 2012.

Narvaez, G., Giraldo, L. F., Bressan, M., & Pantoja, A. (2021). Machine learning for site-adaptation and solar radiation forecasting. *Renewable energy, 167*, 333-342.

Ni, Q., Zhuang, S., Sheng, H., Kang, G., & Xiao, J. (2017). An ensemble prediction intervals approach for short-term PV power forecasting. *Solar energy, 155*, 1072-1083.

Niu, D., Wang, Y., & Wu, D. D. (2010). Power load forecasting using support vector machine and ant colony optimization. *Expert Systems with Applications, 37*(3), 2531-2539.

Nonnenmacher, L., Kaur, A., & Coimbra, C. F. (2016). Day-ahead resource forecasting for concentrated solar power integration. *Renewable energy, 86*, 866-876.

Ogliari, E., Dolara, A., Manzolini, G., & Leva, S. (2017). Physical and hybrid methods comparison for the day ahead PV output power forecast. *Renewable energy, 113*, 11-21.

Ogliari, E., Gandelli, A., Grimaccia, F., Leva, S., & Mussetta, M. (2016). *Neural forecasting of the day-ahead hourly power curve of a photovoltaic plant.* Paper presented at the International Joint Conference on Neural Networks (IJCNN), 2016

Olatomiwa, L., Mekhilef, S., Shamshirband, S., Mohammadi, K., Petković, D., & Sudheer, C. (2015). A support vector machine–firefly algorithm-based model for global solar radiation prediction. *Solar energy, 115*, 632-644.

Olatomiwa, L., Mekhilef, S., Shamshirband, S., & Petković, D. (2015). Adaptive neuro-fuzzy approach for solar radiation prediction in Nigeria. *Renewable and Sustainable Energy Reviews, 51*, 1784-1791.

Oudjana, S. H., Hellal, A., & Mahamed, I. H. (2012). *Short term photovoltaic power generation forecasting using neural network.* Paper presented at the 11th International Conference on Environment and Electrical Engineering (EEEIC), 2012.

Ozoegwu, C. G. (2019). Artificial neural network forecast of monthly mean daily global solar radiation of selected locations based on time series and month number. *Journal of cleaner production, 216*, 1-13.

Paoli, C., Voyant, C., Muselli, M., & Nivet, M.-L. (2010). Forecasting of preprocessed daily solar radiation time series using neural networks. *Solar energy, 84*(12), 2146-2160.

Pedro, H. T., & Coimbra, C. F. (2012). Assessment of forecasting techniques for solar power production with no exogenous inputs. *Solar energy, 86*(7), 2017-2028.

Pedro, H. T. C., & Coimbra, C. F. M. (2015). Short-term irradiance forecastability for various solar micro-climates. *Solar energy, 122*, 587-602.

Perez, R., Lorenz, E., Pelland, S., Beauharnois, M., Van Knowe, G., Hemker, K., . . . Pomares, L. M. (2013). Comparison of numerical weather prediction solar irradiance forecasts in the US, Canada and Europe. *Solar energy, 94*, 305-326.

Persson, C., Bacher, P., Shiga, T., & Madsen, H. (2017). Multi-site solar power forecasting using gradient boosted regression trees. *Solar energy, 150*, 423-436.

Qing, X., & Niu, Y. J. E. (2018). Hourly day-ahead solar irradiance prediction using weather forecasts by LSTM. *Energy, 148*, 461-468.

Quan, H., Srinivasan, D., & Khosravi, A. (2014). Particle swarm optimization for construction of neural network-based prediction intervals. *Neurocomputing, 127*, 172-180.

Quej, V. H., Almorox, J., Arnaldo, J. A., & Saito, L. (2017). ANFIS, SVM and ANN soft-computing techniques to estimate daily global solar radiation in a warm sub-humid environment. *Journal of Atmospheric and Solar-Terrestrial Physics, 155*, 62-70.

Rajagopalan, S., & Santoso, S. (2009). *Wind power forecasting and error analysis using the autoregressive moving average modeling.* Paper presented at the IEEE Power & Energy Society General Meeting (PES), 2009.

Rana, M., Chandra, R., & Agelidis, V. G. (2016). *Cooperative neuro-evolutionary recurrent neural networks for solar power prediction.* Paper presented at the IEEE Congress on Evolutionary Computation (CEC), 2016.

Rawat, R., Vora, K., Manry, M., & Eapi, G. (2014). *Multi-variable Neural Network Forecasting Using Two Stage Feature Selection.* Paper presented at the 13th International Conference on Machine Learning and Applications (ICMLA), 2014.

Raza, M. Q., & Khosravi, A. (2015). A review on artificial intelligence based load demand forecasting techniques for smart grid and buildings. *Renewable and Sustainable Energy Reviews, 50*, 1352-1372.

Reikard, G. (2009). Predicting solar radiation at high resolutions: A comparison of time series forecasts. *Solar energy, 83*(3), 342-349.

Renno, C., Petito, F., & Gatto, A. (2016). ANN model for predicting the direct normal irradiance and the global radiation for a solar application to a residential building. *Journal of cleaner production, 135*, 1298-1316.

Salcedo-Sanz, S., Casanova-Mateo, C., Pastor-Sánchez, A., & Sánchez-Girón, M. (2014). Daily global solar radiation prediction based on a hybrid Coral Reefs Optimization–Extreme Learning Machine approach. *Solar energy, 105*, 91-98.

Shah, A. S. B. M., Yokoyama, H., & Kakimoto, N. (2015). High-precision forecasting model of solar irradiance based on grid point value data analysis for an efficient photovoltaic system. *IEEE Transactions on Sustainable Energy, 6*(2), 474-481.

Shalev-Shwartz, S., & Zhang, T. (2016). Accelerated proximal stochastic dual coordinate ascent for regularized loss minimization. *Mathematical Programming, 155*(1), 105-145. doi:10.1007/s10107-014-0839-0

Shamshirband, S., Mohammadi, K., Khorasanizadeh, H., Yee, L., Lee, M., Petković, D., & Zalnezhad, E. (2016). Estimating the diffuse solar radiation using a coupled support vector machine–wavelet transform model. *Renewable and Sustainable Energy Reviews, 56*, 428-435.

Shi, H., Xu, M., & Li, R. J. I. T. o. S. G. (2017). Deep learning for household load forecasting—A novel pooling deep RNN. *IEEE Transactions on Smart Grid, 9*(5), 5271-5280.

Shivashankar, S., Mekhilef, S., Mokhlis, H., & Karimi, M. (2016). Mitigating methods of power fluctuation of photovoltaic (PV) sources – A review. *Renewable and*

Sustainable Energy Reviews, 59, 1170-1184. doi:https://doi.org/10.1016/j.rser.2016.01.059

Sobri, S., Koohi-Kamali, S., & Rahim, N. A. (2018). Solar photovoltaic generation forecasting methods: A review. *Energy Conversion and Management, 156*, 459-497.

Srivastava, S., & Lessmann, S. (2018). A comparative study of LSTM neural networks in forecasting day-ahead global horizontal irradiance with satellite data. *Solar energy, 162*, 232-247.

Tang, P., Chen, D., & Hou, Y. (2016). Entropy method combined with extreme learning machine method for the short-term photovoltaic power generation forecasting. *Chaos, Solitons & Fractals, 89*, 243-248.

Tao, Y., & Chen, Y. (2014). *Distributed PV power forecasting using genetic algorithm based neural network approach.* Paper presented at the International Conference on Advanced Mechatronic Systems (ICAMechS), 2014.

Theocharides, S., Makrides, G., Livera, A., Theristis, M., Kaimakis, P., & Georghiou, G. E. (2020). Day-ahead photovoltaic power production forecasting methodology based on machine learning and statistical post-processing. *Applied Energy, 268*, 115023.

Trapero, J. R., Kourentzes, N., & Martin, A. (2015). Short-term solar irradiation forecasting based on dynamic harmonic regression. *Energy, 84*, 289-295.

van der Meer, D., Munkhammar, J., & Widén, J. (2018). Probabilistic forecasting of solar power, electricity consumption and net load: Investigating the effect of seasons, aggregation and penetration on prediction intervals. *Solar energy, 171*, 397-413.

VanDeventer, W., Jamei, E., Thirunavukkarasu, G. S., Seyedmahmoudian, M., Soon, T. K., Horan, B., . . . Stojcevski, A. J. R. e. (2019). Short-term PV power forecasting using hybrid GASVM technique. *Renewable energy, 140*, 367-379.

Verbois, H., Huva, R., Rusydi, A., & Walsh, W. (2018). Solar irradiance forecasting in the tropics using numerical weather prediction and statistical learning. *Solar energy, 162*, 265-277.

Verbois, H., Rusydi, A., & Thiery, A. (2018). Probabilistic forecasting of day-ahead solar irradiance using quantile gradient boosting. *Solar energy, 173*, 313-327.

Verzijlbergh, R. A., Heijnen, P. W., de Roode, S. R., Los, A., & Jonker, H. J. J. (2015). Improved model output statistics of numerical weather prediction based irradiance forecasts for solar power applications. *Solar energy, 118*, 634-645.

Voyant, C., Motte, F., Notton, G., Fouilloy, A., Nivet, M.-L., & Duchaud, J.-L. (2018). Prediction intervals for global solar irradiation forecasting using regression trees methods. *Renewable energy, 126*, 332-340.

Voyant, C., Muselli, M., Paoli, C., & Nivet, M.-L. (2012). Numerical weather prediction (NWP) and hybrid ARMA/ANN model to predict global radiation. *Energy, 39*(1), 341-355.

Voyant, C., Notton, G., Kalogirou, S., Nivet, M.-L., Paoli, C., Motte, F., & Fouilloy, A. (2017). Machine learning methods for solar radiation forecasting: A review. *Renewable energy, 105*, 569-582.

Wan, C., Zhao, J., Song, Y., Xu, Z., Lin, J., & Hu, Z. (2015). Photovoltaic and solar power forecasting for smart grid energy management. *CSEE Journal of Power and Energy Systems, 1*(4), 38-46. doi:10.17775/CSEEJPES.2015.00046

Wang, F., Xuan, Z., Zhen, Z., Li, K., Wang, T., & Shi, M. (2020). A day-ahead PV power forecasting method based on LSTM-RNN model and time correlation modification under partial daily pattern prediction framework. *Energy Conversion and Management, 212*, 112766.

Wang, F., Zhen, Z., Liu, C., Mi, Z., Hodge, B.-M., Shafie-khah, M., & Catalão, J. P. S. (2018). Image phase shift invariance based cloud motion displacement vector calculation method for ultra-short-term solar PV power forecasting. *Energy Conversion and Management, 157*, 123-135.

Wang, G., Su, Y., & Shu, L. (2016). One-day-ahead daily power forecasting of photovoltaic systems based on partial functional linear regression models. *Renewable energy, 96*, 469-478.

Wang, H., Lei, Z., Zhang, X., Zhou, B., & Peng, J. (2019). A review of deep learning for renewable energy forecasting. *Energy Conversion and Management, 198*, 111799.

Wang, H., Yi, H., Peng, J., Wang, G., Liu, Y., Jiang, H., & Liu, W. (2017). Deterministic and probabilistic forecasting of photovoltaic power based on deep convolutional neural network. *Energy Conversion and Management, 153*, 409-422.

Wen, L., Zhou, K., Yang, S., & Lu, X. J. E. (2019). Optimal load dispatch of community microgrid with deep learning based solar power and load forecasting. *Energy, 171*, 1053-1065.

Wolff, B., Kühnert, J., Lorenz, E., Kramer, O., & Heinemann, D. (2016). Comparing support vector regression for PV power forecasting to a physical modeling approach using measurement, numerical weather prediction, and cloud motion data. *Solar energy, 135*, 197-208.

Wu, J., & Chan, C. K. (2013). Prediction of hourly solar radiation with multi-model framework. *Energy Conversion and Management, 76*, 347-355.

Wu, J., Chan, C. K., Zhang, Y., Xiong, B. Y., & Zhang, Q. H. (2014). Prediction of solar radiation with genetic approach combing multi-model framework. *Renewable energy, 66*, 132-139.

Wu, Y.-K., Chen, C.-R., & Abdul Rahman, H. (2014). A novel hybrid model for short-term forecasting in PV power generation. *International Journal of Photoenergy, 2014*.

Xin-gang, Z., & You, Z. (2018). Technological progress and industrial performance: A case study of solar photovoltaic industry. *Renewable and Sustainable Energy Reviews, 81*, 929-936.

Xue, X. (2017). Prediction of daily diffuse solar radiation using artificial neural networks. *International Journal of Hydrogen Energy, 42*(47), 28214-28221.

Yang, C., Thatte, A. A., & Xie, L. (2015). Multitime-scale data-driven spatio-temporal forecast of photovoltaic generation. *IEEE Transactions on Sustainable Energy, 6*(1), 104-112.

Yang, D., Ye, Z., Lim, L. H. I., & Dong, Z. (2015). Very short term irradiance forecasting using the lasso. *Solar energy, 114*, 314-326.

Yang, H.-T., Huang, C.-M., Huang, Y.-C., & Pai, Y.-S. (2014). A weather-based hybrid method for 1-day ahead hourly forecasting of PV power output. *IEEE Transactions on Sustainable Energy, 5*(3), 917-926.

Yona, A., Senjyu, T., Funabashi, T., & Kim, C. (2013). Determination Method of Insolation Prediction With Fuzzy and Applying Neural Network for Long-Term Ahead PV Power Output Correction. *IEEE Transactions on Sustainable Energy, 4*(2), 527-533.

Yona, A., Senjyu, T., Saber, A. Y., Funabashi, T., Sekine, H., & Kim, C.-H. (2007). *Application of neural network to one-day-ahead 24 hours generating power forecasting for photovoltaic system.* Paper presented at the International Conference on Intelligent Systems Applications to Power Systems (ISAP), 2007.

Youssef, A., El-Telbany, M., & Zekry, A. (2017). The role of artificial intelligence in photo-voltaic systems design and control: A review. *Renewable and Sustainable Energy Reviews, 78*, 72-79.

Yun, Z., Quan, Z., Caixin, S., Shaolan, L., Yuming, L., & Yang, S. (2008). RBF neural network and ANFIS-based short-term load forecasting approach in real-time price environment. *IEEE Transactions on power systems, 23*(3), 853-858.

Zaher, A., Thil, S., Nou, J., Traoré, A., & Grieu, S. (2017). Comparative study of algorithms for cloud motion estimation using sky-imaging data. *IFAC-PapersOnLine, 50*(1), 5934-5939.

Zang, H., Cheng, L., Ding, T., Cheung, K. W., Liang, Z., Wei, Z., . . . Distribution. (2018). Hybrid method for short-term photovoltaic power forecasting based on deep convolutional neural network. *IET Generation, Transmission and Distribution, 12*(20), 4557-4567.

Zhang, J., Verschae, R., Nobuhara, S., & Lalonde, J.-F. J. S. E. (2018). Deep photovoltaic nowcasting. *Solar energy, 176*, 267-276.

Zhen, Z., Liu, J., Zhang, Z., Wang, F., Chai, H., Yu, Y., . . . Lin, Y. (2020). Deep Learning Based Surface Irradiance Mapping Model for Solar PV Power Forecasting Using Sky Image. *IEEE Transactions on Industry Applications, 56*(4), 3385-3396.

Zheng, J., Zhang, H., Dai, Y., Wang, B., Zheng, T., Liao, Q., . . . Song, X. J. A. E. (2020). Time series prediction for output of multi-region solar power plants. *Applied Energy, 257*, 114001.

Zjavka, L. J. I. R. P. G. (2020). PV power intra-day predictions using PDE models of polynomial networks based on operational calculus. *IET Renewable Power Generation, 14*(8), 1405-1412.